THE MODAL REDUCTION METHOD FOR SIMULATION OF GROUNDWATER FLOW AND MULTI-SPECIES CONTAMINANT TRANSPORT IN FRACTURED POROUS MEDIA

by

Keni Zhang

A thesis submitted to the Faculty of Graduate Studies of the University of Manitoba in partial fulfillment of the requirement for the degree of Doctor of Philosophy in Geological Engineering

Winnipeg, Manitoba, Canada, 2000

THE UNIVERSITY OF MANITOBA

FACULTY OF GRADUATE STUDIES

*****

COPYRIGHT PERMISSION PAGE

The Modal Reduction Method for Simulation of Groundwater Flow and Multi-Species Contaminant Transport in Fractured Porous Media

BY

Keni Zhang

A Thesis/Practicum submitted to the Faculty of Graduate Studies of The University of Manitoba in partial fulfillment of the requirements of the degree of Doctor of Philosophy

Abstract

It is now widely recognized that fractures can play an important role in groundwater flow and contaminant transport in geologic media. As open fractures generally offer the path of lower hydraulic resistance, direct transport of a contaminant entering a fractured rock system will be primarily along the fractures. However, contaminant diffusion from the fractures to the porous matrix can significantly reduce migration rates along the fractures. In order to simulate such processes as diffusion into the matrix block, advection and dispersion along the fractures, decay or biodegradation of the contaminants, and perhaps advection in the matrix (if it is sufficiently permeable), a robust and efficient numerical techniques must be used. A multi-dimensional multi-species contaminant transport problem can easily introduce hundreds of thousand to millions of unknowns. Using traditional numerical approaches, it is very difficult to solve these type transport problems. This is especially true for the transport problem in fractured media, due to the complexity of problem and limitations of computer resources. Therefore, an effective algorithm for reducing the original equation system may be of great assistance in simplifying the problem. The Arnoldi or Lanczos reduction technique uses orthogonal matrix transformations to reduce the discretized transport equation system. The reduced equation system is much smaller compared to the original one. The new system can be solved by a standard solution scheme with very little computational effort. This research focuses on extending the application of the two reduction techniques to the simulation of groundwater flow and multi-species contaminant transport in fractured porous media. Several very efficient two-dimensional numerical models based on the reduction methods have been developed. The developed models include dual-porosity groundwater flow

model, dual-porosity decay chain transport model, dual-porosity TCE biodegradation transport model, discrete fracture flow model, and discrete fracture multi-species contaminant transport model. These models are suitable for solving flow and transport problems using the most popular three approaches (continuum, dual-porosity and discrete fracture approach) for the fractured porous media.

The difficulties of using the reduction techniques have been overcome, such as implementation of boundary conditions, choice of a common starting vector and computation of leakage terms for the dual-porosity approach. Moreover, the "shift" technique has been introduced. Using the "shift" technique, the diagonal dominant property of the matrix to be solved can be improved. This property lead to great enhancement of the iterative solution convergence rate and the convergence rate for Lanczos or Arnoldi reduction recursion process. In addition, use of the "shift" technique can extend the application of the Arnoldi reduction method to solve large Peclet number problems. The proposed numerical method has been verified by several comparisons between analytical solutions and the reduction method solutions. The developed models show great saving in computing time and storage space for the examples compared to traditional methods and LTG method. A problem with about 7 million unknowns had been solved using the proposed method. Therefore, the aforementioned approach will allow for a variety complex, high-resolution problems to be solved for on a personal computer.

Acknowledgments

The research described in this thesis was carried out in the Geotechnical Group of the Department of Civil and Geological Engineering, The University of Manitoba, under the guidance of Dr. Allan Woodbury. I would like to thank Allan for all the help, advice, support and funding that he provided during the course of this research. His encouragement and constant enthusiasm were deeply appreciated and constituted a great source of motivation. I have benefited greatly in many ways from working with him during the past four years. I am also grateful to Dr. Scott Dunbar (University of British Columbia) for his advice and help; in particular during the period of my staying in UBC campus in the summer of 1998. In addition I would like to thank him for openly sharing his expertise on the modal reduction techniques.

I wish to thank Dr. Henian Li (EDS Systemhouse Canada) for always keeping his door open and for giving invaluable help on various aspects of the numerical methods used in this work. Special thanks are extended to Dr. Douglas Ruth for all of the help and support he has given me over the years and for his suggestions regarding this research. I would like to express my appreciation to Ingrid Trestrail for giving me help regarding funding and university daily affair.

I am grateful to my wife, Ran Deng, and my son Eric Zhang for their support and encouragement during the course of my study. They tolerated many late nights and lost weekends while I worked. Special thanks are extended to my parents (Zhonglian Zhang and Rongdi Li) and my parents-in-law (Tianqi Deng and Junqing Peng) for providing me with the emotional support required to complete this research.

Contents

List of Figures

List of Tables

Chapter 1

Introduction

1.1 Background

Increased interest in fractured porous media has resulted from harmful waste storage programs and industrial pollutants, especially those associated with high-level radioactive waste or mining tailings. Many countries are seriously considering siting final repositories for nuclear waste in such environments, at depths ranging from a few tens of meters to 500 m or even a kilometer [Neretnieks, 1993]. It is now widely recognized that fractures can play an important role in the transport of contaminants in a groundwater system. As open fractures generally offer the path of lower hydraulic resistance, direct transport of a contaminant entering a fractured rock system will be primarily along the fractures. Transport through the rock matrix by advection may be small in comparison because of the relatively low hydraulic conductivity of the rock itself.

A number of mathematical models describing groundwater flow and contaminant transport in fractured porous media have been developed over the past two decades. The distinction between these models arises from differences in the conceptual model upon which they are based and the methods used to solve the governing equations. There are three popular models, including continuum, dual-

porosity and discrete fracture models. The continuum model treats the fractured porous medium as a single continuum which is similar to the classical continuum representation of an unfractured porous medium [Bear, 1972]. The properties of the porous medium and the individual fractures are averaged over a Representative Elementary Volume (REV) to define macroscopic properties describing bulk groundwater flow and contaminant transport. For many applications involving large-scale areal simulation, the single-continuum porous media approach to a fractured system has been justified and is reasonable. This is because the area of interest is sufficiently large to effectively be an REV. This approach has been used by Berkowitz *et al.*[1988], Schwartz and Smith [1988], Long *et al.*[1982], and others to investigate groundwater flow and contaminant transport in the fractured porous media. As the single continuum approach requires only lumped parameters representing the average behavior of the media over a small REV, it needs less computational effort and is relatively easy to use compared to dual-porosity approach and discrete fracture approach. However, this approach cannot always adequately represent groundwater flow and solute transport in fractured geologic media. More explicit descriptions of the fracture matrix system may have to be considered [Long *et al.* 1982].

The dual-porosity (or double-porosity) model was first introduced by Barenblatt *et al.* [1960]. Such an approach assumes two overlapping continua in which two porosities and permeabilities are associated with the fractured medium. The primary porosity and permeability are those of the porous, but low-permeability blocks that are separated by fractures. The secondary porosity and permeability are associated with fractures, where the permeability is generally high and the porosity is low. In order to use the dual-porosity approach, two sets of properties must be known, one for the fractures and another for the blocks. The two systems

are linked through a leakage term representing the fluid or solute mass exchange between them. It is also assumed that the porous matrix blocks act as sources (or sinks) that feed (or drain) the fractures with fluid or solute mass. Examples of using the dual-porosity approach to simulate flow in fractured media include Barenblatt *et al.* [1960], and Huyakorn *et al.* [1983]. Solute transport in fractured media is more difficult to simulate than the simulation of groundwater flow, but it has been modeled both analytically and numerically. Numerical models for solving the contaminant transport problem using the dual-porosity approach include those of Bibby [1981], Huyakorn *et al.* [1983a], and Sudicky [1990]. For geometrically simple fractured media, analytical solutions have been developed. Tang *et al.* [1981], and Sudicky and Frind [1982] present analytical solutions based on the dual-porosity approach. One of the most critical components of dual-porosity models is the source/sink term that describes the exchange of water or contaminant mass between the fracture and porous matrix. The source/sink term needs to capture the local-scale microscopic processes with a relatively simple term for use in a macroscopic dual-porosity model. The shortcomings of this approach are that fracture patterns and porous matrix blocks are assumed to be of simple geometry with uniform size and shape and that the advection of solutes in each block is typically ignored.

Dual-porosity models of varying complexity have been widely used to simulate the flow of fluid, heat, or transport of solute in a fractured porous media. Many research projects have been conducted in the application of the dual-porosity approach, evaluation of the coupling term, parameter estimation, and numerical algorithms for implementation of the approach. The following discussion reviews the works that have been done in recent years. A more complete review of the previous work, main ideas and methodologies in this field can be found in the

monograph edited by Bear *et al.* [1993] (see Neretnieks [1993]).

The influence of parameters in the dual-porosity approach for various models have been widely investigated. Tomasko *et al.* [1989] developed a type-curve methodology for modeling radionuclide transport through a dual-porosity system using four dimensionless parameters, including dimensionless velocity, dispersion coefficients, solute storage enhancement coefficients and time constants. Sensitivity of the parameters were analyzed and their importance were investigated.

The coupling term between fracture and matrix block is a key parameter for the dual-porosity approach. Zimmerman and Bodvarsson [1989] developed an approximate analytical solution for the problem of a Newtonian fluid infiltrating into a porous spherical block. It was reported that the instantaneous and cumulative fluxes into the sphere can be predicted with very high accuracy by their model. Dykhuizen [1990] presented a quasi-static formulation for the coupling term for dual-porosity models. His model retains the original simplicity as proposed by Barenblatt *et al.* [1960], but is not restricted to very slow transient flow. Bai [1997] presented an algorithm for computing the solution of coupled processes. Instead of solving the coupled system of equations using special functions as practiced by most analytical methodologies, his algorithm offers a direct solution technique using the method of differential operators in the Laplace domain.

Several strategies have been proposed to model the matrix-fracture interaction in a dual-porosity system by Arbogost [1992]. Among these are (1) to directly compute the internal flow within the matrix blocks as it is affected at the blocks' surfaces by the external fracture flow and (2) to define the matrix-fracture interaction by a "transfer function". His simplified dual-porosity model for two phase flow has a nonlinear matrix fracture interaction, and it is more general than similar existing transfer function models.

Novak [1993] presented a dual-porosity chemical transport model. His study examined systems that include chemical reactions and changes in retardation caused by precipitation. The finite difference technique and a chemical equilibrium simulator based on the Villars-Cruise-Smith algorithm are used in the model.

Lao and Booker [1996] developed a finite element method for analyzing contaminant transport in dual-porosity media using a time-stepping approach. In their approach, the flux exchange that occurs between the fluid in the fractures and the matrix block is represented by a linear hereditary process. Their study shows that all the hereditary information necessary to carry the solution forward from time to time is contained in the values of certain hereditary variables at current time step so that it is not necessary to store the complete time history and consequently a more efficient numerical process can be developed.

Fillion and Noyer [1996] used a dual-porosity model to simulate groundwater flow with automatic mesh generation and parameter calibration. The numerical investigation focused on the mesh generation for discretization of fracture and matrix domain has also been done by Taniguchi and Fillion [1996].

Pini and Putti [1997] used the parallel finite element Laplace transform method to solve the equation of non-equilibrium contaminant transport in a dual-porosity system. When the sorption reaction is represented by a first-order kinetic relationship, the equation takes the form of a convection-dispersion partial differential equation with an integral term describing the mass transfer between the matrix and fracture. This type of problems can be solved efficiently in Laplace space. A similar approach was also adopted by Sudicky [1990]

Transport of contaminants in dual-porosity formations was shown to occur in three distinct regimes: fracture, dual-porosity and total porosity transport [Os-

tensen, 1998]. In Ostensen's study, a formation parameter called transport length, was used to describe the controlling of dual-porosity transport. Conventional two-well tracer tests were used to estimate the transport length. The effect on tracer tests of random heterogeneity and anisotropy in the formation was analyzed.

Besides the approaches mentioned previously, the discrete fracture model has also been widely used. This approach requires that the geometry and hydraulic properties of each fracture be specified. The early numerical studies of solute transport in discrete random fracture networks neglect any mass transport interactions that occur between the fractures and the porous matrix blocks, and also the consideration of matrix diffusion. These works are described by Schwartz *et al.* [1983], and Smith and Schwartz [1984]. Some recently developed numerical models incorporate matrix diffusion by using the principle of superposition of fracture elements onto porous matrix elements to solve the coupled fracture-matrix groundwater flow and solute transport equations. This type of model was used by Sudicky and Mclaren [1991], Therrien and Sudicky [1996], and Vanderkwaak and Sudicky [1996]. Advective transport in the matrix is also accounted in these models.

In recent years, many studies have been done using the discrete fracture approach. Some interesting examples may include the following. Liggett and Medina [1988] presented a three-dimensional flow model. The flow in a 3D network of discrete fractures is calculated by the boundary element method. In their model, the flow in any fracture is considered two-dimensional but these fractures may be connected in a three-dimensional network. The authors claim that the boundary element is extraordinarily effective in computing flow in three-dimensional networks of fractures and the requirement for data is much less than for the comparable finite element analysis.

Casas *et al.* [1990] developed a stochastic discrete fracture network model for the investigation of possible nuclear waste repository sites in crystalline environments and used this model to predict the flow and transport properties of the medium. The model assumed that fractures can be represented as circular discs; the density, orientation and size of which can be inferred from in situ geometric observations. However, the flow in their model is assumed to be restricted to idealized channels within the fracture planes, the hydraulic conductivities of which must be inferred from hydraulic tests. The parameters of a probability distribution function of the hydraulic properties of these channels are inferred from local scale hydraulic injection tests in boreholes. In their transport model, microscopic dispersion in the fractures and retardation effects due to unevenness of the flow paths were taken into account.

A comparison between transport simulation in the flow-calibrated discrete model and tracer tests of the field experiment was conducted by Dverstorp *et al.* [1992]. Field tracer migration in sparsely fractured rock was analyzed with a discrete fracture network model. They concluded that the uneven spatial distribution of flow and tracer, the complex dispersive behavior, and channeling effects that have been observed in the field experiment can be reproduced by the discrete fracture transport model.

Huyakorn *et al.* [1994] developed a sophisticated three-dimensional, three phase numerical model for simulating the movement of non-aqueous-phase liquids (NAPL's) by using dual-porosity and discrete fracture approaches. The model accommodates a wide variety of boundary conditions, including withdrawal and injection well conditions which are treated rigorously using fully implicit schemes. A Galerkin procedure with upstream weighting of fluid mobilities, storage matrix lumping, and fully implicit treatment of nonlinear coefficients and well conditions

was used in the model. The nodal connective schemes and the computational effective numerical schemes were also discussed in their paper.

1.2 Multi-species contaminant transport in fractured media

The most common multi-species contaminant transport problems are caused by either radionuclide decay chain, biodegradation or chemical reaction. Previous works related to the simulation of transport of decay chain in porous media can be categorized into two groups: analytical solutions and numerical models. Analytical solutions can, in spite of their limitations to some simple problems provide effective alternatives for predicting the transport of multi-member decay chains in groundwater [Lester *et al.*, 1975; Haderman, 1980; Gureghian and Jasen 1985]. For more complicated problems, numerical methods have been widely used. The equations described radionuclide transport can embody most of the physical and chemical processes known. The main processes may include advective, retardation, dispersion, radioactive decay, and molecular diffusion. Solving of the decay chain equations can be computationally and computer memory intensive. This results from the requirement of solving several equations for different species at the same time, which is caused by chains arising from parent to daughter transformation. Domenico and Schwartz [1990] classified the known numerical methods for solving decay chain problems into two type approaches,"two-step" or "one-step". The "two-step" approach first provides an approximate concentration by considering advection and dispersion only. The results are then corrected to account for the changes of mass due to the decay and transformation. This method requires iterations between the two steps until the specified convergence criterion is met. This approach has been used by Liu and Narasimhan [1989] and Narasimhan *et*

al. [1986]. The "one step" approach solves all of the equations with advection, dispersion, decay and transformation simultaneously using either a finite element or finite different method. Comparing to the "two-step" approach, this method is numerically complicated but more rigorous. Examples of this approach can be found in the works of Miller and Benson [1983], Willis and Rubin [1987], and Li *et al.* [1998].

Similar to the radionuclide decay chain problem, the simulation of chlorinated solvents such as trichloroethylene (TCE) transport in the groundwater system also involves multi-species transport. During the course of migration, in the absence of oxygen, TCE will be reductively transformed to three isomers of dichloroethene (DCE) which are further converted to vinyl chloride and finally to ethene. McCarty and Semprini [1994] have a detailed discussion of this type of TCE biodegradation. Recent research into numerical modeling of TCE transport is found in the works of Woodbury and Li [1998]. The analytical solutions for this type problem are provided in the work of Sun *et al.* [1999] and Sun *et al.* [1999a].

For the modeling of multi-species radionuclides or TCE transport in fractured rocks, only a limited number of studies have been done. These studies mainly focus on analytical solutions and numerical solutions of simple conceptual models for the reason of problem complexity. Most analytical solutions are restricted to single fracture or parallel fractures and one-dimension. Numerical models all require high memory allocations and are computationally intensive. These greatly limit the application of numerical methods to solve the real world problems of multi-species transport in fractured media.

Sudicky and Frind [1984] presented an analytical solution by Laplace transforming radionuclide transport equations for a two-member decay chain in a single fracture. Their solution takes into account advection along the fracture, molecu-

lar diffusion from the fracture to the porous medium, adsorption on the fracture face, adsorption in the rock matrix, and radioactive decay. The solution for the daughter product is in the form of a double integral which is evaluated by Gauss-Legendre quadrature. They concluded that the daughter product may advance ahead of the parent nuclide even when the half-life of the parent is longer. Other similar analytical solutions include the work of Chen [1986], Chen and Li [1997], and Rasmuson [1984].

Hodgkinson and Maul [1988] developed a semi-analytical solution for arbitrary length decay chains in fractured rock. They assume fractures are identical and parallel to each other. The following physical and chemical phenomena are considered in their solution: advection through the fractures, linear equilibrium on the fracture surfaces, the hydrodynamic dispersion in the rock matrix, and decay and in-growth for the chains of all the members. Talbot's algorithm is used for the numerical inversion of the analytical solutions to the Laplace-transformed equations to obtain the time-dependent solutions.

Lee and Lee [1995] developed a one-dimensional stochastic analytical model using continuous in-time Markov processes for radionuclide transport of decay chain of arbitrary length in the fractured rock media. In their model, the planar fracture in the rock matrix is considered as a finite number of compartments in series. Therefore, the medium is continuous in view of various processes associated with nuclide transport but discrete in medium space. Processes including advection, diffusion into matrix, and radioactive decay chain are taken into account in the model. However, they neglect the both longitudinal and transverse dispersions in the fracture. They compute the expectation and variance of nuclide distribution for compartment or fracture medium by calculating the transition probability for nuclides from the transition intensity between the compartments utilizing the

Chapman-Kolmogorov equation.

Huyakorn *et al.* [1983b] developed a finite element model for simulation of radionuclide decay chain transport in a naturally fractured porous medium system. The dual-porosity approach, discrete fracture approach or combination of these two approaches are used in their model to represent the actual physical system. Advection and hydrodynamic dispersion in the fractures, as well as diffusion in the porous matrix and chain decay or in-growth of solution species, have been taken into account in the model. For the dual-porosity approach, the blocky fractured system is represented by using either a prismatic or spherical idealization of matrix blocks. Two governing equations are written for solute transport in the fractures and diffusion in the porous matrix blocks, respectively, for each species. These equations are coupled together by mass exchange terms and the parent to daughter transform terms. They used a numerical scheme of combining a two-dimensional, upstream-weighted, finite-element approximation for transport in the fractures with a one-dimensional Galerkin approximation for diffusion within the individual matrix blocks. Two schemes are provided for solving of the equations: iterative solution scheme or direct solution schemes. Both schemes are computationally intensive. For the discrete fracture model, they neglect the mass exchange between the fracture and matrix, and write the equations for fractures in local coordinate system, which can be very difficult for relatively complicated fracture system.

Codell [1995] reported that the American Nuclear Regulatory Commission was developing a finite-different model for transport of chain decay radionuclides in porous and fractured media. The dual-porosity concept is to be used in their model. The Laplace transform is applied to the advection-dispersion-decay equation for the fractures and matrix blocks. After the transformed equation is solved by using the finite different method, nodal concentrations in the time domain are

obtained using a Laplace inversion algorithm to invert the Laplace domain nodal concentrations.

1.3 Numerical methods

Over the past two decades, rapid advancements have been made in the development of numerical solution techniques for groundwater flow and contaminant transport modeling. Sudicky and Huyakorn [1991] provide a detailed review on the development of numerical methods. They concluded that the recent modeling advancements center in four key aspects. The first of numerical modeling research concerns development and application of efficient matrix solution techniques for flow and transport problems with a large number of degrees of freedom. The second aspect is the development of stable and accurate numerical schemes for handling advective-dominated transport problems. The third aspect concerns the recent development of improved techniques for handling nonlinearities in the variably saturated flow problems. The final aspect of recent modeling is the development of multiphase models for simulating the migration of NAPL organic chemicals.

Sudicky and Huyakorn [1991] concluded that the Preconditioned Conjugate Gradient (PCG) iterative solution approach may be the most promising method for handling large sparse matrix equations from two- and three-dimensional numerical approximations. Modifications of the standard PCG procedure have been made to deal with the asymmetric matrix equations. One of such modification made by Behie and Forsyth [1984] is known as the ORTHOMIN procedure, which has been applied increasingly in the subsurface contaminant transport and variably saturated flow simulation [Sudicky, 1990; Therrien and Sudicky, 1996]. Other widely used direct solving methods which may improve the accuracy, efficiency

or stability of the solutions include the upstream weighted residual and Petrov-Galerkin schemes [Huyakon and Pinder, 1983], the Laplace Transform Galerkin (LTG) technique [Sudicky, 1989], and Arnoldi/Lanczos modal reduction method (ARM or LRM) [Dunbar and Woodbury 1989; Woodbury *et al.* 1991]. Farrell *et al.* [1998] has made a comparative analysis between the method LTG and ARM with an attention focused on efficiency and accuracy. For the homogeneous materials, he found that the LTG method maintains a higher degree of accuracy than does the ARM. However, in terms of efficiency, the Arnoldi method attains a predefined level of accuracy faster than does the LTG method. For the heterogeneous hydraulic conductivity field, the level of accuracy achieved by the ARM and the LTG method are similar. Compared to the tradition time-marching approach, both methods are stable and robust, and greatly out-perform the traditional approach in efficiency. A potential shortcoming of the LTG formulation was recently reported by Xu and Bruseau [1995]. In their work, they showed that the negative dispersion which is inherent in the Galerkin finite element scheme can be potentially problematic when the LTG method is applied to highly advective problems under high grid Peclet number conditions. In addition, the LTG method is known to be limited to problems involving linear mass transport in steady flow fields.

The Arnoldi method is a modal reduction technique based on the recursive Arnoldi algorithm. Using this algorithm a matrix differential equation can be transformed into a smaller system of equations. The size of the reduced system is dependent on the number of modes or Arnoldi vectors chosen, which is much less than the size of the original equation system. The reduced system is then solved using a time-stepping scheme such as the Crank-Nicolson approach. The solution of the original equation is then obtained from the reduced space using a matrix-vector multiplication. Compared with conventional methods the main

advantage of the ARM is its high efficiency.

The modal reduction technique was first introduced to groundwater hydrology by Dunbar and Woodbury [1989]. They applied the Lanczos method to solve the groundwater flow problem. Later, Woodbury *et al.* [1991] and Nour-Omid *et al.* [1991] used the Arnoldi reduction method to solve the contaminant transport problems. All these applications have demonstrated great efficiency of the modal reduction technique. In 1994, Dunbar *et al.* made a detailed discussion of several implementation difficulties for the Lanczos method, including the choice of starting vector and implementation of time-dependent boundary conditions, etc. For the purpose of improving the approximation of the eigenvalues of the problem and thus increase the convergence rate of the method, Farrell [1997] developed a "shift" version of the ARM. Li [1996] extended the Lanczos methods to solve unsymmetric groundwater problems and applied this method to the multi-species decay chain transport problem [Li *et al.* [1998]).

1.4 Objective and research methodology

Multi-species contaminant transport in fractured porous media has been examined using a variety of underlying physical models such as the continuum, dual-porosity and discrete fracture models. Analytical and numerical solutions of contaminant transport problems using these models for flow and single species contaminant transport problems have been in existence for many years and have been developed for application to both unsaturated soils and saturated geologic media. There are several numerical models available for the simulation of multi-species transport in fractured porous media, such as FTRANS, STAFF3D [Huyakorn, 1983b], TRACR3D [Travis, 1984], TOUGH2 [Pruess, 1991], and FRAC3DVS [Sudicky and McLaren, 1992], FracMan/MAFIC [Golder Associates, Inc, 1994]. However,

most of these models are limited by the efficiency and accuracy of the available solvers and the complexity of the problems. The mass exchange between fracture and matrix is a complicated process for the dual-porosity approach. The coupling term has been investigated for many years in groundwater hydrology [Zimmerman and Bodvarsson, 1989; Dykhuizen, 1990]. An efficient scheme for computing the transient coupling term for mass transport modeling is very important.

The primary objective of this study is to provide effective numerical tools for solving the real world engineering problems in evaluation of environmental impact of high-level radioactive waste, mining tailings, accidental chemical spills, and improperly designed or maintained chemical transportation and storage facilities. Several efficient numerical approaches for the simulation of two or three-dimensional groundwater flow and multi-species solute transport in fractured media, such as the transport problem of decay chain components or TCE and its biodegradation products will be presented. In order to simulate groundwater flow and contaminant transport behavior in fractured media, the flow and contaminant transport equations will be discussed and the mass exchange term between fracture and matrix block will be examined. The consideration of multiple dimensional problems allows for a more realistic representation of the physical system of the real world. However, even a transport problem of single species in two or three dimensions can introduce tens to hundreds of thousand of unknowns. By the traditional numerical approaches, it is very difficult to solve the multi-species transport problem, especially for the transport problem in fractured media, due to the complexity of problem and limitation of computer resources. Therefore, an effective algorithm for reducing the original equation system may be of great assistance in simplifying the problem.

The dual-porosity and discrete fracture approaches will be introduced for the

solute transport in fractured media. The dual-porosity approach is suitable for the case of incomplete information about the fracture distributions. The mathematical models for dual-porosity approach by using parallel fracture model and spherical model are developed. An explicit expression for the mass exchange between the porous matrix and fractures is obtained, which is a function of recent concentration and history concentration of the solute and its parent species in the fracture. The discrete fracture approach requires that the geometry and the hydraulic properties of each fracture be specified. Using a superimposing technique, one final system of equations for the whole domain will be obtained. This approach is applicable for the detailed simulation of solute transport in fractured porous media. Processes of advection, mechanical dispersion, molecule diffusion, biodegradation, decay and in-growth due to the decay of parent species are fully accounted for, except the advection in the porous matrix for dual-porosity approach, which is considered negligible. The traditional Galerkin technique is used to discretize the flow and transport equations. The Lanczos or Arnoldi algorithm is applied to reduce the original equation system, which in turn can be solved by a suitable time integration algorithm such as Crank-Nicolson method. Using a matrix-vector multiplication, the solution of original equation at a particular time can be sought. This approach achieves a tremendous advantage in computation CPU time and computer storage memory over classic methods. When a problem involves large numbers of unknowns or with a large band width, the reduction procedure may not be efficiently implemented by a direct solution method, a fast and robust accelerated iterative solver-ORTHOMIN [Vinsome, 1976] or PCG solver is employed. All the numerical models developed will be verified by comparison with analytical solutions. Several field scale example simulations covering a range of flow and solute transport problems in different fractured geological media will

be presented.

The behavior of a radionuclide decay chain or TCE transport in fractured porous media is not completely understood. Further study of the contaminant transport behavior is necessary for the simulation of multi-species transport in fractured media. In this study, the influences of uncertainty in the distribution of fractures on the contaminant transport will also be investigated.

In particular, the following will be examined in this study:

1. The transport behavior of decay chain radionuclides and TCE biodegradation contaminants (in anaerobic conditions) in saturated fractured porous media. The influence of randomly distributed fractures on multi-species contaminant transport will be examined.

2. Detailed governing equations describing groundwater flow and multi-species contaminants transport (decay chain radionuclides and TCE) in fractured porous media using dual-porosity and discrete fracture approach will be studied. The conditions under which these equations can be written in a form suitable for the Arnoldi or Lanczos reduction methods.

3. How can the calculation of fluid or mass exchange between fracture and matrix block for dual-porosity approach be made more efficient.

4. The applicability and performance of the Lanczos or Arnoldi methods for solving various flow and multi-species mass transport equations with different time-dependent boundary conditions.

5. Improvement of the accuracy and efficiency of the reduction techniques, especially for problems with large Peclet number and heterogeneous media.

In general, the accuracy and efficiency of the numerical methods for simulation of multi-species transport in fractured media and the implementation of the methods are the key issues in this work. In order to achieve the objectives, the following schemes or methodology will be adopted:

1. The fluid or mass exchange term in the dual-porosity model is a function of groundwater head or concentration history of the contaminant, and concentration and concentration history of its parent species. For the groundwater flow problem, this term can be written in a recursive form. It is expected to be more efficient compared to the iterative scheme used in most numerical methods using dual-porosity model. By writing the mass exchange term in recursive form, reduction of the discretized system of equations can be implemented. For the transport problem, the mass exchange term can be computed directly in reduced space and the solution is sought through a superposition scheme. This method is expected to be more efficient compared to the computation in the original space.

2. The groundwater flow and contaminant transport equations will be developed in a form which is suitable for the reduction methods. Several reasonable assumptions will be made in the development of the equations. The Lanczos and Arnoldi reduction methods are used to reduce the size of equation systems. Solving the reduced equations will be more efficient than directly solving the original equations.

3. The general form of the time-dependent first and second type boundary conditions will be examined. By grouping the same time history boundary nodes and considering the different time history groups separately, the first and second type time-dependent boundary conditions can be implemented

in the reduction methods.

4. Because of the complexity of multi-species transport, the common starting vector for the Arnoldi reduction method will be carefully selected and the equation system solver will be chosen to achieve extra efficiency and robustness of the adopted numerical techniques. Two schemes for choosing the common starting vector will be presented. Further efficiency is achieved by using features of FORTRAN 90 for programming.

5. The "shift" technique will be re-introduced and improved. It is expected that this technique can greatly enhance the convergence rate of the iterative solution procedures and the convergence rate of the recursion process. The new technique makes the application of ARM to problems with large Peclet number and large time step size possible.

6. The efficiency and accuracy of the reduction methods will be evaluated through the comparison of the results of reduction methods and the tradition time-stepping methods or LTG method. The flow and transport models will be verified by using published analytical solutions, real field data, and results of generic transport problems solved using different numerical methods.

7. The modal reduction methods will be extended to solve problems of long-term and large-scale groundwater flow and multi-species contaminant transport in fractured media.

Chapter 2

The Reduction Techniques

2.1 Introduction

In this chapter, the Lanczos reduction method (LRM) and the Arnoldi reduction method (ARM) are reviewed. First, the general reduction procedure of a differential equation system is examined. Application of the finite element or finite difference method to the governing groundwater flow or mass transport equation subject to initial and boundary conditions results in a matrix differential equation of the form

$$\mathbf{M}\dot{\mathbf{c}} + \mathbf{K}\mathbf{c} = \mathbf{f} \tag{2.1}$$

where $\mathbf{c}$ is a vector of unknowns at the nodes of the finite element mesh, $\mathbf{K}$ is the "conductivity" matrix, $\mathbf{M}$ is the "capacity" matrix and $\mathbf{f}$ is a vector which contains the effects of the boundary conditions as well as source/sink terms. Both $\mathbf{M}$ and $\mathbf{K}$ are $n \times n$ matrices, where n is the number of nodes in the mesh. Matrix $\mathbf{M}$ is symmetric and positive-definite. Matrix $\mathbf{K}$ is symmetric for groundwater flow problems and unsymmetric for contaminant transport problems.

The traditional approach for solving the above matrix differential equation is to apply a finite difference approximation to the time derivative followed by a time-stepping routine such as the Crank-Nicolson scheme. This method first discretizes

equation (2.1) in time, and then obtains solutions by recursive substitutions. For instance, the Crank-Nicolson algorithm gives

$$\mathbf{M}'\mathbf{c}^{k+1} = \mathbf{K}'\mathbf{c}^{k} + \frac{1}{2}\Delta t(\mathbf{f}^{k+1} + \mathbf{f}^{k}) \tag{2.2}$$

where $\mathbf{M}' = \mathbf{M} + \Delta t\mathbf{K}/2$, $\mathbf{K}' = \mathbf{M} - \Delta t\mathbf{K}/2$, Δt is the time step and k denotes the time level.

It is apparent that the cost of solving the above equation system will be a function of the size of the matrices $\mathbf{K}$ and $\mathbf{M}$, as well as the number of time steps required to reach the desired time. Recently, there has been research into reduction methods to solve these problems, including the Lanczos reduction method and the Arnoldi reduction method. These methods project the large system into a very small subspace (a "Krylov" space) constructed using M-orthogonal vectors, giving a small-sized system of the first order differential equations of the form

$$\mathbf{H}\dot{\mathbf{w}} + \mathbf{w} = \mathbf{g} \quad \text{or} \quad \mathbf{T}\dot{\mathbf{w}} + \mathbf{w} = \mathbf{g} \tag{2.3}$$

where $\mathbf{H}$ (or $\mathbf{T}$) is a $m \times m$ matrix, m is the total number of M-orthogonal Arnoldi (or Lanczos) vectors required to solve the original system of equations, $\mathbf{g}$ is an m-element vector. The advantage of reduction is that $m \ll n$. Approximate solutions in the subspace can then be obtained by solving the reduced system (2.3) using any time-stepping scheme. The solution in the original space is obtained by a transformation (a matrix-vector multiplication).

The LRM applies the Lanczos algorithm [Lanczos, 1950] to the symmetric matrix $\mathbf{K}^{-1}$, using a three term recurrence to construct the tridiagonal matrix $\mathbf{T}$. The ARM method applies the Arnoldi algorithm [Arnoldi, 1951] to the unsymmetric matrix $\mathbf{K}^{-1}$. In the Arnoldi reduction process, the recurrence involves all previously produced vectors, resulting in a upper Hessenberg matrix $\mathbf{H}$. Details

can be seen in the works of Dunbar and Woodbury [1989], Nour-Omid and Glough [1984], and Nour-Omid *et al.* [1991].

The reduction methods have the potential to render problems with large discretization into equivalent systems of much smaller size. Consequently, large savings in computer time and memory are realized, especially for multi-species transport problems which require only one reduction process for all the equation systems.

The reduction method was first introduced to solve groundwater problems by Dunbar and Woodbury [1989]. In 1990, Woodbury *et al.* applied the reduction method to the single species contaminant transport problem. In 1998, Li *et al.* extended the Lanczos method to solve multi-species decay chain transport problem. Later, Woodbury and Li [1998] extended the application of the Arnoldi method to the TCE transport in porous media.

Due to the difficulties of choice of common starting vector, the work of Woodbury and Li is limited to special decay boundary conditions and constant retardation factors for all species. Moreover, a number of mathematical challenges have also hindered the application of the reduction methods. One of the most important challenges is the implementation of complicated first type or second type boundary conditions in the reduction methods. Both the choice of common starting vector and boundary condition implementation will be investigated in this research.

2.2 Lanczos reduction method

The Lanczos reduction process begins by multiplying the symmetric matrix $\mathbf{K}^{-1}$ to both sides of equation (2.1):

$$\mathbf{K}^{-1}\mathbf{M}\dot{\mathbf{c}} + \mathbf{c} = \mathbf{K}^{-1}\mathbf{b}\mu(t) \tag{2.4}$$

where $\mathbf{b}$ is a time independent vector and $\mu(t)$ is a scalar time function such that $\mathbf{f}(t) = \mathbf{b}\mu(t)$.

The method generates a set of Lanczos vectors $\mathbf{q}_1, \mathbf{q}_2, ..., \mathbf{q}_m$ $(m \ll n)$ to form a M-orthogonal matrix, $\mathbf{Q} = (\mathbf{q}_1, \mathbf{q}_2, ..., \mathbf{q}_m)$. The algorithm can be described as:

Start from an initial vector $\mathbf{r}_0 = \mathbf{K}^{-1}\mathbf{b}$ and $\mathbf{q}_0 = 0$, then calculate for j=0, 1, 2, ..., m-1, recursively,

$$(1) \qquad \chi_{j+1} = (\mathbf{r}_j^t \mathbf{M} \mathbf{r}_j)^{\frac{1}{2}},$$

$$(2) \qquad \mathbf{q}_{j+1} = \frac{1}{\chi_{j+1}} \mathbf{r}_j,$$

$$(3) \qquad \varphi_{j+1} = \mathbf{q}_{j+1}^t \mathbf{M} \mathbf{K}^{-1} \mathbf{M} \mathbf{q}_{j+1},$$

$$(4) \qquad \mathbf{r}_{j+1} = \mathbf{K}^{-1}\mathbf{M}\mathbf{q}_{j+1} - \varphi_{j+1}\mathbf{q}_{j+1} - \chi_{j+1}\mathbf{q}_j,$$

Thus, the matrix $\mathbf{Q} = [\mathbf{q}_1, \mathbf{q}_2, ..., \mathbf{q}_m]$ and the tridiagonal matrix $\mathbf{T}$ are formed

$$\mathbf{T} = \begin{bmatrix} \varphi_1 & \chi_2 & & & & \\ \chi_2 & \varphi_2 & \chi_3 & & & \\ & \chi_3 & \varphi_3 & \cdots & & \\ & & \cdots & \cdots & \cdots & \\ & & & \cdots & \varphi_{m-1} & \chi_m \\ & & & & \chi_m & \varphi_m \end{bmatrix} \tag{2.5}$$

From the above algorithm, the following relationships hold

$$\mathbf{K}^{-1}\mathbf{M}\mathbf{Q} = \mathbf{Q}\mathbf{T} + \mathbf{r}\mathbf{e}_m^t \tag{2.6}$$

and

$$\mathbf{Q}^t\mathbf{M}\mathbf{Q} = \mathbf{I} \qquad \mathbf{Q}^t\mathbf{M}\mathbf{r} = 0 \tag{2.7}$$

where $\mathbf{I}$ is the $m \times m$ identity matrix, the m-vector $\mathbf{e}_m$ is the mth column of matrix $\mathbf{I}$ and $\mathbf{r}$ is a residual vector. The superscript t denotes transpose of that matrix or vector.

The two equations in (2.7) refer to the M-orthogonality property. The Rayleigh-Ritz reduction process is then used to reduce the size of equation (2.1). Multiplying equation (2.1) by $\mathbf{Q}^t\mathbf{M}$, substituting the approximate transformation

$$\mathbf{c} = \mathbf{Q}\mathbf{w} \tag{2.8}$$

into the original equation, and applying (2.6) and (2.7), the reduced system (2.3) is obtained, where $\mathbf{g}$ is given by:

$$\mathbf{g} = \chi_1 \mathbf{e}_1 \mu(t) \tag{2.9}$$

The approximate solution to the original equation (2.1) can be obtained by transforming the solution $\mathbf{w}$ according to (2.8). The LRM is only for solving groundwater flow problems which have a symmetric $\mathbf{K}$ matrix.

2.3 Arnoldi reduction method

The ARM may also be appropriately described as a subspace method. However, unlike the LRM method where the Krylov subspace is formed using the symmetric matrix $\mathbf{MK}^{-1}\mathbf{M}$, the ARM generates the subspace using the unsymmetric matrix $\mathbf{MK}^{-1}\mathbf{M}$.

The application of the ARM to the mass transport problem is also initiated by multiplying (2.1) by $\mathbf{K}^{-1}$ and the equation in the form of (2.4) is obtained. Application of m steps of the recursive Arnoldi algorithm to the matrix $\mathbf{K}^{-1}\mathbf{M}$, the reduced system of equations is formed.

The Arnoldi reduction process can be concluded as follows. It is almost identical to the Lanczos reduction method.

Start from a vector $\mathbf{r}_0 = \mathbf{K}^{-1}\mathbf{b}$ and $\mathbf{q}_0 = 0$, then calculate for j=0, 1, 2, ..., m-1, recursively,

(1) $\chi_{j+1} = (\mathbf{r}_j^t \mathbf{M} \mathbf{r}_j)^{\frac{1}{2}}$,

$$(2) \qquad \mathbf{q}_{j+1} = \frac{1}{\chi_{j+1}}\mathbf{r}_j,$$

$$(3) \qquad \varphi_{j+1} = \mathbf{q}_{j+1}^t \mathbf{M}\mathbf{K}^{-1}\mathbf{M}\mathbf{q}_{j+1},$$

$$(4) \qquad \psi_{j+1}^{(j+1-i)} = \mathbf{q}_i^t \mathbf{M}\mathbf{K}^{-1}\mathbf{M}\mathbf{q}_{j+1}, \quad i = 1, 2, ..., j,$$

$$(5) \qquad \mathbf{r}_{j+1} = \mathbf{K}^{-1}\mathbf{M}\mathbf{q}_{j+1} - \varphi_{j+1}\mathbf{q}_{j+1} - \sum_{i=1}^{j} \psi_{j+1}^{(i)}\mathbf{q}_{j+1-i},$$

The M-orthogonal matrix $\mathbf{Q} = [\mathbf{q}_1, \mathbf{q}_2, ..., \mathbf{q}_m]$ and the Hessenberg matrix $\mathbf{H}$ are formed

$$\mathbf{H} = \begin{bmatrix} \varphi_1 & \psi_2^{(1)} & \psi_3^{(2)} & & \psi_{m-1}^{(m-2)} & \psi_m^{(m-1)} \\ \chi_2 & \varphi_2 & \psi_3^{(1)} & & \cdots & \cdots \\ & \chi_3 & \varphi_3 & \cdots & \cdots & \cdots \\ & & \cdots & \cdots & \cdots & \\ & & & \cdots & \psi_{m-1}^{(1)} & \psi_m^{(2)} \\ & & & \cdots & \varphi_{m-1} & \psi_m^{(1)} \\ & & & & \chi_m & \varphi_m \end{bmatrix} \tag{2.10}$$

Analogous to the LRM, equations (2.6) and (2.7) are also valid for the Arnoldi reduction method.

The same Rayleigh-Ritz reduction process as in the LRM is used. Using equation (2.8) for approximate transformation, the reduced system of equations in the form of (2.3) is obtained. The reduced system of equations is then solved using a suitable time stepping procedure such as the Crank-Nicolson method. Woodbury *et al.* [1990] indicated that the time required for the time stepping procedure is not significant if $m \ll n$. It is noted that using the equation (2.8) for transformation of the subspace solution is computationally inexpensive and contributes little to the overall computational cost. At this point it should be stated that the reduction procedure for both the LRM and the ARM can be implemented using either direct or iterative solvers. In this research, both direct and iterative versions of the reduction process have been implemented.

Compared to conventional methods, the main advantage of the reduction method is its efficiency in computing time and storage. The efficiency can be

further enhanced by using a larger time step without violating the Courant constraint [Farrell, 1997]. However, the efficiency to be gained from the ARM is currently only available for transport problems involving steady state groundwater flow. If a problem involve transient flow, the $\mathbf{K}$ matrix must be reformulated and the reduction process repeated each time the velocity field changes. This process is computationally expensive and severely reduces the efficiency of the reduction method, because the reduction process is based on the conductivity matrix $\mathbf{K}$.

The convergence rate for both the iterative solution procedure for the reduction process and the recursion procedure for the reduction process itself depends on the properties of $\mathbf{K}$. The properties of the matrix can be changed by a "shift" method [Farrell, 1997] which greatly enhances the convergence rate. Detailed discussions of application of the shifted Arnoldi method to the problem of flow and transport in discretely fractured media are presented in next chapter.

Chapter 3

Theoretical Development—Flow and Decay Chain Transport

3.1 Physical system

Clay aquitards and consolidated rocks are often considered to be safe geological formations in which to dispose of hazardous waste because of their low hydraulic conductivity. In this case, dissolved contaminants released from hazardous waste facilities migrate mainly by molecular diffusion, which is a relatively slow process; however, these geological materials often contain high conductivity fractures which can greatly enhance the migration rate of dissolved contaminants. As the open fractures generally offer the path of least hydraulic resistance, the transport of a contaminant entering a fractured rock system will be primarily along the fracture. At the same time, contaminants also migrate through the rock matrix by advection.

Figure 3-1 illustrates a commonly occurring geological feature that forms a physical system of groundwater flow and contaminant transport in a fractured porous medium. The physical system consists of a fractured porous medium and a waste facility, such as a mining tailings pit or a dump site, situated on the top of the medium. If fractures exist on the side or bottom of the waste site, the

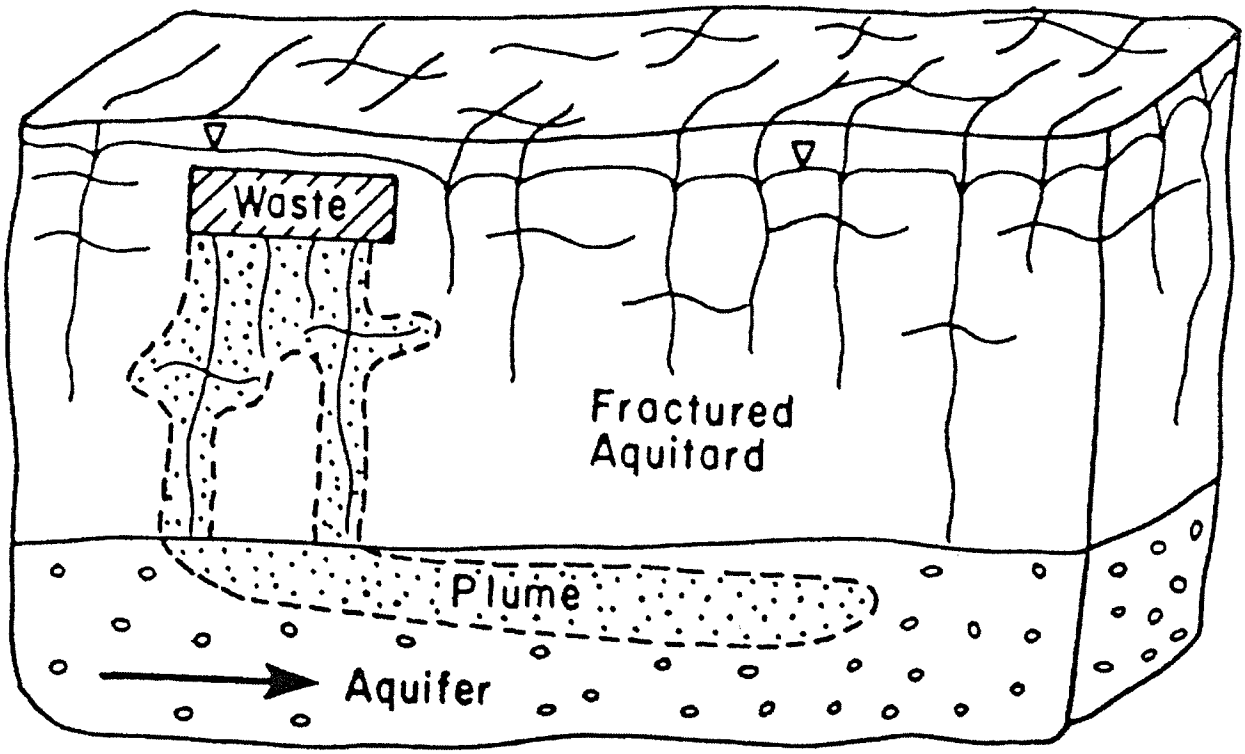

Figure 3-1 One of the most commonly observed physical system of groundwater flow and contaminant transport in fractured porous media (modified from Therrien *et al.*, 1996)

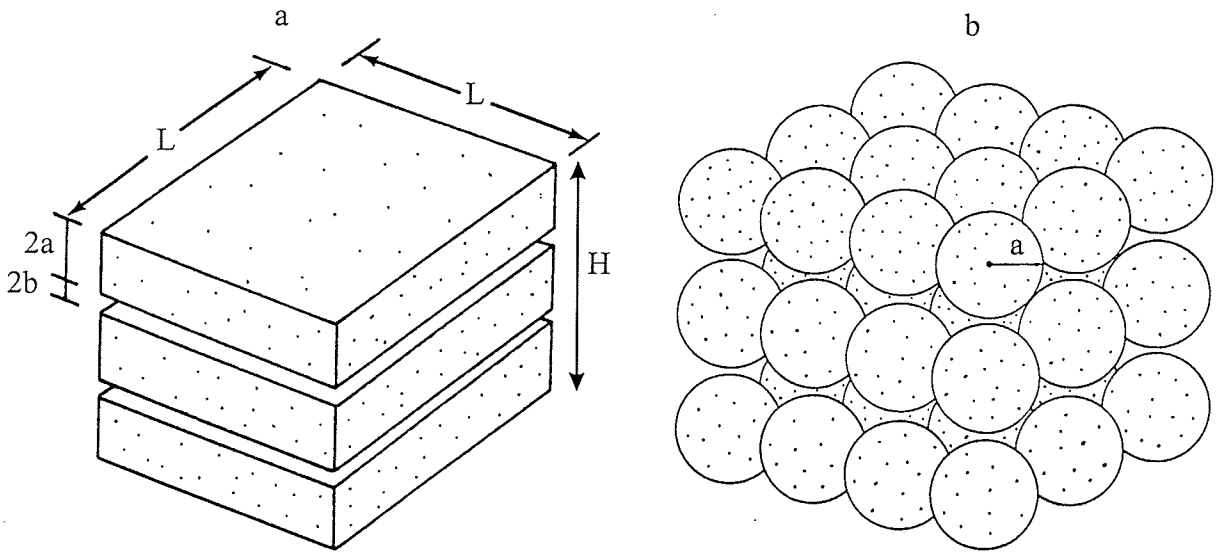

Figure 3-2 Dual-porosity conceptual models: (a) parallel fracture model, (b) spherical block model (after Huyakorn *et al*, 1983)

contaminant that originates from the source may migrate along the fractures by advection and dispersion in the aqueous phase. It further diffuses into the porous matrix, sorbs onto the fracture surfaces and the suspended or filtered colloids, and may decay for some radioactive chemical contaminants. The contaminants in the fracture can distribute among four phases: mass in the solution phase, on the fracture surface, on mobile colloids, and on filtered colloids [Ibaraki and Sudicky, 1995].

The distribution of fractures can be very complicated. For a naturally fractured porous medium, the fractures are interconnected in three dimensions. In order to simplify the system, one can use a family of parallel fractures or two orthogonal families of parallel fractures to represent the physical system. In the work presented herein, the physical system is simulated by using both the dual-porosity approach and the discrete fracture approach separately. For the dual-porosity approach, two conceptual models, the parallel fracture model and the blocky fracture model (see Figure 3-2), are used. For the discrete fracture approach, the fractures can be randomly distributed as one or two-dimensional plates. The theoretical development in this study is for three dimensional problems.

3.2 Properties of contaminant transport

Multi-species contaminant transport in the fractured porous media is a very complicated physical and chemical process. This research focuses on the transport of decay chain radionuclides and multi-species TCE biodegradation contaminants.

The water moving in the fractures in the rock may transport dissolved radionuclides from a repository for radioactive waste or radioactive mining tailings. The assessment of how much and at what rate the nuclides are carried by the moving water is governed by the flow rate of the water in the rock, pathways, and

on the retardation of the radionuclides by physical and chemical interactions with the rock [Neretnieks, 1993]. Domenico and Schwartz [1990] concluded that the magnitude and direction of advective transport are controlled by (1) the hydraulic conductivity distribution within the flow field, (2) the configuration of the water table or potentiometric surface, (3) the presence of sources or sinks, and (4) the shape of the flow domain. Other important processes that influence decay chain transport may include retardation and radioactive decay.

The water flow rate calculations are based on flow models for fractured media. Based on the calculated flow rate, velocity of the flow can be determined. The flow velocity is then used in the transport models. However, the radionuclides do not move with the velocity of water in general. Their velocity will deviate from the average velocity. This is because of the effect of diffusion. Small molecules or ions diffuse in a concentration gradient and can move from high concentration to low concentration locations. With only advection and dispersion active, the classical advection-dispersion equation results. It has been used extensively to describe non active contaminant transport in porous media. It is easily modified to account for the influences of decay. The same equation can be used to describe contaminant transport in the fractures or matrix blocks.

In most circumstances, radionuclides will adsorb on the surfaces of the rock minerals. These processes may considerably retard the radionuclides which, in some instances, can be expected to move many orders of magnitude slower than the flow. For a given flow rate the retardation will be greater for a nuclide if there are more exposed surfaces at which the nuclides can interact. This is because the radionuclides not only interact with the fracture surface, but may also diffuse into the matrix and sorb onto the inner surfaces of the rock matrix. The inner surfaces in the matrix blocks are much larger compared to the fracture surfaces

in contact with the flowing water. Therefore diffusion into the matrix may lead to considerable increase in retardation.

In addition, decay of the radionuclides has a significant impact on the transport of contaminants. The concentration of a radionuclide may decrease due to the decay of that species or increase due to the decay of its corresponding parent species changing into that species. Each radionuclide may have more than one parent species and may also have more than one daughter species.

The dissolved species may also experience kinetic effects caused by physical processes [Neretnieks, 1993]. One such process that has a very large impact for solute transport in fractured rock is the diffusion in and out of zones in which the water is moving so slowly that it can be assumed to be stagnant. Such stagnant zones can be expected in fractures with uneven surfaces and with fracture filling materials.

The presence of colloids may enhance the transport of radionuclides in groundwater by reducing retardation effects [van der Lee *et al.*, 1992; Baek and Pitt, 1996]. Colloids existing in groundwater act as carriers, adsorbing radionuclides onto their large surface area and moving with the groundwater. When the colloidal particles are vigorously filtered onto the fracture surfaces, contaminant migration is not significantly enhanced because of the low colloid mobility, even when the sorption capacity of the colloid is large [Ibaraki and Sudicky, 1995].

In addition, properties of the fractured media greatly influence the transport capacity of the individual fractures. Fracture apertures are known to span several orders of magnitude. Fractures offer paths to a contaminant entering a fractured rock system. Therefore the size of apertures is a key parameter that influences the fracture hydraulic resistance. The porosity and conductivity of the fractures and porous matrix media are the two most important parameters determining the

groundwater flow velocity. The flow velocity determines the transport capacity of the fractured porous media through advection.

Except for decay, all the properties mentioned for decay chain transport also influence TCE transport. In addition, TCE biodegradation is an important property that influences its transport. Biodegradation is the transformation of organic chemicals mediated by living organisms through enzymes. Microorganisms degrade organic chemicals as a source of energy and for their growth, although most of the degradative enzymes are not used directly for growth. The rate of biodegradation of an organic chemical is dependent on chemical and environmental conditions, and on the microorganisms that are present. Extensive laboratory and modeling work has been performed in recent years to examine the contaminant biodegradation properties in the fractured porous media [Vogel and McCarty, 1985; MacQuarrie *et al.* 1990; and Semprini, *et al.*, 1995]. In this research, only the dissolved-phase contaminant transport will be considered and the complicated biodegradation procedure will be simplified as a first order decay process.

3.3 Governing equations

3.3.1 Groundwater flow equations

(1) Dual porosity approach

The partial differential equations describing groundwater flow in dual-porosity fractured media are obtained by considering a representative elementary volume (REV) consisting of a sufficiently large number of matrix blocks and fractures. The dimensions of each of these blocks are assumed to be small relative to the scale of the problem. The geometry of the matrix blocks is taken here to consist of either parallel slabs or spherical "blocks", as shown in Figure 3-2. Because the matrix block dimensions are assumed to be small relative to the scale of the problem,

the hydraulic heads on the surface of each matrix block will be approximately uniform and flow in the block will be essentially one-dimensional. At each point in the domain, there are two overlapping continua, one for the matrix blocks and the other for the fractures.

The partial differential equation of flow in fracture continuum takes the form [Barenblatt *et al.*, 1960, Huyakorn *et al.*, 1983]

$$\frac{\partial}{\partial x_i}(T_{ij}\frac{\partial h}{\partial x_j}) = S\frac{\partial h}{\partial t} - \Gamma - q_w \tag{3.1}$$

i,j=1, 2

where h is the hydraulic head in the fracture, T_{ij} and S are the fracture transmissivity and storage coefficient of the formation, Γ is the volumetric rate of fluid transferring from porous matrix blocks to fractures per unit volume, and q_w is the volumetric rate of fluid flow via sinks or sources.

The term Γ represents the fluid-flux interaction between the porous matrix and the fracture. In general, it is a function of both time and space. There are three popular alternative mathematical models for describing Γ. Detailed description of these models can be found in Huyakorn *et al.* [1983]. In this research, both the unsteady parallel fracture and blocky fracture models are used, although the approach discussed herein can be extended to any fracture model.

The fluid interaction at the interface of the matrix block and fracture can be obtained by solving a one-dimensional governing equation with appropriate initial condition and boundary conditions at the rock matrix-fracture interface. For the dual-porosity parallel fracture, Γ can be expressed as

$$\Gamma = (-\frac{2K'H}{a[a+b]})(\sum_{n=0}^{\infty}\int_0^t \frac{\partial h}{\partial \tau}e^{-\omega_n(t-\tau)}d\tau) \tag{3.2}$$

where a, b are the half thickness of matrix block and fracture, H is the aquifer

thickness, K' is the hydraulic conductivity of the matrix, and ω_n is a constant given by

$$\omega_n = \pi^2(2n+1)^2 K'/(4S'_s a^2) \tag{3.3}$$

where S'_s is the specific storage of the rock matrix.

In a similar way, Γ for the spherical blocky matrix is given by

$$\Gamma = (-\frac{6K'H}{a[a+b]})(\sum_{n=1}^{\infty} \int_0^t \frac{\partial h}{\partial \tau} e^{-\omega_n(t-\tau)} d\tau) \tag{3.4}$$

where

$$\omega_n = \pi^2 n^2 K'/(S'_s a^2)$$

and a for the blocky model is the radius of a spherical "block".

(2) Discrete fracture approach

The description of groundwater flow in a discretely fractured porous media requires governing equations for both the porous matrix and the fracture system. The governing equation for flow in the porous matrix is described by the traditional groundwater flow equation for porous media [Bear, 1972]:

$$\frac{\partial}{\partial x_i}(K'_{ij}\frac{\partial h'}{\partial x_j}) + q' = S'_s \frac{\partial h'}{\partial t} \tag{3.5}$$

i, j=1, 2, 3

where h' is the hydraulic head in the matrix, K'_{ij} and S'_s are the hydraulic conductivity and specific storage of the porous matrix. The effect of any source or sink on the flow in the matrix such as a fluid exchange with the fractures or extraction by pumping is represented in (3.5) by q'.

The fluid flux q_i in any direction i, at any point within the matrix can be defined accordingly by using the Darcy equation:

$$q_i = -K'_{ij}\frac{\partial h'}{\partial x_i} \tag{3.6}$$

i,j =1, 2, 3

In one version of the discrete fracture approach, the fractures are idealized as two-dimensional plates. This implies that the hydraulic head is uniform across the fracture width. The equation for groundwater flow in a fracture of aperture $2b$ is:

$$2b\frac{\partial}{\partial x_i}(K\frac{\partial h}{\partial x_j}) - q_n \mid_{I^-} + q_n \mid_{I^+} = 2bS_s\frac{\partial h}{\partial t} \tag{3.7}$$

i, j=1,2

where h is the hydraulic head in the fracture, S_s and K are the specific storage and hydraulic conductivity of the fracture, and the two q_n terms represent the normal components of the fluid leakage flux across the boundary interfaces (I^- and I^+) that separate the fracture and the porous matrix. It is this leakage term together with an assumed continuity in the head along the interface that provides the link between the flow equations for each fracture and porous matrix. K is given by [Bear, 1972]

$$K = \frac{\rho g(2b)^2}{12\mu} \tag{3.8}$$

where ρ and μ are the fluid density and viscosity, respectively, and g is the acceleration of gravity.

By combining (3.8) with the one-dimensional form of the Darcy equation, the fluid flux q_f along the axis of a fracture is [Sudicky and McLaren, 1992]

$$q_f = -\frac{\rho g(2b)^2}{12\mu}\frac{dh}{dl} \tag{3.9}$$

3.3.2 Radionuclide decay chain transport equations

(1) Dual-porosity approach

The governing equations for transport of radionuclide component p ($p = 1, 2..., P$) in the fractures using a dual-porosity approach can be written in the following form

[Huyakorn *et al.* 1983b, 1983a]

$$\frac{\partial}{\partial x_i}(D_{ij}\frac{\partial C_p}{\partial x_j}) - v_i\frac{\partial C_p}{\partial x_i} = R_p\frac{\partial C_p}{\partial t} + R_p\lambda_p C_p - \sum_{m'=1}^{M}\zeta_{pm'}R_{m'}\lambda_{m'}C_{m'}$$
$$-(\frac{1-\phi}{\phi})\Gamma_p \qquad\qquad p = 1, 2, ..., P \quad i, j = 1, 2 \tag{3.10}$$

where C_p is the concentration of species p, t is the time, x_i is the spatial coordinate, D_{ij} is the hydrodynamic dispersion tensor, v_i represents the flow velocity in fractures along the x_i direction, λ_p and R_p are the first-order decay constant and the retardation coefficient of species p in the fractures, respectively, $\zeta_{pm'}$ is the fraction of parent component m' transforming into component p, M is the total number of parent components transforming into the component p, $R_{m'}$, $\lambda_{m'}$ and $C_{m'}$ are the retardation coefficient, decay constant, and the concentration of the parent species m', Γ_p is the volumetric rate of mass exchange of component p between the rock matrix and fracture, and the ϕ is the secondary fracture porosity which is defined as the volume of fractures per unit volume of the entire porous medium. For the parallel fracture model, the secondary fracture porosity is given by

$$\phi = \frac{b}{a+b} \tag{3.11}$$

where a and b are the half thickness of matrix block and fracture. The similar expression for the spherical block model can also be derived if the packing of the spheres is known.

For linear-reversible equilibrium sorption, the retardation coefficient R_p or R_m in fracture can be further defined as [Freeze and Cherry, 1979]

$$R = 1 + \frac{K_d^*}{b} \tag{3.12}$$

where K_d^* is the fracture wall distribution coefficient $[L]$.

As mentioned earlier, the two most popular conceptual models for the fractured porous medium are the parallel fracture-prismatic block and spherical block models [Huyakorn et al., 1983a]. Both models are depicted in Figure 3-2. The mass transfer between the matrix block and fracture (Γ_p) can be written in the terms of concentration gradient at their interface using Fick's law. For the parallel fractured model, the expression of Γ_p takes the form:

$$\Gamma_p = -\frac{D'}{a}\frac{\partial C'_p}{\partial z}\,|_{z=a} \tag{3.13}$$

where z is a local coordinate with the origin at the center of the matrix block, D' is the molecular diffusion coefficient of the rock matrix, and C'_p is concentration of radionuclide component p in the matrix block.

The corresponding expression for the spherical model is given by:

$$\Gamma_p = -\frac{3D'}{a}\frac{\partial C'_p}{\partial r}\,|_{r=a} \tag{3.14}$$

where r is the radial distance from the center of the sphere.

The development of equation (3.10) is based on the following major assumptions [Huyakorn *et al.*, 1983b, 1983a]:

1. Contaminant transport in the fractures is two-dimensional and is controlled by both hydrodynamic dispersion and advection.

2. The local sorption equilibrium isotherm can be considered linear.

3. Chemical reaction or radioactive decay or ingrowth effects can be described by a first-order term.

4. The fractured porous medium is macroscopically uniform and can be approximated by the parallel fracture-prismatic block conceptual model or by the spherical block model.

5. Transport in the matrix blocks is dominated by molecular diffusion, and this can be described by an one-dimensional diffusion equation in Cartesian or spherical coordinates.

6. For the spherical model the block diameter is small in comparison with overall transport distance.

Equation (3.10) represents a system of P partial differential equations linked together by the decay chain terms, which account for transformation of parent to daughter components. In order to solve equation (3.10), boundary conditions and initial conditions are required. The initial conditions can be expressed as

$C_p = C_p^0$ at $t=0,\ p=1,\ 2,\ldots,\ P$

The common boundary conditions are the first or second type with constant or transient concentration. A decaying source condition can be described by a set of mass-balance equations, known as Bateman's system of ordinary differential equations [Bateman, 1910]

$$\frac{d\tilde{C}_p}{dt} = -\lambda_p \tilde{C}_p + \sum_{m'=1}^{M} \zeta_{pm'} \lambda_{m'} \tilde{C}_{m'} \tag{3.15}$$

where $\tilde{C}_p$ denotes the boundary concentration of species p. For a general P-component decay chain in the sequence:
(1)→(2).....→(P-1)→(P), the analytical solution of (3.15) was given by Harada *et al.* [1980]

$$\tilde{C}_p = \tilde{C}_p^0 e^{-\lambda_p t} + \lambda_{p-1} \tilde{C}_{p-1}^0 \sum_{m'=p-1}^{p} e^{-\lambda_{m'} t} [\prod_{\substack{k=p-1 \\ k \neq m'}}^{p} (\lambda_k - \lambda_{m'})]^{-1} + \ldots$$

$$+ \lambda_{p-1}\lambda_{p-2}\ldots\lambda_1 \tilde{C}_1^0 \sum_{m'=1}^{p} e^{-\lambda_{m'} t} [\prod_{\substack{k=1 \\ k \neq m'}}^{p} (\lambda_k - \lambda_{m'})]^{-1} \tag{3.16}$$

p=1, 2,.....,P

The superscript 0 on boundary concentration $\tilde{C}_p$ in the above equation denotes the initial boundary concentration value of that species.

In equation (3.10), the mass exchange term Γ_p is related to the concentration gradient at the interface between the matrix blocks and fractures. The concentration gradient may be computed by solving the diffusion equation for contaminant concentration in the matrix block. For the prismatic block, the equation representing one-dimensional diffusion in the block takes the form [Huyakorn *et al.*, 1983b]

$$\frac{\partial}{\partial z}(D'\frac{\partial C'_p}{\partial z}) = \phi' R'_p \frac{\partial C'_p}{\partial t} + \phi' R'_p \lambda_p C'_p - \sum_{m'=1}^{M} \zeta_{pm'} \phi' R'_{m'} \lambda_{m'} C'_{m'} \qquad (3.17)$$

p=1, 2, ..., P

where $C'_{m'}$ is the concentration of p's parent species m' in the slab, ϕ' is the matrix porosity, R'_p and $R'_{m'}$ are the retardation coefficients of component p and m' in the block respectively. The retardation coefficient in the matrix is given by [Freeze and Cherry, 1979]:

$$R' = 1 + \frac{\rho_b}{\phi'} K_d \qquad (3.18)$$

where ρ_b is the bulk density of the matrix and K_d is the equilibrium distribution coefficient describing a linear Freundlich adsorption isotherm.

The solution of equation (3.17) must satisfy the following initial conditions.

$C'_p = C'^0_p$ at t=0, p=1, 2,..., P

The appropriate boundary conditions are of the form

$C'_p = C_p$ at z=a, p=1, 2,..., P

$\frac{\partial C'_p}{\partial z} = 0$ at z=0, p=1, 2,..., P

For spherical blocks, the corresponding system of equations is

$$\frac{1}{r^2}\frac{\partial}{\partial r}(r^2 D'\frac{\partial C'_p}{\partial r}) = \phi' R'_p \frac{\partial C'_p}{\partial t} + \phi' R'_p \lambda_p C'_p - \sum_{m=1}^{M} \zeta_{pm} \phi' R'_m \lambda_m C'_m \qquad (3.19)$$

p=1, 2,..., P

which must be solved subject to

$C'_p = C'^0_p$ at *t=0, p=1, 2,..., P*

$C'_p = C_p$ at *r=a, p=1, 2,..., P*

$\frac{\partial C'_p}{\partial r} = 0$ at *r=0, p=1, 2,..., P*

The systems (3.10) and (3.17) or (3.19) are related together through the parent-daughter decay chain and the mass exchange terms. For a real-world problem, this most likely would result in a large system of equations. In order to solve these problems, a robust and effective scheme to reduce and solve the equation system is necessary.

(2) Discrete fracture approach

Similar to the formulation of the flow problem using the discrete fracture model, two equations will be used to describe the decay chain contaminant transport in fractured porous media for each species: one for the fracture and another for the porous matrix. In contrast with the dual-porosity model, the advection in the porous matrix is also taken into account in the discrete fracture model. The coupling between the two equations is provided by the continuity in concentration at the fracture-matrix interface and by the equality of the normal component of the solution mass flux across this interface.

For the species p, the equation governing mass transport in the porous matrix is given by

$$\frac{\partial}{\partial x_i}(D'_{ij}\frac{\partial C'_p}{\partial x_j}) - v'_i\frac{\partial C'_p}{\partial x_i} = R'_p\frac{\partial C'_p}{\partial t} + R'_p\lambda_p C'_p - \sum_{m'=1}^{M}\zeta_{pm'}R'_{m'}\lambda_{m'}C'_{m'} \qquad (3.20)$$

p=1, 2,...,P $\quad$ i,j=1,2,3

The notation above is the same as in equation (3.10), except that the parameters are for the porous matrix.

The equation describing radionuclide decay chain transport in a fluid-filled fracture can be written as follow (modified from Sudicky and McLaren, 1992)

$$(2b)[R_p\frac{\partial C_p}{\partial t} + v_i\frac{\partial C_p}{\partial x_i} - \frac{\partial}{\partial x_i}(D_{ij}\frac{\partial C_p}{\partial x_j}) + R_p\lambda_p C_p - \sum_{m'=1}^{M}\zeta_{pm'}R_{m'}\lambda_{m'}C_{m'}]$$
$$-\Lambda_n\,|_{I^-} + \Lambda_n\,|_{I^+} = 0 \qquad i,\ j = 1,2 \qquad p=1,2,...,P \qquad (3.21)$$

The two terms involving Λ_n represent the mass loss (or gain) of solute mass across the fracture-matrix interfaces I^- and I^+ due to fluid leakage and hydrodynamic dispersion. The retardation factor R_p is defined by equation (3.12). In (3.21), it is assumed that the adsorption characteristics of both fracture walls are identical.

Λ_n along interface I^+ interface can be written as:

$$\Lambda_n\,|_{I^+} = [q_n C_p - \phi D_n\frac{\partial C_p}{\partial \mathrm{n}}]\,|_{I^+} \qquad (3.22)$$

where q_n is the normal component of the Darcy flux, and D_n and $\partial C_p/\partial$n are the dispersion coefficient and concentration gradient, respectively, acting perpendicular to the fracture-matrix interface I^+. Λ_n along interface I^- can be determined in the same way.

3.4 Numerical techniques for flow modeling

The numerical solution of the governing flow equations for both the dual-porosity and discrete fracture models are obtained by applying the standard Galerkin finite

element method for spatial discretization. Their solution is complicated because strong contrasts in material properties are likely to exist between the fractures and the porous matrix. In addition, a multi-dimensional model can easily involve many hundreds to thousands of unknowns. Therefore, an efficient and robust numerical technique is necessary to solve the governing equations. Dunbar and Woodbury [1989] have shown that the Lanczos algorithm is well suited for solving large groundwater flow problems, particularly when the time duration is long. The Lanczos algorithm uses orthogonal matrix transformations to reduce the finite element equations to a much smaller tridiagonal system of first-order differential equations. A standard tridiagonal solution algorithm can solve this new system with little computational effort. A matrix-vector multiplication is then used to obtain the original solutions at desired time steps. Solution techniques for flow equations for both the dual-porosity and discrete fracture models are discussed in the following sections.

3.4.1 Dual-porosity approach

Consider now the following flow equation obtained by substituting (3.2) or (3.4) into (3.1).

$$\frac{\partial}{\partial x_i}(T_{ij}\frac{\partial h}{\partial x_j}) - S\frac{\partial h}{\partial t} + q_w - \sigma\sum_{i=0}^{\infty} I_i = 0 \qquad i=1,\ 2 \tag{3.23}$$

where

$$I_i = \int_0^t \frac{\partial h}{\partial \tau} e^{-\omega_i(t-\tau)} d\tau \tag{3.24}$$

and σ for a parallel fracture model is

$$\sigma = \frac{2K'H}{a(a+b)} \tag{3.25}$$

or for a blocky fracture model

$$\sigma = \frac{6K'H}{a(a+b)} \tag{3.26}$$

If a finite difference approach is adopted to solve (3.23) and if the time step size Δt is assumed constant, at time step k+1, the time integration in (3.24) can be approximated by

$$I_i^{k+1} \approx \frac{h^1 - h^0}{\Delta t}\int_0^{t_1} e^{-\omega_i(t_{k+1}-\tau)}d\tau + \frac{h^2 - h^1}{\Delta t}\int_{t_1}^{t_2} e^{-\omega_i(t_{k+1}-\tau)}d\tau + ... + \frac{h^{k+1} - h^k}{\Delta t}\int_{t_k}^{t_{k+1}} e^{-\omega_i(t_{k+1}-\tau)}d\tau \tag{3.27}$$

where the superscripts of h (*0, 1, ..., k* and *k+1*) denotes the groundwater heads at different time steps.

From (3.27), it is easy to show that the relation between I_i^k and I_i^{k+1} can be expressed as:

$$I_i^{k+1} = e^{-\omega_i \Delta t} I_i^k + \frac{1 - e^{-\omega_i \Delta t}}{\omega_i \Delta t}(h^{k+1} - h^k) \tag{3.28}$$

Note equation (3.28) is in a recursive form and can be rewritten as a function of groundwater hydraulic head history.

$$I_i^{k+1} = \epsilon_i(h - h^k) + \delta_i(\epsilon_i(h^k - h^{k-1}) + \delta_i(...\epsilon_i(h^2 - h^1) + \delta_i(\epsilon_i(h^1 - h^0))..)) \tag{3.29}$$

where

$$\delta_i = e^{-\omega_i \Delta t}$$

$$\epsilon_i = \frac{1 - e^{-\omega_i \Delta t}}{\omega_i \Delta t}$$

The assumption of a constant time step is not necessary. However, without this assumption δ_i and ϵ_i must be re-evaluated for each different time step. In order to use the Lanczos reduction method, it is assumed here that the storage coefficient

S is a constant for all the fractures. For the traditional solution methods, this assumption is not necessary.

After substituting (3.29) into (3.23), discretization of (3.23) by Galerkin finite element method leads to the following system of first-order differential equations

$$\mathbf{M}\dot{\mathbf{h}} + \mathbf{K}\mathbf{h} - \sigma\frac{\mathbf{M}}{S}\sum_{i=0}^{\infty}\epsilon_i\mathbf{h} - \sigma\frac{\mathbf{M}}{S}\sum_{i=0}^{\infty}[-\epsilon_i\mathbf{h}^k + \delta_i(\epsilon_i(\mathbf{h}^k - \mathbf{h}^{k-1}) + \delta_i(...\epsilon_i(\mathbf{h}^2 - \mathbf{h}^1) + \delta_i(\epsilon_i(\mathbf{h}^1 - \mathbf{h}^0))..))] = \mathbf{f} \tag{3.30}$$

where $\mathbf{h}$ is a vector of hydraulic heads at nodes of a finite element mesh, $\mathbf{K}$ and $\mathbf{M}$ are the conductivity matrix and capacity matrix respectively. Both of these matrices are symmetric and positive definite. The right hand side vector $\mathbf{f}$ includes the effects of source terms as well as boundary conditions. In the next section, system (3.30) is reduced in size by means of the Lanczos reduction method.

3.4.2 Application of the Lanczos reduction method

Background of the method The Lanczos method begins by constructing an orthogonal set of vectors, known as Lanczos vectors [Nour-Omid, 1987]. This method uses the transformation $\mathbf{h} = \mathbf{Q}\mathbf{w}$, where $\mathbf{Q}$ is a $\mathbf{M}$ orthogonal matrix (i.e., $\mathbf{Q}^t\mathbf{M}\mathbf{Q} = \mathbf{I}$, the identity matrix). $\mathbf{Q}$ consists of m Lanczos vectors each of dimension n, i.e. $\mathbf{Q}$ is a $n \times m$ matrix. The Lanczos reduction process may be started with a vector $\mathbf{r}_0$ which depends on the right-hand side of the discretized system of equations. Equation (3.30) is transformed by multiplying it by $\mathbf{M}\mathbf{K}^{-1}$ and substituting the transformation $\mathbf{h} = \mathbf{Q}\mathbf{w}$. The reduced equation is obtained by taking advantage of the orthogonality of the Lanczos vectors. $\mathbf{r}_0$ is chosen to be $\mathbf{K}^{-1}\mathbf{f}$. The vector $\mathbf{f}$ includes the influences of non-zero boundary conditions and the effects of sources/sinks of the problem at any time. Detailed discussion of the Lanczos reduction method can be found in the following references [Lanczos,

1950; Simon, 1984; Nour-Omid, 1989]. The algorithm for the method is detailed in Chapter 2.

The Lanczos method does not require an actual inversion of the stiffness matrix $\mathbf{K}$ [Dunbar *et al*, 1994], even though there are many references to $\mathbf{K}^{-1}$ in the Lanczos algorithm. The $\mathbf{K}^{-1}\mathbf{f}$ are actually computed by solving the system $\mathbf{Kx} = \mathbf{f}$. This is accomplished by performing one factorization of the $\mathbf{K}$ matrix followed by m back-solves for each Lanczos process.

Both the direct and iterative solution methods are used for different versions of the Lanczos reduction process. For the dual-porosity flow model, the direct solution method is adopted. In the direct solution version, a Cholesky decomposition and a series of back-solves are used to carry out the Lanczos reduction. This is, of course, a direct as opposed to an iterative scheme. In addition, for the dual-porosity flow model, time-marching by the Crank-Nicolson method and direct solvers are typically used for the solution of (3.30) as a basis for overall timing comparisons between traditional method and the LRM. It has been pointed out that perhaps iterative solvers such as conjugate gradients should be used instead of direct solvers for the Crank-Nicolson solution of (3.30).

It is recommended that iterative solvers be used to carry out the Lanczos reduction in place of direct solvers if the Lanczos method is applied to three-dimensional problems, or where an arbitrary sparsity structure is encountered. It should be noted that whatever method is used to compute the solutions to $\mathbf{Kx} = \mathbf{f}$, the overhead cost will be the same for both the direct integration of (3.30) and the Lanczos method. The total computational effort of a Lanczos process is approximately equal to solving equation $\mathbf{Kx} = \mathbf{f}$ for m time steps, no matter what solution method is used.

During the Lanczos decomposition, each Lanczos vector generated is subject

to loss of $\mathbf{M}$ orthogonality with respect to earlier vectors due to computer runoff error and cancelation. This means that $\mathbf{Q}^t\mathbf{M}\mathbf{Q} \neq \mathbf{I}$. Therefore, the orthogonality must be monitored. When loss of orthogonality has occurred, reorthogonalization must be implemented (Simon, 1984).

Another important issue for the Lanczos method is the criterion for terminating the recursion when a sufficient number of Lanczos vectors has been computed. In this work an approach described by Dunbar and Woodbury [1989] is adopted. Numerical experiments have shown that the number of Lanczos vectors needed is dependent on the inhomogeneity of aquifer hydraulic properties and element grid size. However, in a typical case for a problem of 5,000 nodes, less than 100 vectors are needed.

Following the Lanczos reduction method, the following reduced system of equations is created

$$\mathbf{T}\dot{\mathbf{w}} + \mathbf{w} - \sigma\frac{\mathbf{T}}{S}\sum_{i=0}^{\infty}\epsilon_i\mathbf{w} - \sigma\frac{\mathbf{T}}{S}\sum_{i=0}^{\infty}[-\epsilon_i\mathbf{w}^k + \delta_i(\epsilon_i(\mathbf{w}^k - \mathbf{w}^{k-1}) + \delta_i(...\epsilon_i(\mathbf{w}^2 - \mathbf{w}^1) + \delta_i(\epsilon_i(\mathbf{w}^1 - \mathbf{w}^0))..))] = \mathbf{g} \tag{3.31}$$

where $\mathbf{w}$ is the solution vector with a length of m in reduced space, $\mathbf{T} = \mathbf{Q}^t\mathbf{M}\mathbf{K}^{-1}\mathbf{M}\mathbf{Q}$, is a $m \times m$ tridiagonal matrix, and $\mathbf{Q}$ is a $n \times m$ matrix. Note that m is much less than total number of original equations, n. This is due to the fact that the recursion for determining the Lanczos vectors would be terminated after $m \ll n$ steps and these basis states capture the essence of the solution. $\mathbf{g} = \mathbf{Q}^t\mathbf{M}\mathbf{K}^{-1}\mathbf{f}$ is the right-hand side vector of the equation system and can be determined from equation (2.9).

The reduced system of equations can be solved by any time integration technique. Note the solution at each time level does not need to be transformed back to the original unknowns. Only the original solutions $\mathbf{h}$ at the desired time steps or locations are computed by the matrix-vector multiplication $\mathbf{h}$=$\mathbf{Q}\mathbf{w}$. The Lanczos

reduction method therefore yields a large saving in computer memory storage and solving the reduced system is much faster than time-marching the original equation system (3.30). For a medium-sized real field problem with several thousands to several ten thousands solving time steps, the solution data for all time steps can easily involve hundreds of megabytes to even several gigabytes. However, the total reduced solution data ($\mathbf{w}$) are much less than total original solution data ($\mathbf{h}$). Typically, the total reduced solution data may be only 1.0% or less of the total original solution data. The original solution for any desired time step or location can be retrieved from the reduced solution data in future with very little computational effort.

Initial and boundary conditions Proper implementation of initial and boundary conditions is a key to efficient use of the Lanczos reduction method. When the boundary conditions are complicated, the reduction method may lose its advantage by having to re-evaluate the vector $\mathbf{g}$. This subject is discussed in more detail below. If all the boundary conditions can be written in terms of one time varying function, the reduction method will be most efficient. This situation may include a single well system, or multi-well system with the same linearly dependent pumping rates. For different time-dependent boundary conditions, these can be divided into several groups and each group can be implemented separately.

Initial conditions must also be treated properly. They can be eliminated from the solution by writing $\mathbf{h}$ as the sum of the initial conditions $\mathbf{h}^0$, plus a transient part $\mathbf{v}(t)$:

$$\mathbf{h}(t) = \mathbf{h}^0 + \mathbf{v}(t), \qquad \mathbf{h}(0) = \mathbf{h}^0, \qquad \mathbf{v}(0) = 0 \tag{3.32}$$

Substituting the above equations into (3.30), one can obtain a differential

equation for the transient $\mathbf{v}$:

$$\mathbf{M}\dot{\mathbf{v}} + \mathbf{K}\mathbf{v} - \sigma\frac{\mathbf{M}}{S}\sum_{i=0}^{\infty}\epsilon_i\mathbf{v} - \sigma\frac{\mathbf{M}}{S}\sum_{i=0}^{\infty}[-\epsilon_i\mathbf{v}^k + \delta_i(\epsilon_i(\mathbf{v}^k - \mathbf{v}^{k-1}) + \delta_i(...\epsilon_i(\mathbf{v}^2 - \mathbf{v}^1) + \delta_i(\epsilon_i(\mathbf{v}^1 - \mathbf{v}^0))..))] = \mathbf{f} - \mathbf{K}\mathbf{h}^0 \tag{3.33}$$

Equation (3.33) has the same form of left hand side as the original equation (3.30) for $\mathbf{h}$. The only difference between (3.30) and (3.33) is that the new equation has a right hand side of $\mathbf{f} - \mathbf{K}\mathbf{h}^0$. This is because $\mathbf{M}\dot{\mathbf{h}}^0 = \mathbf{0}$, since $\mathbf{h}^0$ is not a function of time. In this way the initial vector $\mathbf{w}^0$ can be set equal to the zero vector, $\mathbf{0}$.

The right-hand vector $\mathbf{f}$ is time-dependent if the boundary conditions are time-dependent or wells have a non-constant pumping history. Therefore the right hand side vector of the reduced equation $\mathbf{g} = \mathbf{Q}^t\mathbf{M}\mathbf{K}^{-1}(\mathbf{f}-\mathbf{K}\mathbf{h}^0)$, is also time-dependent. Unfortunately, the vector $\mathbf{g}$ would have to be evaluated at each time step during the solution of the small tridiagonal system. This would be very time consuming and completely negates any benefits in efficiency afforded by the small system. The Lanczos decomposition is spatial in nature. Therefore, to retain the time-dependent effects which arise in the vector $\mathbf{g}$, the vector $\mathbf{f}$ must be decomposed into spatial and temporal components, i.e. $\mathbf{f} = \mathbf{b}\mu(t)$. Here $\mu(t)$ represents the temporal behavior of the boundary conditions or sink/sources. The vector $\mathbf{K}^{-1}\mathbf{b}$ then becomes the starting vector which is transformed to the constant part of vector $\mathbf{g}$.

For multiple time-history boundary conditions, Dunbar and Woodbury [1989] proposed a scheme that groups the boundary conditions and wells into N parts with each part having the same individual time history pattern:

$$\mathbf{f} = \sum_{j=1}^{N}\mathbf{b}_j\mu_j(t) + \mathbf{f}_0 - \mathbf{K}\mathbf{h}^0 \tag{3.34}$$

Its corresponding reduced right hand side vector has form

$$\mathbf{g} = \sum_{j=1}^{N} \mathbf{g}_j \mu_j(t) + \mathbf{g}_0 \tag{3.35}$$

At each time step, $\mathbf{g}$ is updated individually for every group boundary conditions. Investigation in this research indicates that this scheme is appropriate for one dimensional problems; however, it may not converge (or converge slowly) for multi-dimensional problems. A new scheme is developed below for the multiple-group time-history boundary condition problems based on the principle of superposition. Similar ideas have been proposed by Li [1998].

According to Dunbar's scheme, one can start by writing right hand side of (3.33) in the form of (3.34). Due to homogeneous initial conditions (the influence of initial conditions has been eliminated from the left hand side of the equation), equation (3.33) can be split into several systems of equations equivalent to,

$$\mathbf{M}\dot{\mathbf{v}}_0 + \mathbf{K}\mathbf{v}_0 - \sigma\frac{\mathbf{M}}{S}\mathbf{v}_0 - \sigma\frac{\mathbf{M}}{S}\mathbf{u}_0 = \mathbf{f}_0 + \mathbf{K}\mathbf{h}^0 \tag{3.36}$$

$$\mathbf{M}\dot{\mathbf{v}}_i + \mathbf{K}\mathbf{v}_i - \sigma\frac{\mathbf{M}}{S}\mathbf{v}_i - \sigma\frac{\mathbf{M}}{S}\mathbf{u}_i = \mu_i(t)\mathbf{b}_i \qquad i = 1, ..., N \tag{3.37}$$

where $\mathbf{u}_i$ is compact notation for the known part of the leakage terms, N is the time history group number, and $\mathbf{v} = \sum_{i=0}^{N} \mathbf{v}_i$. The right hand side of equation (3.36) is not a time dependent function. It denotes the influence of the steady state boundary conditions and the initial conditions.

The modified reduction method generates Lanczos vectors by using their corresponding starting vectors $\mathbf{K}^{-1}(\mathbf{f}_0 - \mathbf{K}\mathbf{h}^0)$ and $\mathbf{K}^{-1}\mathbf{b}_i$ for each equation system. $\mathbf{Q}_i$ and $\mathbf{T}_i$ are produced for all the equation systems. After the Lanczos reduction process, equations (3.36) and (3.37) will be reduced to:

$$\mathbf{T}_0\dot{\mathbf{w}}_0 + \mathbf{w}_0 - \sigma\frac{\mathbf{T}_0}{S}\mathbf{w}_0 - \sigma\frac{\mathbf{T}_0}{S}\mathbf{y}_0 = \mathbf{g}_0 \tag{3.38}$$

$$\mathbf{T}_i\dot{\mathbf{w}}_i + \mathbf{w}_i - \sigma\frac{\mathbf{T}_i}{S}\mathbf{w}_i - \sigma\frac{\mathbf{T}_i}{S}\mathbf{y}_i = \mu_i(t)\mathbf{g}_i \qquad i = 1, ..., N \tag{3.39}$$

where $\mathbf{y}_i$ denotes a reduced vector of known part of the leakage terms in compact notation, and $\mathbf{v}_i = \mathbf{Q}_i\mathbf{w}_i$.

In this approach, N Lanczos processes are needed, but only one decomposition of matrix $\mathbf{K}$ needs to be computed. For a limited number of boundary condition time histories, this approach is expected to be very efficient. In most cases boundary conditions can be grouped into similar time history patterns. Therefore the Lanczos method is still efficient. The computation effort for each Lanczos process is about the same as solving the original equation system for m time steps. When more Lanczos processes are required or when $(N+1) \times m > tn$ (tn is the total required solution time steps), the Lanczos method would not be efficient.

Choice of Starting Vector The convergence of the Lanczos method is sensitive to the starting vector which is used to compute the first Lanczos vector. The best starting vector for the method is the steady state solution [Dunbar and Woodbury 1989]. From equation (3.30), Note that the leakage terms of the dual-porosity flow problem are zero at steady state. The starting vector for each Lanczos process can simply be chosen as $\mathbf{K}^{-1}\mathbf{b}$, a vector parallel to its steady solution. Using the boundary condition data at the moment when all the data are non-zero determines the vector $\mathbf{b}$. Before the reduction procedure, the Dirichlet boundary conditions need to be partitioned from the original equation system.

Computer implementation The Lanczos method for solving the dual-porosity flow problem is set up in the following stages:

1. The coefficients δ_i and ϵ_i for updating of the leakage terms are computed.

2. The matrices $\mathbf{K}$, $\mathbf{M}$ are formed. The initial and boundary conditions are applied to the discretized equation system to form the right-hand side vector $\mathbf{f}$.

3. The matrix $\mathbf{K}$ is factored by the Cholesky decomposition method.

4. The Lanczos decomposition is performed. The Lanczos vectors $\mathbf{Q}$, right hand side $\mathbf{g}$, and matrix $\mathbf{H}$ are formed. $\mathbf{Q}$ is then stored on a disk file for future references.

5. The small $m \times m$ system of first order differential equations is decomposed using a standard tridiagonal solver.

6. The leakage terms are evaluated and a back solve is performed at each time step.

7. If there are more than one boundary condition time history patterns, repeat step 4 to 6 for the next group boundary conditions.

8. A matrix-vector multiplication computes the solution to the original problem for all the desired time or a dot product of two m entry vectors to obtain the original solution for any location. Computation for the original solutions can be performed during solving of the reduced system or any time after solving of the system.

9. If there are more than one group time-dependent boundary conditions, add the solutions of different groups together.

Updating the leakage terms of the reduced equation system is needed at each time step, and they are related to the solution history. By using the following

equation, it is possible to avoid the storage of all the hydraulic head time history data.

At time $k \times \Delta t$, the leakage terms can be written as

$$\mathbf{I}^k = \sigma \frac{\mathbf{T}}{S} \sum_{i=0}^{\infty} \mathbf{I}_i^k \tag{3.40}$$

Then, the correction term at time $(k+1) \times \Delta t$ can be written as:

$$\mathbf{I}^{k+1} = \sigma \frac{\mathbf{T}}{S} \sum_{i=0}^{\infty} \varpi_i (\mathbf{I}_i^k + \epsilon_i \mathbf{w}^k) - \sigma \frac{\mathbf{T}}{S} \sum_{i=0}^{\infty} \epsilon_i \mathbf{w}^k \tag{3.41}$$

Evaluation of the leakage terms of $\mathbf{I}_i$ involves an infinite exponential series summation. Therefore, updating the right hand side requires the storage of three extra arrays for $\mathbf{I}_i$, δ_i and ϵ_i with a length of the number of truncated terms for the infinite exponential series. Huyakorn *et al.* [1983] showed that the rate of convergence of the series depends directly on the dimensionless parameter $t^* = K't/(S_s' a^2)$. It is sufficiently accurate to determine a' such that $t^* = 0.5$ and $a \geq a'$, where a' is an effective thickness. They indicated that the computational efficiency can be greatly improved by replacing the actual semi-thickness of the matrix block, a, with the effective thickness, a'. Only within this effective thickness is the hydraulic head h' in the matrix block affected by the change of head at the block-fracture interface. Using a' instead of a, very small truncation errors are introduced by retaining only the first several terms of the series. My experience indicates that with less than 20 truncated terms a very high accuracy can be achieved. Updating the leakage terms in reduced space is based on the reduced leakage terms and solutions of the last time step. If 20 truncated terms are used, at each time step only about $(22+m) \times m$ multiplications are required to update the leakage terms. It is very economic compared to the computation for the original equation system which needs $(22+n) \times n$ multiplications by using the equation (3.41) to update the leakage terms. This recursive scheme is also more efficient compared to the iterative scheme proposed by Huyakorn *et al.* [1983].

3.4.3 Discrete fracture approach

The most advanced approach for simulating groundwater flow in fractured porous media is the discrete fracture approach. However, this approach is limited by the large computational overheads associated with traditional modeling methods. One primary reason is because of the vastly different flow velocities between the fractures and the matrix blocks, which results in sharp groundwater head gradients near the fracture-matrix interface. In addition, for most field problems, the formations contain complex randomly-distributed networks of discrete fractures. In order to simulate the sharp hydraulic head gradients at the interface between fractures and the matrix, a fine time and spatial discretization is needed. The discretization can easily involve many tens to hundreds of thousands of unknowns and time steps. In this work, the Lanczos reduction method is extended to the modeling of groundwater flow using the discrete fracture approach.

The numerical solutions of the governing equations (3.5) and (3.7) for transient groundwater flow in fractured porous media using the discrete fracture approach are also obtained by applying the standard Galerkin finite element method for spatial discretization, and then reducing the finite element system by the Lanczos algorithm. The discretization method is discussed as follows.

The trial solutions for h and h' are defined according to

$$h'(x_i,t) \approx \hat{h}'(x_i,t) = \sum_I N_I(x_i) h'_I(t) \tag{3.42}$$

$$h(x_j,t) \approx \hat{h}(x_j,t) = \sum_J \Omega_J(x_j) h_J(t) \tag{3.43}$$

where x_i (i=1,2,3) and x_j (j=1,2) are the spatial coordinates, I and J are nodal indices ranging from 1 to n' and n, n' and n are the total number of nodes in porous matrix and fracture respectively, and N_I and Ω_J are linear interpolation functions.

It is now required that the residual generated, when trial solutions are substituted into (3.5) and (3.7), is minimized in the following sense:

$$\int_V [\frac{\partial}{\partial x_i}(K'_{ij}\frac{\partial h'}{\partial x_j}) - S'_s\frac{\partial h'}{\partial t} - q']N_I dV = 0 \tag{3.44}$$

i,j=1,2,3; I=1,2, , n'

$$\int_A [2b\frac{\partial}{\partial x_i}(K_{ij}\frac{\partial h}{\partial x_j}) - 2bS_s\frac{\partial h}{\partial t} - q_n\mid_{I^-} + q_n\mid_{I^+}]\Omega_J dA = 0 \tag{3.45}$$

i,j=1,2; J=1,2,...,n

where V denotes the porous matrix 3D domain and A denotes the fracture 2D domain.

Application of Green's theorem and introducing of (3.42) and (3.43) into (3.44) and (3.45) reduces the order of the second derivative terms and then forces the resulting residual orthogonal to all the weighting functions. In the Galerkin method, the weighting functions are chosen to be identical to the interpolation functions. By subdividing the integrals over the porous matrix domain V into piecewise elemental contributions of volume V^e and the fracture domain A into fracture elements of area A^e, a system of algebraic equations is obtained.

Because we have the condition that $h' = h$ for nodes common to a fracture areal element and volumetric porous matrix element, and because common nodes receive numerical contributions from both types of elements, the two discretized equations for the porous matrix and fracture can be superimposed. The discrete equations obtained by the method discussed above are independent of the choice of element type. The block elements and fracture elements are generated such that they correspond to each other. The nodes comprising the fracture elements are therefore all common to nodes comprising the porous matrix elements. The commonality of these nodes thus ensures the continuity of hydraulic head at the fracture matrix interface. Also, by superimposing the contributions at each node

from both element types, the exchange flux terms q_n cancel internally and need not be calculated explicitly. The final system of the algebraic equations for the superimposed fracture and matrix element system has the following form:

$$\sum_{J=1}^{n'} \dot{h}_J [\sum_e \int_{V^e} S'_s N_I N_J dV + \sum_{ef} (2b) \int_{A^e} S_s \Omega_I \Omega_J dA] +$$
$$\sum_{J=1}^{n'} h_J [\sum_e \int_{V^e} K'_{i'j'} \frac{\partial N_I}{\partial x_{i'}} \frac{\partial N_J}{\partial x_{j'}} dV + \sum_{ef} (2b) \int_{A^e} K_{ij} \frac{\partial \Omega_I}{\partial x_i} \frac{\partial \Omega_J}{\partial x_j} dA] = \tag{3.46}$$
$$\sum_{J=1}^{n'} [\sum_e \int_{V^e} q' N_I N_J dV + \sum_e \int_s \frac{\partial h'}{\partial \mathrm{n}} K'_{\mathrm{n}} N_I ds + (2b) \sum_{ef} \int_l \frac{\partial h}{\partial \mathrm{n}} K_{\mathrm{n}} \Omega_I dl]$$

I=1, 2, ... , n'; i', j'=1, 2, 3; i, j=1, 2

where $\sum_e$ and $\sum_{ef}$ refer to the summation over volumetric matrix and areal fracture elements, respectively, that are connected to node J, s and l represent the areal and linear boundaries of the three-dimensional and the two-dimensional elements, and n denotes the direction normal to the boundary. The last two terms on the right hand side of equation (3.46) represent flux contributions due to any imposed natural boundary conditions.

Equation (3.46) can be easily written using a matrix notation as

$$\mathbf{M}\dot{\mathbf{h}} + \mathbf{K}\mathbf{h} = \mathbf{f} \tag{3.47}$$

The notation here is the same as in (3.30). Equation (3.47) can conveniently be reduced by the Lanczos algorithm to a small system. An iterative version of the LRM is implemented for the discrete fracture approach. The PCG solver is used in the Lanczos reduction process. A similar scheme as the one discussed in last section to solve (3.47) can be used.

The efficiency of the LRM will be determined by the number of Lanczos vectors (m) used and the efficiency of solving equation $\mathbf{K}\mathbf{x} = \mathbf{b}$. In the LRM, the $\mathbf{K}$ matrix can be manipulated to facilitate the PCG solution through a "shift" technique. A

similar technique has been introduced by Farrell [1998] for the Arnoldi reduction method. Equation (3.47) can be rewritten as:

$$\mathbf{M}\dot{\mathbf{h}} + (\mathbf{K} + \varrho\mathbf{M})\mathbf{h} - \varrho\mathbf{M}\mathbf{h} = \mathbf{f} \tag{3.48}$$

$\mathbf{K}$ is replaced with $\mathbf{K}+\varrho\mathbf{M}$ in the reduction process. If an appropriate value of ϱ is selected, the iterative solution convergence rate will be enhanced dramatically. This is because for optimal convergence rates, the matrix to be solved by the PCG method should be diagonally dominant, like the mass matrix $\mathbf{M}$ (Meijerink and van der Vorst, 1977). That is, in a row, the diagonal is positive, and sum of the off-diagonals is less than or equal to the diagonal, with strict inequality for at least one row in the matrix. Experience indicates that ϱ should have a value that makes $\mathbf{K}$ and $\varrho\mathbf{M}$ similar in absolute value. If $\varrho \geq 2/\Delta t$ (Δt is the time-marching step size), the convergence rate in the reduction process should not be worse than the classic iterative solution method for the original equation system. This is because the matrix $\mathbf{K}+2/\Delta t\mathbf{M}$ parallels to the left-hand side matrix of the original equation system after the temporal approximation by the Crank-Nicolson scheme.

Following the LRM, a reduced system of equations is created

$$\mathbf{T}\dot{\mathbf{w}} + \mathbf{w} - \varrho\mathbf{T}\mathbf{w} = \mathbf{f} \tag{3.49}$$

The above reduced equation system can be easily solved using the same scheme as discussed for the dual-porosity flow model.

3.5 Transport modeling techniques for the dual-porosity approach

3.5.1 Solution of diffusion equations in matrix blocks

In order to determine the mass exchange between the fracture and matrix block, the diffusion equation in the porous matrix blocks must be solved first. Figure 3-3 shows the discretization of porous matrix block for the two type conceptual models. Discretization of the mass diffusion transport equation can be performed by applying the traditional Galerkin finite element technique.

First we focus our attention on the equations for the prismatic matrix block. By applying the Galerkin technique to equation (3.17), one will get the one dimensional finite-element equations for the matrix block in matrix notation:

$$\phi' R'_p \mathbf{M}\dot{\mathbf{c}}'_p + \mathbf{K}\mathbf{c}'_p + \phi'\lambda_p R'_p \mathbf{M}\mathbf{c}'_p - \sum_{m'=1}^{M} \zeta_{pm'}\phi' R'_{m'}\lambda_{m'}\mathbf{M}\mathbf{c}'_{m'} = \mathbf{f}_p \tag{3.50}$$

p=1, 2, ..., P

Using standard linear basis functions and the boundary conditions, the $n' \times n'$ conductivity matrix $\mathbf{K}$, $n' \times n'$ capacity matrix $\mathbf{M}$ and right hand vector $\mathbf{f}_p$ can be determined. The node number n' of the discretized matrix block is small. In most cases, it is in the range of several tens of nodes.

Using the temporal approximation by the way of finite differences, such as the Crank-Nicolson method, the following tridiagonal set of equations can be obtained for the porous matrix block associated with an arbitrary node J in the fracture domain. Let us consider the pth species for now:

$$\begin{aligned}
&\beta_1 C'^{k+1}_{p,1} + \gamma_1 C'^{k+1}_{p,2} = d_1 \\
&\alpha_i C'^{k+1}_{p,i-1} + \beta_i C'^{k+1}_{p,i} + \gamma_i C'^{k+1}_{p,i+1} = d_i \qquad i = 2, 3, ..., n'-1 \\
&C'^{k+1}_{p,n'} = C^{k+1}_{p,J}
\end{aligned} \tag{3.51}$$

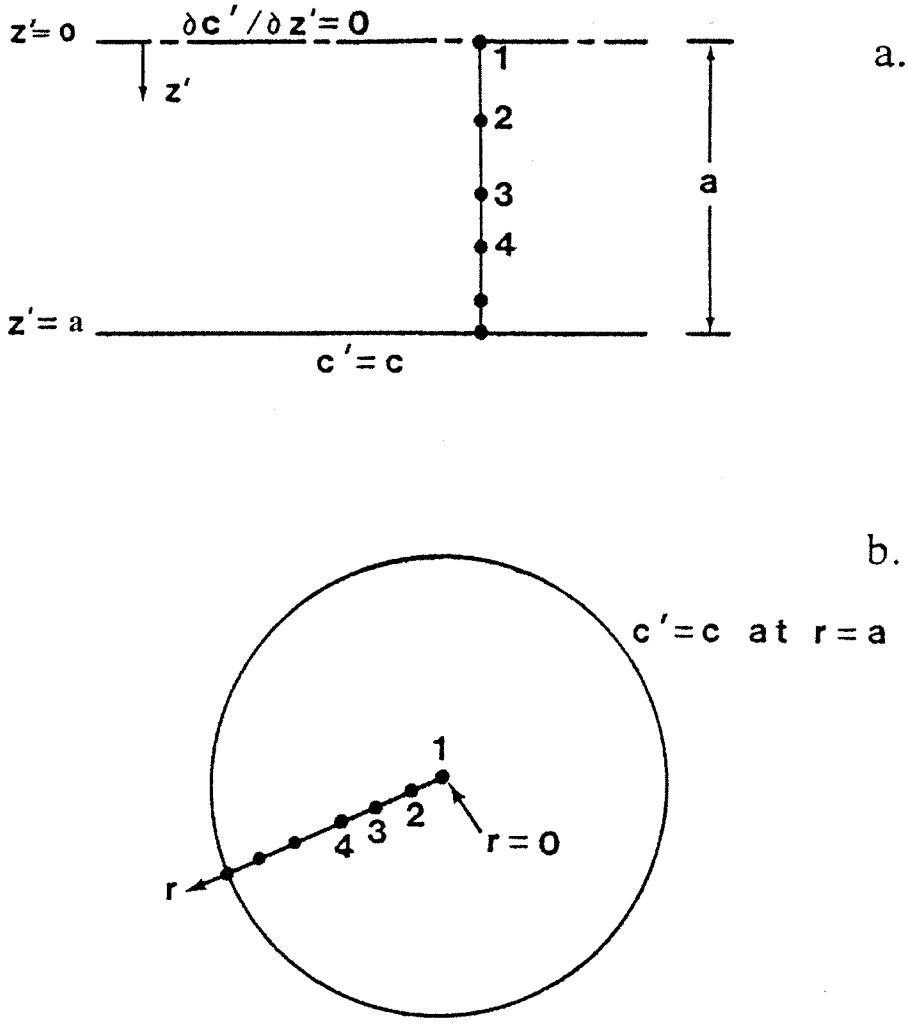

Figure 3-3 Discretization of porous matrix blocks: (a) prismatic block, and (b) spherical block (after Huyakorn *et al*, 1983)

where $C_{p,J}^{k+1}$ is the concentration of component p at node J in the fracture domain, the superscript k+1 denotes the current time level. The coefficients α_i, β_i and γ_i in the left hand side of the equation can be easily determined from equation (3.50). The right hand side vector of equation system (3.51) is given by:

$$\begin{aligned}\mathbf{d}_i = \quad & (\frac{\phi' R'_p \mathbf{M}}{\Delta t} - \frac{\mathbf{K} + \phi' \lambda_p R'_p \mathbf{M}}{2}) \mathbf{c}_p^{'k} \\ & + \sum_{m'=1}^{M} \frac{\zeta_{pm'} \phi' \lambda_{m'} R'_{m'} \mathbf{M}}{2} (\mathbf{c}_{m'}^{'k+1} + \mathbf{c}_{m'}^{'k}) \end{aligned} \tag{3.52}$$

where Δt is the finite difference time step size. In order to simplify the equations, Δt has been assumed to be a constant for all the time steps. Moreover, each block is assumed homogeneous.

The general solution of above equation system can be expressed in the form

$$\begin{bmatrix} C_{p,1}^{'k+1} \\ C_{p,2}^{'k+1} \\ \cdots \\ C_{p,n'-2}^{'k+1} \\ C_{p,n'-1}^{'k+1} \end{bmatrix} = \mathbf{A} \begin{bmatrix} d_1 \\ d_2 \\ \cdots \\ d_{n'-2} \\ d_{n'-1} \end{bmatrix} + \mathbf{A} \begin{bmatrix} 0 \\ 0 \\ \cdots \\ 0 \\ -\gamma_{n'-1} C_{p,J}^{k+1} \end{bmatrix} \tag{3.53}$$

where $\mathbf{A}$ is defined as

$$\begin{aligned} \mathbf{A} &= \begin{bmatrix} \beta_1 & \gamma_1 & 0 & \cdots & 0 & 0 \\ \alpha_2 & \beta_2 & \gamma_2 & \cdots & 0 & 0 \\ \cdots & \alpha_i & \beta_i & \gamma_i & \cdots & \cdots \\ 0 & \cdots & \alpha_{n'-2} & \beta_{n'-2} & \gamma_{n'-2} & 0 \\ 0 & 0 & 0 & \cdots & \alpha_{n'-1} & \beta_{n'-1} \end{bmatrix}^{-1} \\ &= \begin{bmatrix} a_{11} & a_{12} & \cdots & a_{1n'-2} & a_{1n'-1} \\ a_{21} & a_{22} & \cdots & \cdots & a_{2n'-1} \\ \cdots & \cdots & \cdots & \cdots & \cdots \\ a_{n'-21} & a_{n'-22} & \cdots & a_{n'-2n'-2} & a_{n'-2n'-1} \\ a_{n'-11} & a_{n'-12} & \cdots & \cdots & a_{n'-1n'-1} \end{bmatrix} \end{aligned} \tag{3.54}$$

From equation (3.53), it is easy to show that the concentration solutions for any species in the matrix block consists of two parts. The first part (part I) is

caused by the concentration history of that species and its parent species, and the second part (part II) is caused by the corresponding node current concentration in the fracture (i.e. caused by the term $\gamma_{n'-1}C_{p,J}^{k+1}$).

The general solution of any species for any node in the matrix block can be written as

$$C_{p,i}^{\prime k+1} = \bar{C}_{p,i}^{\prime k} + \varpi_i C_{p,J}^{k+1} \tag{3.55}$$

$i = 1, 2, ...n' - 1$, $p = 1, 2, ..., P$

where $\bar{C}_{p,i}^{\prime k}$ is the solution to part I, and ϖ_i is a constant solution coefficient for computing the solution to part II, which can be calculated by

$$\begin{bmatrix} \varpi_1 \\ \cdots \\ \varpi_i \\ \cdots \\ \varpi_{n'-1} \end{bmatrix} = -\gamma_{n'-1} \begin{bmatrix} a_{1n'-1} \\ \cdots \\ a_{in'-1} \\ \cdots \\ a_{n'-1n'-1} \end{bmatrix} \tag{3.56}$$

where the right-hand side vector of the above equation is the last column (column $n'-1$) of matrix $\mathbf{A}$. It can be obtained by solving the equation system (3.51) with a right hand side of (0,0,...,0,1). It is interesting to note that the solution coefficients may be very small for the nodes far from the fractures and the influences of fracture concentration on these nodes can be neglected.

The solution to part I is obtained by setting $\gamma_{n'-1} = 0$ in equation (3.51) and solving the equation directly. The solution to part II is computed simply by multiplying ϖ_i with $C_{p,J}^{k+1}$.

Substituting equation (3.55) into (3.13), the mass exchange term Γ_p at time step k+1 can be calculated

$$\Gamma_p^{k+1} = -\frac{D'}{a\Delta z}(C_{p,J}^{k+1} - \varpi_{n'-1}C_{p,J}^{k+1} - \bar{C}_{p,n'-1}^{\prime k}) \tag{3.57}$$

After the solution to part I is obtained, substituting Γ_p of different species into its corresponding transport equation for the fractures, the concentrations of that

species in the fractures can be solved without requiring the solution of current concentration in the matrix block. After the contaminant concentrations in the fractures are determined, the solution to part II for the matrix block at current time step can be updated. The summation of the solutions to part I and part II forms the final concentration solution for the matrix blocks.

The spherical block model has the same discretized system of equations as the parallel fracture model. Its tridiagonal equation system and the exchange terms can be obtained in a manner similar to that described above. The only differences are the coefficients of the equations. The two matrices $\mathbf{M}$ and $\mathbf{K}$ for the spherical block model [in equation (3.50)] are determined by

$$\mathbf{K} = \sum_{n'-1} [\mathbf{K}]^e; \qquad \mathbf{M} = \sum_{n'-1} [\mathbf{M}]^e \tag{3.58}$$

where n' is the total nodes in the block domain. The element matrices are given as follows:

$$[\mathbf{K}]^e = \frac{D'}{3\Delta r_i^2}(r_i^3 - r_{i-1}^3) \begin{bmatrix} 1 & -1 \\ -1 & 1 \end{bmatrix} \tag{3.59}$$

$$[\mathbf{M}]^e = \frac{1}{60\Delta r_i^2} \begin{bmatrix} M_{11} & M_{12} \\ M_{21} & M_{22} \end{bmatrix} \tag{3.60}$$

where,

$$M_{11} = 2r_i^5 - 20r_{i-1}^3 r_i^2 + 30r_{i-1}^4 r_i - 12r_{i-1}^5$$

$$M_{12} = M_{21} = 3r_i^5 - 5r_{i-1}r_i^4 + 5r_{i-1}^4 r_i - 3r_{i-1}^5$$

$$M_{22} = 12r_i^5 - 30r_{i-1}r_i^4 + 20r_{i-1}^2 r_i^3 - 2r_{i-1}^5$$

$i = 1, ..., n' - 1$

In above two equations, Δr_i is the grid size of a spherical element associated with node i and r_i is the local coordinate of the node.

3.5.2 Reduction of the transport equations in fractures using the Arnoldi algorithm

In order to fully illustrate the method only a simple case of multi-species decay chain transport is considered. It is supposed that any species in the decay chain has only one direct parent component and 100% of the parent component will decay to a daughter component. This means that $\zeta = 1$, except the first species in the decay chain is without a parent component. However, the procedure for solving the equations presented can easily be generalized.

By applying the Galerkin finite element method [Huyakorn and Pinder, 1983] to the equation (3.10) and considering the case of only one direct parent species, the following set of linear equations are produced

$$R_p \mathbf{M}\dot{\mathbf{c}}_p + \mathbf{K}\mathbf{c}_p + \lambda_p R_p \mathbf{M}\mathbf{c}_p - \lambda_{p-1} R_{p-1} \mathbf{M}\mathbf{c}_{p-1} - \frac{1-\phi}{\phi}\mathbf{M}\mathbf{u}_p = \mathbf{f}_p \qquad (3.61)$$

$p = 1, 2, ..., P$

where $\mathbf{c}_p$ is the vector of species p's concentration with n unknowns at the nodes of the mesh, $\mathbf{c}_{p-1}$ is the vector of parent species's concentration which is known, $\dot{\mathbf{c}}_p$ is the vector of concentration derivative with respect to time t, $\mathbf{u}_p$ is the vector of mass exchange rate between fracture and matrix block, $\mathbf{f}_p$ is a time-dependent force vector containing the effects of the initial and boundary conditions in the fractures, $\mathbf{M}$ is a positive-definite and symmetric capacity matrix, and $\mathbf{K}$ is a unsymmetrical conductivity matrix which depends on D_{ij} and velocity v. Both $\mathbf{K}$ and $\mathbf{M}$ have a size of $n \times n$.

For the first species ($p = 1$), which has no parent species, the term related to $\mathbf{c}_{p-1}$ does not exist in equation (3.61). The elements of $\mathbf{u}_p$ can be determined by equation (3.57). It is a function of time and location; however it can be divided into two independent parts. One part relates to C_p and the other part relates to the concentration history of the species and its parent species, and also relates to

present concentration of the parent species. The second part can be predetermined before the solution of the equations.

By using the Arnoldi algorithm [Arnoldi, 1951; Woodbury *et al.*, 1990; Nour-Omid *et al.*, 1991], the size of these equations can be reduced to a series of small ordinary differential equations of the form

$$R_p\mathbf{H}\dot{\mathbf{w}}_p + \mathbf{w}_p + \lambda_p R_p\mathbf{H}\mathbf{w}_p - \lambda_{p-1}R_{p-1}\mathbf{H}\mathbf{w}_{p-1} - \frac{1-\phi}{\phi}\mathbf{H}\mathbf{y}_p = \mathbf{g}_p \tag{3.62}$$

where $\mathbf{H}$ is a $m \times m$ upper Hessenberg matrix, m is much smaller than n, and $\mathbf{w}_p$, $\mathbf{w}_{p-1}$, $\mathbf{g}_p$ and $\mathbf{y}_p$ are reduced vectors of $\mathbf{c}_p$, $\mathbf{c}_{p-1}$, $\mathbf{f}_p$ and $\mathbf{u}_p$ respectively.

The Arnoldi reduction method uses orthogonal matrix transformations to reduce the equation (3.61) to a much smaller upper Hessenberg system of first-order differential equation by approximating the solution of $\mathbf{c}_p$ with $\mathbf{Q}\mathbf{w}_p$. $\mathbf{Q}$, a $n \times m$ matrix, consists of the first mth Arnoldi vectors which is created during the Arnoldi process. The details of determination of the matrix $\mathbf{Q}$ and $\mathbf{H}$ and the reduction procedures can be found in Chapter 2.

From equation (3.57), the reduced mass exchange vector $\mathbf{y}_p$ can be determined. It is in the following form

$$\mathbf{y}_p = -\frac{D'}{a\Delta z}[(1-\varpi_{n'-1})\mathbf{w}_p - \bar{\mathbf{w}}'_{p,n'-1}] \tag{3.63}$$

where $\bar{\mathbf{w}}'_{p,n'-1}$ corresponds to $\bar{\mathbf{c}}'_{p,n'-1}$ in reduced space.

Equation (3.62) was obtained based on the assumption of homogeneous matrix blocks throughout the domain, namely, D', R'_p and ϕ' are constants in the whole domain. This assumption makes the system reduction relatively easy. For the traditional iterative or direct solving schemes, the assumption is not necessary. In order to make the problem simple, the reduced initial condition vectors are all supposed to be zero, i.e,

$$\bar{\mathbf{w}}'^{0}_{p,i} = 0$$

$i = 1, ..., n' - 1$

Equation (3.62) can be solved by a suitable time integration algorithm such as Crank-Nicolson scheme. As the **H** is an upper Hessenberg matrix, it can be easily decomposed into the product of an upper triangular matrix and a lower bidiagonal matrix. Note that the Arnoldi method shows a great advantage here in that only one process is required to reduce multiple equation systems simultaneously. Also, the solution to the reduced system (3.62) using the Crank-Nicolson time-stepping scheme is economic because the reduced system size is much smaller than the original system. This also yields a large saving in storage required by the reduction method. Therefore, solving of the reduced system is more efficient than direct solving of the original equation system. Woodbury *et al.* [1990] indicated that the penalty with the time-stepping procedure is not significant if $m \ll n$.

In **w** space, equation (3.50) is still valid and the coefficients are still the same. However, now the equations are corresponding to the reduced nodes. Therefore the solutions for the matrix can be directly substituted into equation (3.63). This is because the current species concentration in the matrix block can be written as a function of the species and its parent species concentration and concentration history in the fracture. After reduction, the function is still the same. This property affords additional efficiency in computing time and memory storage for the Arnoldi reduction method. At each time step, the mass exchange terms are computed in the reduced space and only require solving m 1-D diffusion equations. For the original equation system, in order to determine mass exchange terms n 1-D diffusion equations need to be solved.

It is important to mention that the solution of $C'_{p,i}$, the concentration at ith node in the matrix, can be directly computed from the reduced space solutions

for the ith node by:

$$\mathbf{c}'_{p,i} = \mathbf{Q}\mathbf{w}'_{p,i} \tag{3.64}$$

$i = 1, 2, ..., n' - 1$

Note, it is not necessary to compute concentrations for all the nodes. For a matrix block corresponding to a specific fracture node J, various node concentrations can be obtained by the dot product of Jth row of matrix $\mathbf{Q}$ and vector $\mathbf{w}'_{p,i}$.

3.5.3 Choice of common starting vector

The choice of the starting vector is a very important factor influencing the convergence and accuracy of the Arnoldi reduction method. For the multi-species transport problem, a common starting vector must be chosen for all the equation systems to minimize the residual errors. Li *et al.* [1999] showed that any vector parallel to the vectors $\mathbf{f}_p$ $(p = 1, 2, ..., P)$ is a suitable starting vector for the Arnoldi process in reducing the equation system (3.62). It is also required that all the right-hand side vectors $\mathbf{f}_p$ must be parallel to each other. However, in most cases these vectors are not parallel to each other. It is shown here that these vectors can be partitioned into two parts, each of which is parallel to each other. Two approaches for choosing the common starting vector for most common transient and constant type Dirichlet boundary conditions are presented below.

A simple case is discussed here where a 2nd-type boundary condition is zero and there are no other source/sinks. The concentration vector $\mathbf{c}_p$ in equation (3.61) is for all the nodes in the domain, including the first-type boundary nodes. The submatrices of $\mathbf{M}$ and $\mathbf{K}$ without the influence of first type boundary nodes can be obtained by partitioning-out the rows and columns from $\mathbf{M}$ and $\mathbf{K}$ corresponding to the first type boundary nodes. After partitioning, all the entries of

$\mathbf{f}_p$ are zero except contributions from first type boundary nodes

Let Φ be the set of index values of all nodes, and $\Psi_1 \subset \Phi$ be the subset of index values of all first type nodes, $\Omega \subset \Phi$ be the subset of index values of all nodes which are not first type boundary nodes but are in an element which has one or more first type boundary nodes, and $\Upsilon \subset \Phi$ be the subset of all other nodes.

After partitioning, the ith entries of the $\mathbf{f}_p$ can be written as

$$f_{pi} = -\sum_{j \in \Psi_{1i}} [R_p M_{ij} \dot{C}_{pj} + K_{ij} C_{pj} + \lambda_p R_p M_{ij} C_{pj} - \lambda_{p-1} R_{p-1} M_{ij} C_{p-1j} - \frac{1-\phi}{\phi} M_{ij} \Gamma_{pj}] \tag{3.65}$$

where Ψ_{1i} denotes the subset of index values of first type boundary nodes which are in the same element as node i.

It follows that $f_{pi} = 0$, when $i \in \Upsilon$ because the subset Ψ_{1i} is empty. When $i \in \Omega$, f_p has:

$$f_{pi} = -\sum_{j \in \Psi_{1i}} [K_{ij} C_{pj} + M_{ij} F(C_{pj})] \tag{3.66}$$

where $F(C_{pj})$ is a function of C_{pj} and can be written as

$$F(C_{pj}) = R_p \dot{C}_{pj} + \lambda_p R_p C_{pj} - \lambda_{p-1} R_{p-1} C_{p-1j} - \frac{1-\phi}{\phi} \Gamma_{pj} \tag{3.67}$$

Two schemes are used to find the common starting vector for different species. The first scheme assumes that the two vectors formed by $\sum_{j \in \Psi_{1i}} K_{ij}$ and $\sum_{j \in \Psi_{1i}} M_{ij}$ for all nodes are parallel to each other, so it can be writen

$$\sum_{j \in \Psi_{1i}} M_{ij} = \eta \sum_{j \in \Psi_{1i}} K_{ij}. \tag{3.68}$$

where η is a constant.

This assumption is valid provided that all the first type boundary nodes have similar connections, the discretized element grids have same size and the hydraulic

properties are homogeneous in the first type boundary area. The first two conditions can be implemented during the discretization of the modeling domain. The last condition is true for most situations due to the fact that typical sites have relative small source areas.

In this way, a vector $\mathbf{b}$ for all the species can be determined. Its elements are computed by following equation:

$$b_i = \begin{cases} 0 & i \in \Upsilon \\ -\sum_{j \in \Psi_{1i}} K_{ij} & i \in \Omega \end{cases} \tag{3.69}$$

$i = 1, 2, ..., n$

All the right hand side vectors $\mathbf{f}_p$ $(p = 1, 2, ..., P)$ in equation (3.61), which are only affected by first type boundary conditions, are parallel to the vector $\mathbf{b}$. They can be determined and are of the form:

$$\mathbf{f}_p = (\tilde{C}_p + \eta F(\tilde{C}_p))\mathbf{b} \tag{3.70}$$

The values of $F(\tilde{C}_p)$ and $\tilde{C}_p$ at any moment can be determined easily based on the given first type boundary conditions for steady state boundary or the equation (3.16) for the decay boundary. It has been shown that $\mathbf{K}^{-1}\mathbf{b}$ is the only choice of a starting vector for the decay chain problem [Li *et al.*, 1999].

Another scheme for determination of the common starting vector is based on the principle of superposition. Equation (3.61) can be considered to be the superposition of two equations. The two equations have the right hand side of the two parts of equation (3.66), respectively. The common starting vector for the first equation can be determined in the same way as first scheme. The determination of common starting vector for the second equation is also similar to the first scheme except that the vector $\mathbf{b}$ is computed from the matrix $\mathbf{M}$.

$$b_i = \begin{cases} 0 & i \in \Upsilon \\ -\sum_{j \in \Psi_{1i}} M_{ij} & i \in \Omega \end{cases} \tag{3.71}$$

$i = 1, 2, ..., n$

The right-hand sides of the two superposition equations can be rewritten as

$$\mathbf{f}_p^{(1)} = \tilde{C}_p \mathbf{b}^{(1)} \tag{3.72}$$

$$\mathbf{f}_p^{(2)} = F(\tilde{C}_p) \mathbf{b}^{(2)} \tag{3.73}$$

Using the second scheme, two Arnoldi processes are required and two reduced equation systems must be solved. Even though additional computations are required compared to a single Arnoldi process, this method can still achieve great efficiency. The second scheme is more general compared to the first scheme and does not require the assumptions of equation (3.68). Therefore, more complicated boundaries, such as multiple sources and non-zero second type boundary conditions can be implemented for the ARM in the similar way.

The final reduced system is obtained by using a common starting vector $\mathbf{K}^{-1}\mathbf{b}$ in the Arnoldi algorithm.

$$R_p \mathbf{H}\dot{\mathbf{w}}_p + \mathbf{w}_p + R_p \lambda_p \mathbf{H}\mathbf{w}_p + \frac{D'(1-\phi)}{a\Delta z \phi}(1 - \varpi_{n'-1})\mathbf{H}\mathbf{w}_p =$$
$$\chi_1(\tilde{C}_p + \eta F(\tilde{C}_p))\mathbf{e}_1 + R_{p-1}\lambda_{p-1}\mathbf{H}\mathbf{w}_{p-1} + \frac{D'(1-\phi)}{a\Delta z \phi}\bar{\mathbf{w}}'_{n'-1} \tag{3.74}$$

$p = 1, 2, ..., P$

Note that the vector $\mathbf{e}_1$ is the first column of identity matrix (with dimension m), and χ_1 is the M-norm of $\mathbf{K}^{-1}\mathbf{b}$. Equation (3.74) is the reduced system for the first scheme of choosing a starting vector. The second scheme has two reduced equation systems. Both systems are similar to equation (3.74) except the first terms of the right hand side, which are:

$$R_p \mathbf{H}\dot{\mathbf{w}}_p + \mathbf{w}_p + R_p \lambda_p \mathbf{H}\mathbf{w}_p + \frac{D'(1-\phi)}{a\Delta z \phi}(1 - \varpi_{n'-1})\mathbf{H}\mathbf{w}_p =$$
$$\chi_1 \tilde{C}_p \mathbf{e}_1 + R_{p-1}\lambda_{p-1}\mathbf{H}\mathbf{w}_{p-1} + \frac{D'(1-\phi)}{a\Delta z \phi}\bar{\mathbf{w}}'_{n'-1} \tag{3.75}$$

$$R_p\mathbf{H}\dot{\mathbf{w}}_p + \mathbf{w}_p + R_p\lambda_p\mathbf{H}\mathbf{w}_p + \frac{D'(1-\phi)}{a\Delta z\phi}(1-\varpi_{n'-1})\mathbf{H}\mathbf{w}_p =$$
$$\chi_1 F(\tilde{C}_p)\mathbf{e}_1 + R_{p-1}\lambda_{p-1}\mathbf{H}\mathbf{w}_{p-1} + \frac{D'(1-\phi)}{a\Delta z\phi}\bar{\mathbf{w}}'_{n'-1} \tag{3.76}$$

$p = 1, 2, ..., P$

The final solutions of the pth species at desired steps are given by $\mathbf{c}_p = \mathbf{Q}\mathbf{w}_p$ for the first scheme. The concentration solutions for equations (3.75) and (3.76) are obtained in the same way as for the solution of first scheme. Summation of the solutions for the two equations gives the final solutions for the second scheme.

3.5.4 Summary of solution procedure

The solution procedure for the transport of multi-species decay chain radionuclide components using the Arnoldi method can be described as follows.

1. Discretize the fracture and matrix block domains, select an appropriate grid for both domains and determine the time step size for all the solutions.

2. Consider the component that is the first in the order of hierarchy. Compute the coefficient matrix for left hand side of the system of equations (3.51) and then compute the last column of the matrix $\mathbf{A}$ in (3.54). Use (3.56) to compute the solution coefficients ϖ_i for all the matrix block nodes. It is noted that the solution coefficients are the same for all the matrix blocks if matrix blocks are homogeneous. In addition, if the time step size Δt is not a constant, last column of $\mathbf{A}$ and ϖ_i must be re-evaluated at any Δt changing step.

3. The coefficient matrix of (3.51) is factored by a tridiagonal method [Press *et al.*, 1992]

4. Repeat steps 2 and 3 for all species.

5. The matrices $\mathbf{K}$, $\mathbf{M}$, and the common starting vector $\mathbf{K}^{-1}\mathbf{b}$ are formed.

6. Reduce the original system by performing an Arnoldi decomposition. The Arnoldi vectors $\mathbf{Q}$, the Hessenberg matrix $\mathbf{H}$, and the right hand-side vectors $\mathbf{g}_p$ for first time step corresponding to the pth component is determined.

7. The small $m \times m$ systems of first-order differential equation for the components are decomposed into LU forms by Gauss elimination.

8. Update the right-hand side vector $\mathbf{d}$ of equation (3.51) using (3.52), which is a function of the species last time step concentration and its parent species current step and last time step concentration, and then perform the back solve to obtain the solution to part I for the matrix block. Note the concentration used in updating vector $\mathbf{d}$ is the reduced space solution.

9. Update the right-hand side of the fracture equation system (3.74) by substituting the solution to part I for matrix block and concentration of parent species to it. Back solve the equations.

10. Compute the solution to part II and then by summing up the two part solutions to obtain the concentration solution for matrix blocks at the current time step.

11. At desired time steps a matrix vector multiplication is performed for computing the solution to the original problem.

12. Repeat steps 8 to step 11 for all species.

13. Proceed to next time step. Update the vector $\mathbf{g}_p$ and then repeat steps 8 to 12 for all time steps.

14. If the second scheme for determining a common starting vector is used, Repeat steps 5 to 13 for the equation system with second starting vector ($\mathbf{K}$ and $\mathbf{M}$ matrix do not need to be computed again). The final results are obtained by adding solutions of the two Arnoldi processes together.

3.6 Transport modeling techniques for the discrete fracture approach

The discrete fracture approach for simulation of multi-species contaminant transport in fractured porous media is limited by large computational overheads if one uses the traditional numerical methods. One primary reason is because of the vastly different hydraulic properties between the fractures and the matrix blocks, which results in sharp concentration gradients near the fracture-matrix interface. For field scale problems, the formations can contain very complex randomly distributed fractures. Furthermore, the multi-species transport problem requires the simulation of multiple components in the same time, because the contaminant species influence each other during their transport in the groundwater system. In order to simulate the sharp concentration gradients, the complicated fracture networks and the multiple components, a fine time and spatial discretization is needed. The discretization can easily involve many hundreds of thousands to millions of unknowns and time steps. To solve this type of problem, a very efficient numerical method in terms of both CPU time and computer memory must be used. The ARM is the right choice for modeling of multi-species contaminant transport in fractured porous media using the discrete fracture approach.

Sudicky and McLaren [1991] used the LTG method [Sudicky, 1989] to solve the two-dimensional contaminant transport equation using discrete fracture approach. Therrien *et al.*[1992] applied a similar approach to three-dimensional variably

saturated flow and transport problem. Both approaches are limited to the single species transport problem. In the following the discrete fracture approach for multi-species contaminant transport problem will be discussed.

The spatial discretization of the transport equations is identical to that of the flow equations. Similar to the flow problem, we can also perform superposition of the two dimensional areal elements representing the fractures onto the three dimensional volumetric elements representing the porous matrix. This ensures the continuity of the concentration at the fracture-matrix interface and avoids the need to explicitly determine the solute mass exchange terms involving Λ_n in (3.21). The elements can be any type. For a 2D problem, the fractures are represented by one dimensional linear elements and the matrices are represented by two dimensional areal elements. The final superposition form of the discretized equations for species p can be expressed by

$$\sum_{J=1}^{n'} \dot{C}_{p,J}[\sum_e \int_{V^e} R'_p N_I N_J dV + \sum_{ef}(2b)\int_{A^e} R_p \Omega_I \Omega_J dA] +$$
$$\sum_{J=1}^{n'} C_{p,J}[\sum_e \int_{V^e}(D'_{i'j'}\frac{\partial N_I}{\partial x_{i'}}\frac{\partial N_J}{\partial x_{j'}} + v'_{i'}\frac{\partial N_J}{\partial x_{i'}}N_I + R'_p\lambda_p N_I N_J)dV +$$
$$\sum_{ef}(2b)\int_{A^e}(D_{ij}\frac{\partial \Omega_I}{\partial x_i}\frac{\partial \Omega_J}{\partial x_j} + q_i\frac{\partial \Omega_J}{\partial x_i}\Omega_I + R_p\lambda_p\Omega_I\Omega_J)dA] -$$
$$\sum_{m'=1}^{M}\sum_{J=1}^{n'} C_{m',J}[\sum_e \int_{V^e}\zeta_{pm'}R'_{m'}\lambda_{m'}N_I N_J dV + \sum_{ef}(2b)\int_{A^e}\zeta_{pm'}R_{m'}\lambda_{m'}\Omega_I\Omega_J dA]$$
$$= \sum_{J=1}^{n'}[\sum_e D'_{\mathrm{n}}\int_s \frac{\partial C'_p}{\partial \mathrm{n}}N_I ds + (2b)\sum_{ef} D_{\mathrm{n}}\int_l \frac{\partial C_p}{\partial \mathrm{n}}\Omega_I dl] \qquad (3.77)$$

$i,j = 1,2;\ i',j' = 1,2,3;\ I = 1,2,...n';\ p = 1,2...P$

where s and l refer to the areal and linear boundaries of the three-dimensional and two-dimensional elements respectively, i, j, i' and j' refer to the dimension of spatial coordinate system, and $\sum_e$ and $\sum_{ef}$ represent the summation over the 3D porous matrix and 2D fracture elements that are connected to node J. Terms

on right hand side of the equations represent contribution from the boundary conditions, in where n denotes the direction normal to the boundary.

Equation (3.77) can be conveniently written in the form of matrix notation as

$$R_p\mathbf{M}\dot{\mathbf{c}}_p + \mathbf{K}\mathbf{c}_p + \lambda_p R_p \mathbf{M}\mathbf{c}_p - \sum_{m'=1}^{M} \zeta_{pm'}\lambda_{m'}R_{m'}\mathbf{M}\mathbf{c}_{m'} = \mathbf{f}_p \tag{3.78}$$

where the assumption has been made that the ratio of retardation coefficient in matrix and fracture for all species are same,R'_p/R_p=constant. It is easy to prove that this assumption is reasonable. Equation (3.78) is solved by reducing it to a small system using the Arnoldi algorithm in a similar fashion as that used for the dual-porosity model.

An iterative version of the Arnoldi algorithm is implemented for the reduction process. The ORTHOMIN solver is used in the Arnoldi reduction process. In order to improve the convergence rate of the iterative solution procedure, the"shift" technique is adopted. Equation (3.78) can be rewritten as:

$$R_p\mathbf{M}\dot{\mathbf{c}}_p + (\mathbf{K}+\varrho\mathbf{M})\mathbf{c}_p - \varrho\mathbf{M}\mathbf{c}_p + \lambda_p R_p \mathbf{M}\mathbf{c}_p - \sum_{m'=1}^{M} \zeta_{pm'}\lambda_{m'}R_{m'}\mathbf{M}\mathbf{c}_{m'} = \mathbf{f}_p \tag{3.79}$$

where ϱ is shift factor which can be optimally selected based on the numerical range of values in the $\mathbf{M}$ and $\mathbf{K}$ matrices. Experience suggests that the ϱ should have a value that makes $\mathbf{K}$ and $\varrho\mathbf{M}$ in a similar absolute value range.

Replacing $\mathbf{K}$ with $\mathbf{K}+\varrho\mathbf{M}$ can dramatically enhance the iterative convergence rate in ORTHOMIN. This is because for optimal convergence rates, the matrix to be solved by the ORTHOMIN solver should be diagonally dominant. By using the "shift" technique, the diagonal dominant property of the matrix to be solved can be improved. Equally important, the "shift" technique can also increase the convergence rate for the Arnoldi reduction recursion process which means less Arnoldi vectors are required compared to the situation without using this technique [Farrell, 1997]. In addition, using the "shift" technique can extend

the application of the ARM to solve large Peclet number problems. Experience indicates that without using "shift" technique, a problem with a Peclet number larger than 2 is difficult to be solve by ARM. However after using the technique a problem with a Peclet number equal 100 can be solved by ARM.

The final reduced equation system for all species are in form of

$$R_p\mathbf{H}\dot{\mathbf{w}}_p + \mathbf{w}_p - \varrho\mathbf{H}\mathbf{w}_p + \lambda_p R_p\mathbf{H}\mathbf{w}_p - \sum_{m'=1}^{M} \zeta_{pm'}\lambda_{m'}R_{m'}\mathbf{H}\mathbf{w}_{m'} = \mathbf{g}_p \tag{3.80}$$

The traditional time-marching scheme is used to solve reduced system (3.80). The final solutions for desired time steps are obtained by a matrix-vector multiplication. For detailed solution procedures, readers can refer to the last section dealing with the dual-porosity model. The boundary conditions can also be handled in a similar way as that used for the dual-porosity model.

Chapter 4

Theoretical Development—TCE Biodegradation Transport

4.1 Background

TCE degradation in an anaerobic environment can be analyzed by the loss of three chlorine atoms. The process can be described in following several steps [Vogel *et al.*, 1985; Fetter, 1992; Woodbury and Li, 1998]:

First, an enzyme or a cofactor catalyzes the reduction of TCE (HC_2Cl_3), resulting in the loss of one chlorine ion and production of dichloroethene (DCE or $H_2C_3Cl_2$):

$$H^+ + HC_2Cl_3 \rightarrow H_2C_3Cl_2 + Cl^- \tag{4.1}$$

where DCE exists as three different structural isomers 1,1-DCE, cis-DCE and trans-1,2 DCE, respectively. Another chlorine atom is lost from a DCE isomer and vinyl chloride (VC or H_3C_2Cl) is formed:

$$H^+ + H_2C_2Cl_2 \rightarrow H_3C_2Cl + Cl^- \tag{4.2}$$

Finally, the loss of a third chlorine atom produces ethene (H_4C_2):

$$H^+ + H_3C_2Cl \rightarrow H_4C_2 + Cl^- \tag{4.3}$$

All the reactions can be summarized as:

$$TCE \rightarrow \left\{ \begin{array}{c} \text{1,1 DCE} \\ \text{cis-1,2 DCE} \\ \text{trans-1,2 DCE} \end{array} \right. \rightarrow VC \rightarrow Ethene \tag{4.4}$$

Discussion of this type of TCE biodegradation can be seen in the work of Semprini and others [1995]. Wiedemeier *et al.*[1996] presented a detailed case study on this type biodegradation at a former fire training site.

As a single phase, TCE is regarded as dense non-aqueous phase liquid (DNAPL). It has the potential to migrate to great depths. Once present in an aquifer, DNAPL slowly dissolves into flowing groundwater, giving rise to aqueous phase plumes. The life span of TCE and its biodegradation products in subsurface is typically between several days to several thousand days, depending on the groundwater flow conditions.

Migration of TCE and its biodegradation products are governed by the effects of advection, dispersion, sorption and biodegradation. Simulation of this type of contaminant transport in dual-porosity media involves six coupled equations describing the contaminant transport in fractures, and equations describing the contaminant diffusion in the porous matrix. Solving these equations using either the finite element or finite difference equations for a field scale problem would result in a large number of unknowns. This can render the problem almost impractical for anything less than a supercomputer. Therefore numerical techniques must be carefully chosen to achieve efficiency and robustness. Woodbury *et al.* [1990] has shown that the Arnoldi reduction technique is very suitable for solving this type of problem.

4.2 Governing equations

Using the dual-porosity model, two groups of equations describing mass transport in the fractures and matrix blocks are required for each contaminant species. It is assumed that the solutes can sorb onto the fracture walls and onto the solid phase comprising the porous matrix, and their degradation can be described with first-order decay. These equations are coupled together by parent to daughter transformation and the mass exchanges between fractures and matrix blocks. First, the equations of the transport in fractures are discussed:

Let C_p, p=1,2,...,6, be the concentrations of the species, which are TCE, cis-1,2 DCE, Trans-1,2 DCE, 1,1 DCE, VC and ethene respectively. The governing equations for these six species in the fractures can be written in the following form [modified from Woodbury and Li, 1998]:

$$R_1\frac{\partial C_1}{\partial t} = \frac{\partial}{\partial x_i}(D_{ij}\frac{\partial C_1}{\partial x_j}) - v_i\frac{\partial C_1}{\partial x_i} - \lambda_{12}R_1C_1 - \lambda_{13}R_1C_1 - \lambda_{14}R_1C_1 + (\frac{1-\phi}{\phi})\Gamma_1 \tag{4.5}$$

$$R_q\frac{\partial C_q}{\partial t} = \frac{\partial}{\partial x_i}(D_{ij}\frac{\partial C_q}{\partial x_j}) - v_i\frac{\partial C_q}{\partial x_i} + \lambda_{1q}R_1C_1 - \lambda_{q5}R_qC_q + (\frac{1-\phi}{\phi})\Gamma_q \quad \text{for } q = 2,3,4 \tag{4.6}$$

$$R_5\frac{\partial C_5}{\partial t} = \frac{\partial}{\partial x_i}(D_{ij}\frac{\partial C_5}{\partial x_j}) - v_i\frac{\partial C_5}{\partial x_i} + \lambda_{25}R_2C_2 + \lambda_{35}R_3C_3 + \lambda_{45}R_4C_4 - \lambda_{56}R_5C_5 + (\frac{1-\phi}{\phi})\Gamma_5 \tag{4.7}$$

$$R_6\frac{\partial C_6}{\partial t} = \frac{\partial}{\partial x_i}(D_{ij}\frac{\partial C_6}{\partial x_j}) - v_i\frac{\partial C_6}{\partial x_i} + \lambda_{56}R_5C_5 - \lambda_{67}R_6C_6 + (\frac{1-\phi}{\phi})\Gamma_6 \tag{4.8}$$

$i, j = 1, 2$

where Γ_p is the rate of material exchange of species p between the rock matrix and fracture, D_{ij} is the hydrodynamic dispersion tensor in the fracture, v_i represents the flow velocity in fractures along the x_i direction, R_p is the retardation coefficient of species p in the fractures, ϕ is the secondary fracture porosity which is defined as the volume of fractures per unit volume of the entire fractured porous medium, and λ_{IJ} are decay constants. The first sub-index I denotes the parent species and the second sub-index J denotes the daughter species member. The λ are obtained from half-life of the species decay constants $(f_{IJ})_{1/2}$, that is

$$\lambda_{IJ} = \frac{\ln 2}{(f_{IJ})_{1/2}} \tag{4.9}$$

In the dual-porosity model, the domain is assumed to be comprised of matrix blocks that are distributed uniformly in space in a macroscopic sense. The two most popular geometries of the matrix block that have been used consist of either parallel slabs or spherical blocks, as depicted in Figure 3-1 [Huyakorn *et al.*, 1983]. Because their dimensions are assumed to be small relative to the scale of the problem, the concentration at the surface of each matrix block will be approximately uniform and diffusional transport in the block will be essentially one-dimensional. In this work, only the parallel fracture-prismatic block conceptual model for TCE transport is considered. The theory developed here is easily extended to other matrix block types, such as the spherical block.

Equations of the one-dimensional diffusion in a prismatic block can be written as

$$\frac{\partial}{\partial z'}(D'\frac{\partial C_1'}{\partial z'}) = \phi' R_1' \frac{\partial C_1'}{\partial t} + \phi' R_1' \lambda_{12} C_1' + \phi' R_1' \lambda_{13} C_1' + \phi' R_1' \lambda_{14} C_1' \tag{4.10}$$

$$\frac{\partial}{\partial z'}(D'\frac{\partial C_q'}{\partial z'}) = \phi' R_q' \frac{\partial C_q'}{\partial t} + \phi' R_q' \lambda_{q5} C_q' - \phi' R_1' \lambda_{1q} C_1' \qquad q = 2, 3, 4 \tag{4.11}$$

$$\frac{\partial}{\partial z'}(D'\frac{\partial C'_5}{\partial z'}) = \phi' R'_5 \frac{\partial C'_5}{\partial t} + \phi' R'_5 \lambda_{56} C'_5 - \phi' R'_2 \lambda_{25} C'_2 - \phi' R'_3 \lambda_{35} C'_3 - \phi' R'_4 \lambda_{45} C'_4 \tag{4.12}$$

$$\frac{\partial}{\partial z'}(D'\frac{\partial C'_6}{\partial z'}) = \phi' R'_6 \frac{\partial C'_6}{\partial t} + \phi' R'_6 \lambda_{67} C'_6 - \phi' R'_5 \lambda_{56} C'_6 \tag{4.13}$$

where C'_p (p=1...6) is the concentration of pth species, ϕ', D' and R'_p are the porosity, the molecular diffusion coefficient and the retardation coefficient of species p in the matrix block, respectively.

The mass transfer rate between the matrix block and fracture (Γ_p) can be written in the terms of concentration gradient at their interface using Fick's law. The expression of Γ_p for any species takes the form of equation (3.13).

The transport equations are subject to initial and boundary conditions and the boundary conditions can be any type. However, the most common boundary condition is a first type with a constant or transient concentration. For the first type boundary condition with decay, where $\tilde{C}_1^0$, $\tilde{C}_2^0$, $\tilde{C}_3^0$, $\tilde{C}_4^0$, $\tilde{C}_5^0$ and $\tilde{C}_6^0$ are initial source concentrations which are placed on some part of first type boundary, then the concentrations of these six species on the boundary are required to satisfy the following equations [Woodbury and Li, 1998],

$$\frac{\partial \tilde{C}_1}{\partial t} = -\lambda_{12}\tilde{C}_1 - \lambda_{13}\tilde{C}_1 - \lambda_{14}\tilde{C}_1 \tag{4.14}$$

$$\frac{\partial \tilde{C}_q}{\partial t} = \lambda_{1q}\tilde{C}_1 - \lambda_{q5}\tilde{C}_q \qquad \text{for } q = 2,3,4 \tag{4.15}$$

$$\frac{\partial \tilde{C}_5}{\partial t} = \lambda_{25}\tilde{C}_2 + \lambda_{35}\tilde{C}_3 + \lambda_{45}\tilde{C}_4 - \lambda_{56}\tilde{C}_5 \tag{4.16}$$

$$\frac{\partial \tilde{C}_6}{\partial t} = \lambda_{56}\tilde{C}_5 - \lambda_{67}\tilde{C}_6 \tag{4.17}$$

where $\tilde{C}_1$ $\tilde{C}_2$ $\tilde{C}_3$ $\tilde{C}_4$ $\tilde{C}_5$ and $\tilde{C}_6$ are the boundary concentration of these six species respectively. Based on the analytical solution of Bateman's system of ordinary

differential equations [Bateman, 1910] given by Harada *et al.* [1980], the solutions of above equations can be written as:

$$\tilde{C}_1 = \tilde{C}_1^0 e^{-\lambda_1 t} \tag{4.18}$$

$$\tilde{C}_i = (\tilde{C}_i^0 - \frac{\tilde{C}_1^0 \lambda_{1i}}{\lambda_{i5} - \lambda_1}) e^{-\lambda_{i5} t} + \frac{\tilde{C}_1^0 \lambda_{1i}}{\lambda_{i5} - \lambda_1} e^{-\lambda_1 t}, \ i=2,3,4 \tag{4.19}$$

$$\tilde{C}_5 = \hat{C}_5 e^{-\lambda_{56} t} + \sum_{i=2}^{4} \{ \frac{\lambda_{i5}}{\lambda_{56} - \lambda_{i5}} (\tilde{C}_i^0 - \frac{\tilde{C}_1^0 \lambda_{1i}}{\lambda_{i5} - \lambda_1}) e^{-\lambda_{i5} t} + \\ + \frac{\tilde{C}_1^0 \lambda_{1i} \lambda_{i5}}{(\lambda_{56} - \lambda_1)(\lambda_{i5} - \lambda_1)} e^{-\lambda_1 t} \} \tag{4.20}$$

$$\tilde{C}_6 = \hat{C}_6 e^{\lambda_{67} t} + \frac{\hat{C}_5 \lambda_{56}}{\lambda_{67} - \lambda_{56}} e^{-\lambda_{56} t} + \sum_{i=2}^{4} \{ \frac{\lambda_{56} \lambda_{i5}}{(\lambda_{67} - \lambda_{i5})(\lambda_{56} - \lambda_{i5})} (\tilde{C}_i^0 \\ - \frac{\tilde{C}_1^0 \lambda_{1i}}{\lambda_{i5} - \lambda_1}) e^{-\lambda_{i5} t} + \frac{\tilde{C}_1^0 \lambda_{1i} \lambda_{i5} \lambda_{56}}{(\lambda_{67} - \lambda_1)(\lambda_{56} - \lambda_1)(\lambda_{i5} - \lambda_1)} e^{-\lambda_1 t} \} \tag{4.21}$$

where $\lambda_1 = \lambda_{12} + \lambda_{13} + \lambda_{14}$ and $\hat{C}_5$ and $\hat{C}_6$ in equations (4.20) and (4.21) are constants determined by following formulae:

$$\hat{C}_5 = \tilde{C}_5^0 - \sum_{i=2}^{4} \{ \frac{\lambda_{i5}}{\lambda_{56} - \lambda_{i5}} (\tilde{C}_i^0 - \frac{\tilde{C}_1^0 \lambda_{1i}}{\lambda_{i5} - \lambda_1}) + \frac{\tilde{C}_1^0 \lambda_{1i} \lambda_{i5}}{(\lambda_{56} - \lambda_1)(\lambda_{i5} - \lambda_1)} \tag{4.22}$$

$$\hat{C}_6 = \tilde{C}_6^0 - \frac{\hat{C}_5 \lambda_{56}}{\lambda_{67} - \lambda_{56}} - \sum_{i=2}^{4} \{ \frac{\lambda_{56} \lambda_{i5}}{(\lambda_{67} - \lambda_{i5})(\lambda_{56} - \lambda_{i5})} (\tilde{C}_i^0 - \frac{\tilde{C}_5^0 \lambda_{1i}}{\lambda_{i5} - \lambda_1}) \\ + \frac{\tilde{C}_5^0 \lambda_{1i} \lambda_{i5} \lambda_{56}}{(\lambda_{67} - \lambda_1)(\lambda_{56} - \lambda_1)(\lambda_{i5} - \lambda_1)} \} \tag{4.23}$$

The equations for the matrix blocks (equation (4.10)-(4.13)) are solved subject to the assumptions of continuity of the concentration at the fracture-matrix interface, and the zero concentration gradient at the center of the matrix block for all the contaminant species. The two groups of equations for both fractures and matrix blocks are related together through mass exchange terms and the degradation from one species to another. Therefore, in order to get the solutions for all the six species, these equations must be solved at the same time.

4.3 Determination of mass exchange terms

The mass exchange term can be determined based on the equation (3.13) and is a function of the concentration gradient at the matrix block surface. Before the computation is performed, the one-dimensional diffusion equation for the matrix blocks must be solved. However, at the moment of solving the one-dimensional diffusion equation, the corresponding nodal concentration at the fracture (the first type boundary for the equation) is variable and unknown. Due to this fact, most algorithms solve the equation for the matrix block and fracture iteratively to obtain the solutions [Huyakorn *et al.*,1983]. In this thesis, a scheme based on the principle of superposition to solve the equations directly is developed. Figure 3-3(a) shows the discretization of the prismatic matrix block.

A tridiagonal set equations is derived for the porous matrix block associated with node J in the fracture domain. Application of the Galerkin technique to any one of equations (4.10)-(4.13), using the standard linear basis functions, applying their boundary conditions and adopting the finite difference temporal approximation yields the same equation as (3.51). For the TCE problem, P in (3.51) has a value of 6.

Equation (3.51) is the general form for all species. The coefficients α_i, β_i and γ_i in the left hand side and right hand side d_i are given by:

$$\alpha_i = \theta\alpha_i^* + \phi' R_p' \Delta z_{i-1}/(6\Delta t)$$

$$\gamma_i = \theta\gamma_i^* + \phi' R_p' \Delta z_i/(6\Delta t)$$

$$\beta_i = \theta\beta_i^* + \phi' R_p' (\Delta z_{i-1} + \Delta z_i)/(3\Delta t)$$

$$d_i = (\theta - 1)(\alpha_i^* C_{p,i-1}^{'k} + \beta_i^* C_{p,i}^{'k} + \gamma_i^* C_{p,i+1}^{'k}) + \frac{\phi' R_p'}{6\Delta t}[\Delta z_{i-1} C_{p,i-1}^{'k} + 2(\Delta z_{i-1} + \Delta z_i) C_{p,i}^{'k} + \Delta z_i C_{p,i+1}^{'k}] + \bar{d}_i$$

$$\alpha_i^* = \frac{-D'}{\Delta z_{i-1}} + \frac{\lambda\phi' R'_p \Delta z_{i-1}}{6}$$
$$\gamma_i^* = \frac{-D'}{\Delta z_i} + \frac{\lambda\phi' R'_p \Delta z_i}{6}$$
$$\beta_i^* = \frac{D'}{\Delta z_{i-1}} + \frac{D'}{\Delta z} + \frac{\lambda\phi' R'_p}{3}(\Delta z_{i-1} + \Delta z_i)$$
$$\beta_1 = \theta\beta_1^* + \phi' R'_p \Delta z_1/(3\Delta t)$$
$$\gamma_1 = \theta\gamma_1^* + \phi' R'_p \Delta z_1/(6\Delta t)$$
$$d_1 = (\theta - 1)(\beta_1^* C'^k_{p,1} + \gamma_1^* C'^k_{p,2}) + \frac{\phi' R'_p \Delta z_1}{6\Delta t}(2C'^k_{p,1} + C'^k_{p,2}) + \bar{d}_1$$
$$\gamma_1^* = \frac{-D'}{\Delta z_1} + \frac{\lambda\phi' R'_p \Delta z_1}{6}$$
$$\beta_i^* = \frac{D'}{\Delta z_1} + \frac{\lambda\phi' R'_p \Delta z_1}{6}$$

$p = 1, 2...6; \quad i = 2, 3, ..., n' - 1$

where θ is a time-weighting factor. Note that $\theta = 0.5$ for the Crank-Nicolson time-stepping scheme. The one-dimensional element sizes for the matrix block are defined as $\Delta z_i = z_{i+1} - z_i$.

λ and $\bar{d}_i$ for different species are given as follows.

Species 1:

$$\lambda = \lambda_{12} + \lambda_{13} + \lambda_{14}$$
$$\bar{d}_1 = 0$$
$$\bar{d}_i = 0 \qquad i = 2, 3, ..., n' - 1$$

Species 2, 3 and 4:

$$\lambda = \lambda_{j5}$$
$$\bar{d}_1 = (1 - \theta)\phi' R'_1 \lambda_{1j} \frac{\Delta z_1}{6}(2C'^k_{1,1} + C'^k_{1,2}) + \theta\phi' R'_1 \lambda_{1j} \frac{\Delta z_1}{6}(2C'^{k+1}_{1,1} + C'^{k+1}_{1,2})$$
$$\bar{d}_i = \frac{(1 - \theta)\phi' R'_1 \lambda_{1j}}{6}[\Delta z_{i-1} C'^k_{1,i-1} + 2(\Delta z_{i-1} + \Delta z_i) C'^k_{1,i} + \Delta z_i C'^k_{1,i+1}]$$

$$+\frac{\theta\phi' R_1'\lambda_{1j}}{6}[\Delta z_{i-1}C_{1,i-1}^{\prime k+1}+2(\Delta z_{i-1}+\Delta z_i)C_{1,i}^{\prime k+1}+\Delta z_i C_{1,i+1}^{\prime k+1}]$$

$$j=2,3,4; \qquad i=2,3,...,n'-1$$

Species 5:

$$\lambda=\lambda_{56}$$

$$\bar{d}_1=\sum_{j=2}^{4}[(1-\theta)\phi' R_j'\lambda_{j5}\frac{\Delta z_1}{6}(2C_{j,1}^{\prime k}+C_{j,2}^{\prime k})+\theta\phi' R_j'\lambda_{j5}\frac{\Delta z_1}{6}(2C_{j,1}^{\prime k+1}+C_{j,2}^{\prime k+1})]$$

$$\bar{d}_i=\sum_{j=2}^{4}\{\frac{(1-\theta)\phi' R_j'\lambda_{j,5}}{6}[\Delta z_{i-1}C_{j,i-1}^{\prime k}+2(\Delta z_{i-1}+\Delta z_i)C_{j,i}^{\prime k}+\Delta z_i C_{j,i+1}^{\prime k}]$$

$$+\frac{\theta\phi' R_j'\lambda_{j5}}{6}[\Delta z_{i-1}C_{j,i-1}^{\prime k+1}+2(\Delta z_{i-1}+\Delta z_i)C_{j,i}^{\prime k+1}+\Delta z_i C_{j,i+1}^{\prime k+1}]\}$$

$$i=2,3,...,n'-1$$

Species 6:

$$\lambda=\lambda_{67}$$

$$\bar{d}_1=(1-\theta)\phi' R_5'\lambda_{56}\frac{\Delta z_1}{6}(2C_{5,1}^{\prime k}+C_{5,2}^{\prime k})+\theta\phi' R_5'\lambda_{56}\frac{\Delta z_1}{6}(2C_{5,1}^{\prime k+1}+C_{5,2}^{\prime k+1})$$

$$\bar{d}_i=\frac{(1-\theta)\phi' R_5'\lambda_{56}}{6}[\Delta z_{i-1}C_{5,i-1}^{\prime k}+2(\Delta z_{i-1}+\Delta z_i)C_{5,i}^{\prime k}+\Delta z_i C_{5,i+1}^{\prime k}]$$

$$+\frac{\theta\phi' R_5'\lambda_{56}}{6}[\Delta z_{i-1}C_{5,i-1}^{\prime k+1}+2(\Delta z_{i-1}+\Delta z_i)C_{5,i}^{\prime k+1}+\Delta z_i C_{5,i+1}^{\prime k+1}]$$

$$i=2,3,...,n'-1$$

Equations (3.51) have a total of $n'-1$ equations in n' unknowns for each species. Note the concentration at the fracture-matrix interface is continuous. However, the concentration in the fracture at the moment of solving the current diffusion equation is not yet determined. The matrix concentration solutions are a function of the fracture concentration at node J ($C_{p,J}^{k+1}$) which is unknown. After manipulating the equation system, the general solution for any species can be expressed in the form of equation (3.53). The same procedure is adopted to solve

the matrix block equations for TCE as the procedure discussed in Section 3.5.1. The mass exchange term Γ_p at time step k+1 is in the same form as (3.57).

It is assumed that all the matrix blocks have uniform properties. If the matrix block domain is not homogeneous, the mass exchange term must be evaluated for each block, which would be very time consuming for problem with a large numbers of nodes. The time step size Δt is an important parameter for the equation system. If it is constant, the computation of the last column of matrix $\mathbf{A}$ and part II solution coefficient ϖ_i is computed only one time. Otherwise, the last column of $\mathbf{A}$ and ϖ_i must be re-computed whenever Δt changes.

4.4 FEM discretization of the equations in fractures

Applying the Galerkin finite element method (Huyakorn and Pinder, 1983) to the TCE transport equations (4.5)-(4.8) for the fractures, discretized equations for the six species are obtained as follows:

$$R_1\mathbf{M}\dot{\mathbf{c}}_1 + \mathbf{K}\mathbf{c}_1 + \lambda_1 R_1 \mathbf{M}\mathbf{c}_1 - \frac{1-\phi}{\phi}\mathbf{M}\mathbf{u}_1 = \mathbf{f}_1 \tag{4.24}$$

$$R_q\mathbf{M}\dot{\mathbf{c}}_q + \mathbf{K}\mathbf{c}_q + \lambda_{q5} R_q \mathbf{M}\mathbf{c}_q - \lambda_{1q} R_1 \mathbf{M}\mathbf{c}_1 - \frac{1-\phi}{\phi}\mathbf{M}\mathbf{u}_q = \mathbf{f}_q$$
$$q = 2, 3, 4 \tag{4.25}$$

$$R_5\mathbf{M}\dot{\mathbf{c}}_5 + \mathbf{K}\mathbf{c}_5 + \lambda_{56} R_5 \mathbf{M}\mathbf{c}_5 - \lambda_{25} R_2 \mathbf{M}\mathbf{c}_2 - \lambda_{35} R_3 \mathbf{M}\mathbf{c}_3$$
$$-\lambda_{45} R_4 \mathbf{M}\mathbf{c}_4 - \frac{1-\phi}{\phi}\mathbf{M}\mathbf{u}_5 = \mathbf{f}_5 \tag{4.26}$$

$$R_6\mathbf{M}\dot{\mathbf{c}}_6 + \mathbf{K}\mathbf{c}_6 + \lambda_{67} R_6 \mathbf{M}\mathbf{c}_6 - \lambda_{56} R_5 \mathbf{M}\mathbf{c}_5 - \frac{1-\phi}{\phi}\mathbf{M}\mathbf{u}_6 = \mathbf{f}_6 \tag{4.27}$$

where $\mathbf{c}_p$ $(p = 1...6)$ is the vector of concentration of species p with n unknowns at the nodes of the mesh, $\dot{\mathbf{c}}_p$ is the vector of concentration derivative with respect to

time, $\mathbf{u}_p$ is the vector of mass exchange rate between fracture and matrix block, $\mathbf{f}_p$ is a time-dependent force vector containing the effects of the initial and boundary conditions in the fractures, $\mathbf{M}$ is a positive-definite and symmetric capacity matrix, and $\mathbf{K}$ is a unsymmetrical conductivity matrix which depends on D_{ij} and flow velocity v.

The entries of vector $\mathbf{u}_p$ are determined by equation (3.57) which consists of two independent parts. One part relates to the current concentration of the species and the other part relates to the concentration history of the species and its parent species, and also relates to current concentration of the parent species. The second part can be predetermined before the solution of the equations.

A simple case is considered in this thesis where a second type boundary condition is zero and there are no other 2nd type source/sinks. The concentration vector $\mathbf{c}_p$ is for all the nodes in the domain, including the first-type boundary nodes. The submatrices of $\mathbf{M}$ and $\mathbf{K}$ without the influence of first type boundary nodes can be obtained by partitioning-out the rows and columns from $\mathbf{M}$ and $\mathbf{K}$ corresponding to the first type boundary nodes. After partitioning, all the entries of $\mathbf{f}_p$ are zero except contributions from first type boundary nodes.

Let Φ be the set of index values of all nodes, and $\Psi_1 \subset \Phi$ be the subset of index values of all first type nodes and $\Upsilon \subset \Phi$ be the subset of all other nodes that do not directly connect to nodes in Ψ_1.

After partitioning, the ith entries of the right hand side vector $\mathbf{f}_p$ can be written as

$$f_{1i} = -\sum_{j \in \Psi_{1i}} [R_1 M_{ij} \dot{C}_{1,j} + K_{ij} C_{1,j} + \lambda_1 R_1 M_{ij} C_{1,j} - \frac{1-\phi}{\phi} M_{ij} \Gamma_{1j}] \tag{4.28}$$

$$f_{qi} = -\sum_{j \in \Psi_{1i}} [R_q M_{ij} \dot{C}_{q,j} + K_{ij} C_{q,j} + \lambda_{q5} R_q M_{ij} C_{q,j} - \lambda_1 R_{1q} M_{ij} C_{1,j} - \frac{1-\phi}{\phi} M_{ij} \Gamma_{qj}] \qquad q = 2,3,4 \tag{4.29}$$

$$f_{5i} = -\sum_{j\in\Psi_{1i}} [R_5 M_{ij}\dot{C}_{5,j} + K_{ij}C_{5,j} + \lambda_{56}R_p M_{ij}C_{5,j} - \lambda_2 R_2 M_{ij}C_{2,j}$$
$$-\lambda_3 R_3 M_{ij}C_{3,j} - \lambda_1 R_4 M_{ij}C_{4,j} - \frac{1-\phi}{\phi}M_{ij}\Gamma_{5j}] \tag{4.30}$$

$$f_{6i} = -\sum_{j\in\Psi_{1i}} [R_6 M_{ij}\dot{C}_{6,j} + K_{ij}C_{6,j} + \lambda_{67}R_6 M_{ij}C_{6,j} - \lambda_{56}R_5 M_{ij}C_{5,j}$$
$$-\frac{1-\phi}{\phi}M_{ij}\Gamma_{6j}] \tag{4.31}$$

where Ψ_{1i} denotes the subset of index values of first type boundary nodes which are in the same element as node i, K_{ij} and M_{ij} are the elements of matrix $\mathbf{K}$ and $\mathbf{M}$ at ith row and jth column respectively.

The equations (4.28)-(4.31) can be written in a general form:

$$f_{pi} = -\sum_{j\in\Psi_{1i}} [K_{ij}C_{p,j} + M_{ij}F(C_{p,j})] \tag{4.32}$$

$p = 1, 2...6$

where $F(C_{p,j})$ is a function of $C_{p,j}$. The function takes different forms for different species.

It follows that $f_{pi} = 0$, when $i \in \Upsilon$, because the subset Ψ_{1i} is empty. The function $F(C_{p,j})$ can be easily determined from given boundary concentrations. if the first type boundary conditions satisfy with equations (4.14)-(4.17), the boundary concentrations and $F(C_{p,j})$ can be determined based on equations (4.18)-(4.21).

4.5 Implementation of the Arnoldi reduction method

4.5.1 Reduction of the transport equations

By applying the Arnoldi algorithm [Arnoldi, 1951; Woodbury *et al.*, 1990; Nour-Omid *et al.*, 1991; and Woodbury and Li, 1998] to equations (4.24)-(4.27), the

size of these equations can be reduced to a series of small ordinary differential equations of the form

$$R_1\mathbf{H}\dot{\mathbf{w}}_1 + \mathbf{w}_1 + \lambda_1 R_1\mathbf{H}\mathbf{w}_1 - \frac{1-\phi}{\phi}\mathbf{H}\mathbf{y}_1 = \mathbf{g}_1 \tag{4.33}$$

$$R_q\mathbf{H}\dot{\mathbf{w}}_q + \mathbf{w}_q + \lambda_{q5} R_q\mathbf{H}\mathbf{w}_q - \lambda_{1q} R_1\mathbf{H}\mathbf{w}_1 - \frac{1-\phi}{\phi}\mathbf{H}\mathbf{y}_q = \mathbf{g}_q$$
$$q = 2, 3, 4 \tag{4.34}$$

$$R_5\mathbf{H}\dot{\mathbf{w}}_5 + \mathbf{w}_5 + \lambda_{56} R_5\mathbf{H}\mathbf{w}_5 - \lambda_{25} R_2\mathbf{H}\mathbf{w}_2 - \lambda_{35} R_3\mathbf{H}\mathbf{w}_3$$
$$-\lambda_{45} R_4\mathbf{H}\mathbf{w}_4 - \frac{1-\phi}{\phi}\mathbf{H}\mathbf{y}_5 = \mathbf{g}_5 \tag{4.35}$$

$$R_6\mathbf{H}\dot{\mathbf{w}}_6 + \mathbf{w}_6 + \lambda_{67} R_6\mathbf{H}\mathbf{w}_6 - \lambda_{56} R_5\mathbf{H}\mathbf{w}_5 - \frac{1-\phi}{\phi}\mathbf{H}\mathbf{y}_6 = \mathbf{g}_6 \tag{4.36}$$

where $\mathbf{H}$ is a $m \times m$ upper Hessenberg matrix, m is the number of Arnoldi vectors used which is much smaller than n, and $\mathbf{w}_p$, $\mathbf{g}_p$ and $\mathbf{y}_p$ are the reduced vector of $\mathbf{c}_p$, $\mathbf{f}_p$ and $\mathbf{u}_p$ respectively.

The Arnoldi reduction method uses orthogonal matrix transformations to reduce the equations (4.24)-(4.27) to a much smaller upper Hessenberg system of first-order differential equation by approximating the solution of $\mathbf{c}_p$ with $\mathbf{Q}\mathbf{w}_p$. $\mathbf{Q}$, a $n \times m$ matrix, consists of the first mth Arnoldi vectors which is created during Arnoldi reduction process. The details of determination of the matrix $\mathbf{Q}$ and $\mathbf{H}$ and the reduction procedures can be found in the work of Woodbury *et al.* [1990], and Nour-Omid *et al* [1991] and in Chapter 2. The criteria of monitoring and terminating the unsymmetric Lanczos reduction process [Li *et al.*, 1999] can also be applied to the Arnoldi reduction process. By using their criteria, the appropriate number of Arnoldi vectors (m) are selected.

Equations (4.33)-(4.36) are obtained based on the assumption of homogeneous matrix blocks throughout the domain, namely D' and ϕ' are constants in the whole

matrix domain, and R'_p is constant for each species. This assumption makes the system reduction relatively easy.

Equations (4.33)-(4.36) are solved by a suitable time integration algorithm such as the Crank-Nicolson scheme. As $\mathbf{H}$ is an upper Hessenberg matrix and its size is small, it can be easily decomposed into the product of an upper triangular matrix and a lower bidiagonal matrix. Note that the Arnoldi method shows a great advantage here in that only one process is required to reduce the entire multiple equation system simultaneously. Also, the solution to the reduced systems (4.33)-(4.36) using a direct method is economic because the reduced system size is much smaller than the original system. This also gives a large saving in storage required by the reduction method. Therefore, solving of the reduced system is more efficient than direct solving of the original equation system. The penalty with the time-stepping procedure is not significant if $m \ll n$. The original solution for any desired time step or location can be retrieved from the reduced solution data in future with very little computation effort.

It is easy to show that the entries of reduced mass exchange vector $\mathbf{y}_p$ can be computed with equation (3.57), even though that equation is for the unreduced space mass-exchange rate calculation.

In $\mathbf{w}$ space (reduced space), the discretized equations for the matrix blocks are still the same as equation system (3.51):

$$\begin{aligned}
&\beta_1 w_{p,1}^{'k+1} + \gamma_1 w_{p,2}^{'k+1} = d_1 \\
&\alpha_i w_{p,i-1}^{'k+1} + \beta_i w_{p,i}^{'k+1} + \gamma_i w_{p,i+1}^{'k+1} = d_i \qquad i = 2, 3, ..., n' - 1 \\
&w_{p,n'}^{'k+1} = w_{p,J}^{k+1}
\end{aligned} \tag{4.37}$$

$p = 1, 2...6$

Note the equations now correspond to the reduced space nodes and the first type boundary concentrations at the fracture-matrix interface are equal to the

reduced space solutions of corresponding nodes in the fracture. Therefore the solutions for the matrix blocks can be directly substituted into equation (3.57) or reduced form (3.63) to compute the mass exchange rates in reduced space. This is because that the current species concentration in the matrix block can be written in a function of the species and its parent species concentration and concentration history in the fracture. After reduction, the function is still the same. This property affords additional efficiency in computing time and memory storage for the Arnoldi reduction method. At each time step, the mass exchange terms are computed in the reduced space which only requires to solve m 1-D diffusion equations for each species. For original equation system (4.24)-(4.27), n 1-D diffusion equations need to be solved to determine the mass exchange terms.

After the $\mathbf{w}$ space solutions are obtained, the concentration $C'_{p,i}$ at ith node in the matrix, can be directly computed from the reduced space solutions for the ith node by equation (3.64).

Note, it is not necessary to compute concentrations for all the nodes. Only the concentrations at the desired locations and times are computed. For a matrix block corresponding to a specific fracture node J, various node concentrations can be obtained by the dot product of Jth row of matrix $\mathbf{Q}$ and vector $\mathbf{w}'_{p,i}$.

4.5.2 Choice of common starting vector for TCE transport

The choice of the starting vector is a very important factor influencing the convergence and accuracy of the Arnoldi reduction method. For the multi-species transport problem, a common starting vector must be chosen for all the equation systems to minimize the residual errors. Li *et al.* [1999] showed that any vector parallel to the vectors $\mathbf{f}_p$ $(p = 1, 2, ..., 6)$ is a suitable starting vector for the Arnoldi process in reducing the equation system (4.24)-(4.27). It is also required

that all the right-hand side vectors $\mathbf{f}_p$ must be parallel to each other. In most cases these vectors are not parallel to each other. However, these vectors can be partitioned into two parts, each of which is parallel to each other. Two schemes for choosing the common starting vector for most popular transient and constant type Dirichlet boundary conditions are available. A detailed description of these two schemes can be found Section 3.5.3.

The final reduced system is obtained by using a common starting vector $\mathbf{K}^{-1}\mathbf{b}$ in the Arnoldi algorithm, where $\mathbf{b}$ is a constant vector. The reduced right hand side vectors for both schemes are in the following form:

First scheme:

$$\mathbf{g}_p = \chi_1(\tilde{C}_p + \eta F(\tilde{C}_p))\mathbf{e}_1 \tag{4.38}$$

$p = 1, 2, ..., 6$

Second scheme:

$$\mathbf{g}_p^{(1)} = \chi_1^{(1)}\tilde{C}_p\mathbf{e}_1 \tag{4.39}$$

$$\mathbf{g}_p^{(2)} = \chi_1^{(2)}F(\tilde{C}_p)\mathbf{e}_1 \tag{4.40}$$

$p = 1, 2, ..., 6$

Note that the vector $\mathbf{e}_1$ is the first column of identity matrix (with dimension m), χ_1 is the M-norm of $\mathbf{K}^{-1}\mathbf{b}$, η is a constant, and $F(\tilde{C}_p)$ is a function defined in equation (4.32).

The final solutions of the pth species at desired steps or locations are given by $\mathbf{c}_p = \mathbf{Q}\mathbf{w}_p$ for the first scheme. The concentration solutions for the second scheme are obtained in the same way as for the first scheme. In the second scheme, summation of the solutions for the two equations with different right hand sides gives the final solution.

Chapter 5

Verification of the Models

To verify the numerical formulae, the solutions of the proposed models are compared to analytical solutions or solutions obtained by a different numerical models. The first example examines the Lanczos reduction method by simulating a problem involving transient flow to a pumped well fully penetrating a fractured, confined aquifer. The second example investigates the application of the Arnoldi reduction method to single species contaminant transport in parallel fractures. The third and fourth examples show the accuracy and efficiency of the Arnoldi method applied to three species decay chain and seven species biodegradation transport problems, respectively. All the first four examples use the dual-porosity model. The fifth example verifies the discrete fracture flow model by comparison with the dual-porosity flow model. The last verification problem concerns single species contaminant transport in discretely fractured porous media.

5.1 Dual-porosity flow

The first example shows a homogeneous, isotropic and infinite aquifer system with a well at the center. The problem is identical to the Theis problem, except the aquifer is a dual-porosity medium. The dual-porosity aquifer is considered to be

a single horizontal fracture which is analogous to the aquifer-aquitard system. The problem is geometrically symmetric, so only one quarter of the flow field is simulated with 1/4 of the original pumping rate. The dimension of the model is set large enough so that the influence of the boundary cannot be reached in a short time and can be considered of infinite extent. Values of various parameters employed in the simulation are given in Table 5.1. Figure 5-1 shows the grid used. The cross-section for this example is shown in Figure 5-2(a).

Parameter	Value
Number of nodes	550
Number of elements	980
Dimension of aquifer r	2000 m
Fracture Transmissivity T_x, T_y	18.2 m^2/d
Pumping rate, Q	250 m^3/d
Fracture storage coefficient, S	0.002
Hydraulic conductivity of matrix, K'	0.0005 m/d
Specific storage of matrix, S'_s	0.005 m^{-1}
Thickness of matrix block, $2a$	10 m
Fracture aperture, $2b$	0.01 m

Table 5.1: Values of various parameters for verification example 1

To obtain the numerical solution for the example, the fracture domain was discretized into 980 triangular elements and 550 nodes. The grid size is about 0.1 m near the well and 300 m at the outside boundary. Figure 5-3 shows the computed dimensionless drawdown versus dimensionless time at r=48.3 m and 266.22 m compared to the analytical solutions. The analytical solutions are obtained from the solutions of the classical problem of well flow in a confined aquifer-aquitard system [Hantush, 1964]. Note that the parallel fracture dual-porosity model is analogous to the short-term response of the confined aquifer-aquitard

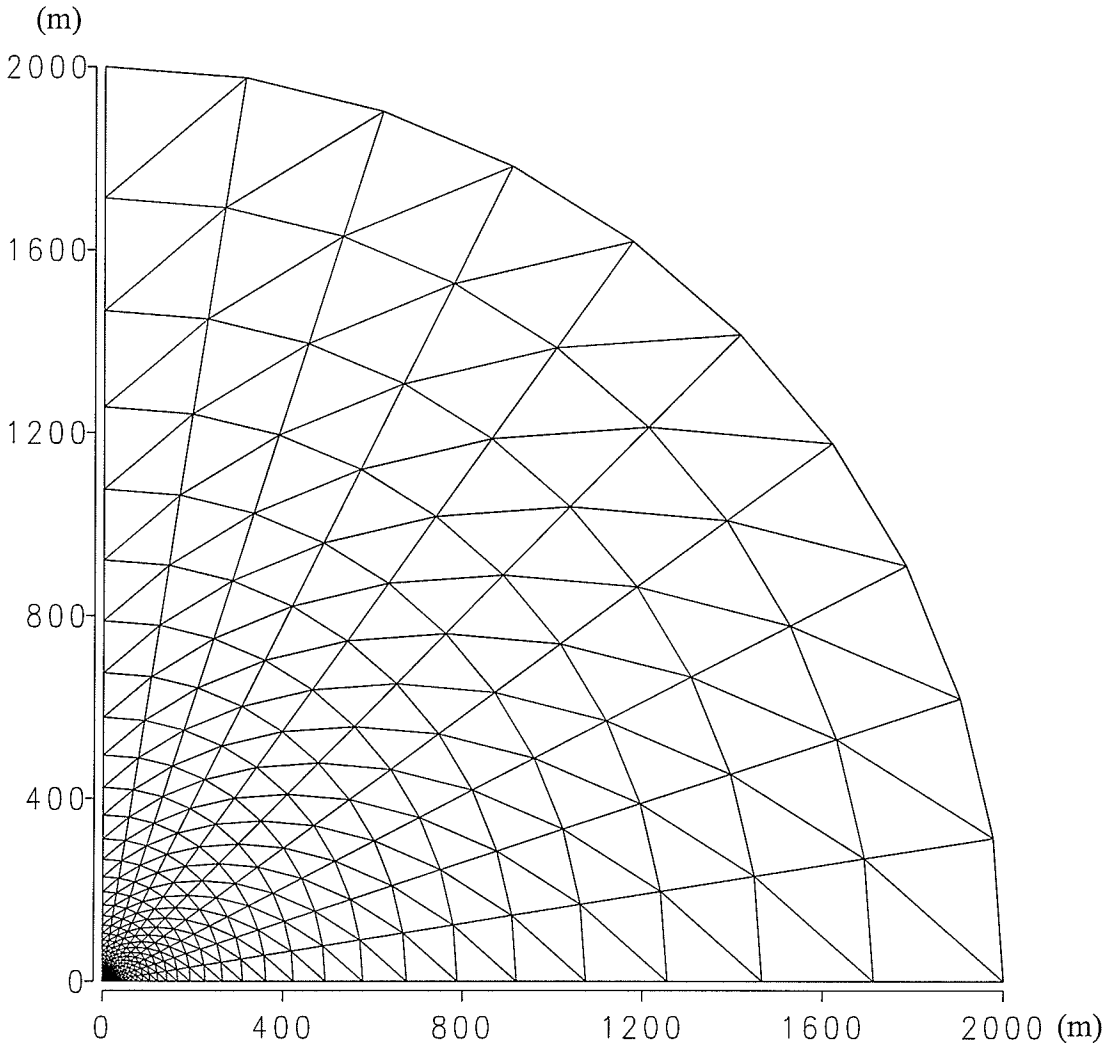

Figure 5-1 Finite element mesh for example 1. Only one quarter of the total field is shown

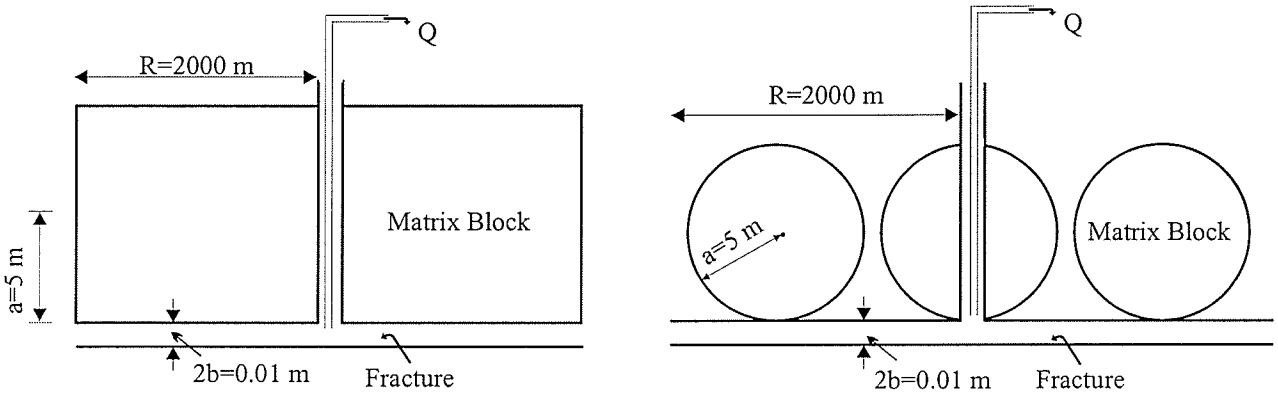

(a) Cross-section of parallel fracture model

(B) Cross-section of spherical block model

Figure 5-2 Cross-section of the two-dimensional flow in dual-porosity media

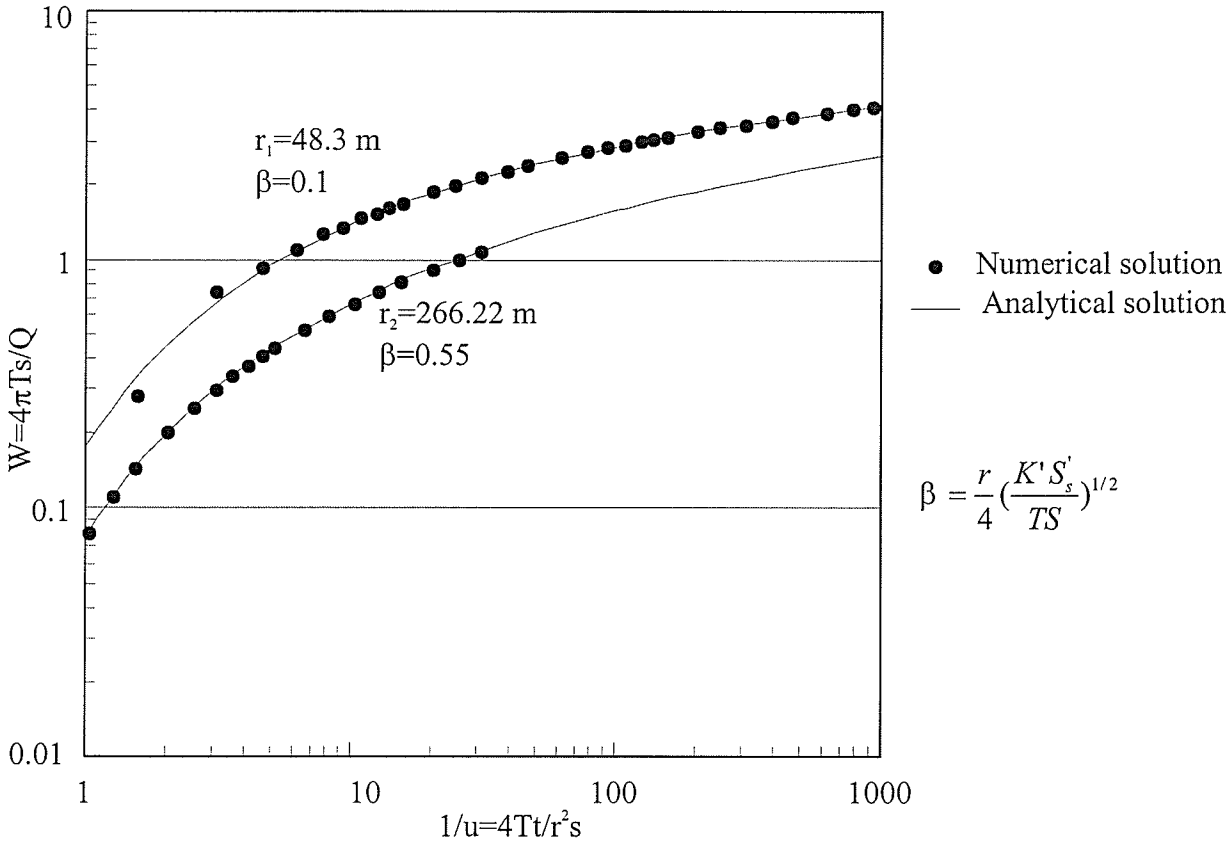

Figure 5-3 Dimensionless fracture drawdown versus dimensionless time, showing the comparison of numerical and analytical solutions for the parallel fracture model

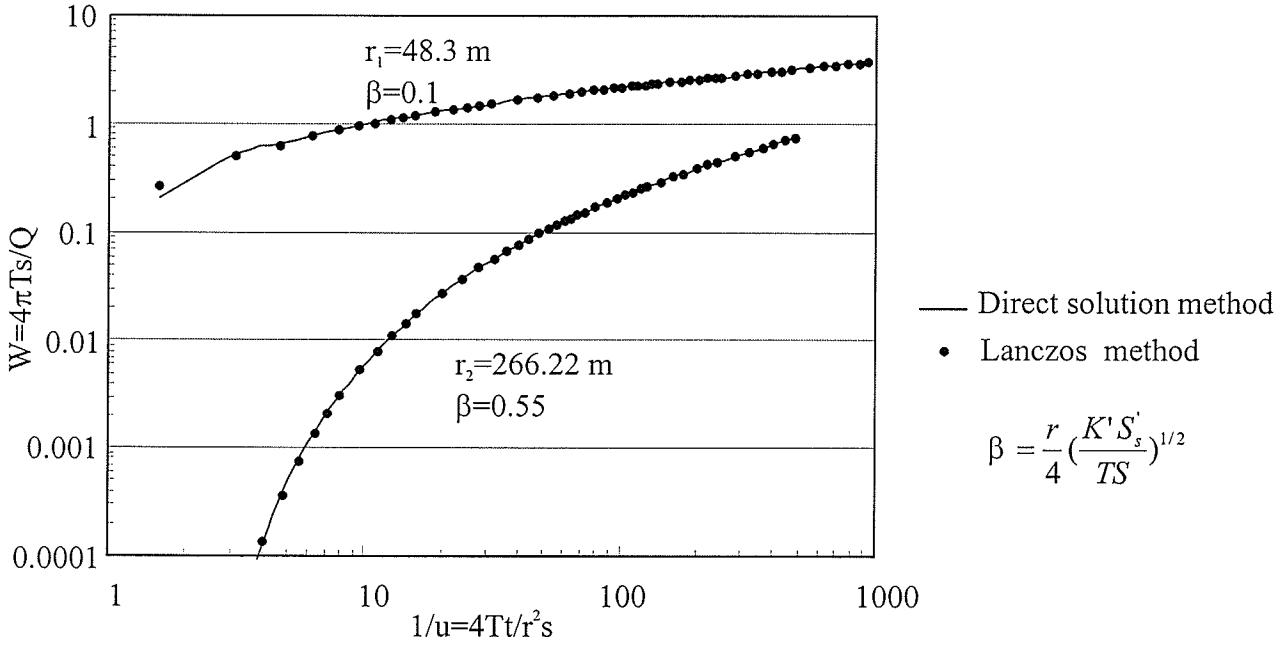

Figure 5-4 Dimensionless fracture drawdown versus dimensionless time for the dual-porosity blocky fracture model

system which can be written as

$$s = (Q/4\pi T)\mathcal{H}(u, \beta)$$

where s is the drawdown and $\mathcal{H}$ is the leaky well-function. By selecting an appropriate β, the analytical solutions can be read from a column of the table of function $\mathcal{H}(u, \beta)$. From Figure 5-3 it can be seen that the results of Lanczos reduction method agree very well with the analytical curves. For this extreme example, in which the ratio between maximum and minimum grid size is 3000, it is expected that more Lanczos vectors may be needed. However only 30 vectors are required. For this small problem with 600 time steps, the reduction method can still achieve about 75 % reduction in time (1:4 in time) compared to the direct solution method.

The same hydraulic parameters are applied to a blocky fracture model with the exception that the prismatic matrix blocks are now replaced by spherical blocks of 5 m radius (see Figure 5-2(b)). Computed dimensionless drawdowns at r=48.3 m and 266.22 m are plotted in Figure 5-4 against dimensionless time. The leakage parameter β is used to identify the type curves. An analytical solution for the problem of well flow in a spherical porous matrix fractured system is not available. Therefore this solution is compared with the solution obtained by the traditional finite element method, which had been verified by Huyakorn *et al.* [1983]. The comparison indicates that both methods agree with each other very well. The blocky model has less drawdown than the parallel fracture model for the same parameters. This is due to the fact that the blocky fracture model has more fracture space than the parallel fracture model in the same domain. The fracture space determines the conductivity of the fractured aquifer system and the higher conductivity causes less drawdown.

5.2 Single species contaminant transport

In order to verify the Arnoldi reduction method for contaminant transport in a dual-porosity medium, an example involving the transport of radionuclides in a parallel-fracture system is investigated. Both longitudinal transport in the fracture and transverse diffusion in the matrix block are examined and the results are compared to analytical solutions. This example is also used to compute solutions for the spherical block model.

In this example (see Figure 5-5), the numerical solution computed using the Arnoldi reduction method is compared against the analytical solution developed by Tang *at al.* [1981]. The input parameters describing the physical system are given in Table 5.2. The boundary condition at the inflow end of the fracture (x=0) is of the first type, with a constant concentration of 1.0. The two dimensional transport region is 10.0 m in length and 1.0 m in width. The region length is sufficiently long such that the concentration profiles do not reach the outflow boundary for the purpose of comparison with the analytical solution, which assumes that the medium is semi-infinite in length. The radionuclide source is located at $x = 0$. The node spacing is Δx=0.25 m for the first meter and 0.5 m for the rest of the domain. A total of 104 triangular elements and 79 nodes are used in the plane of fracture. Discretization in the matrix block is achieved by using 40 linear 1D elements with a minimum 0.0012 m and maximum 0.12 m nodal spacing. A constant time step size of 10 days is used.

Figure 5-6 compares the concentration profiles along the center of the fracture obtained with the Arnoldi reduction method to the analytical results at 100, 1000 and 10,000 days, respectively. Excellent agreement is found between the analytical and the numerical results. Note that for early time values the numerical solution shifts slightly from the analytical solution. This can be improved by using more

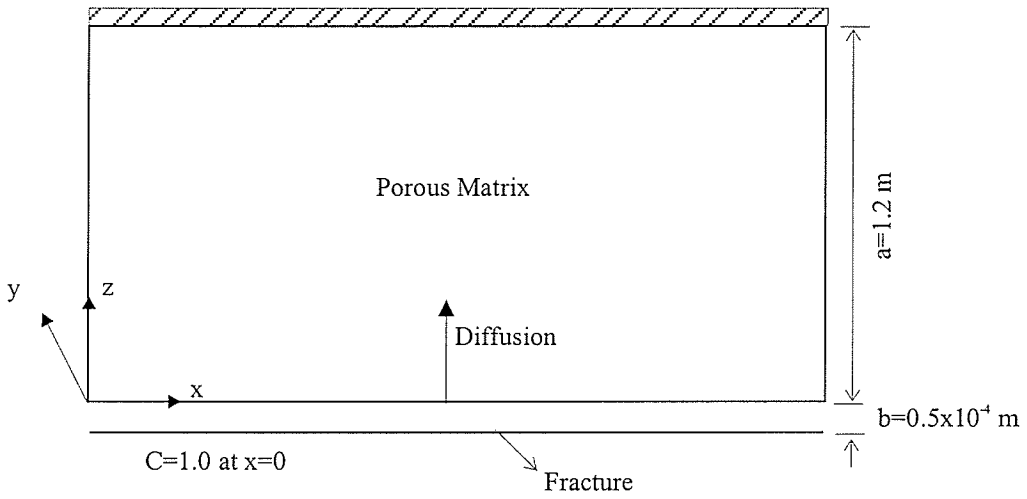

Figure 5-5 Physical system for verification problem 2.

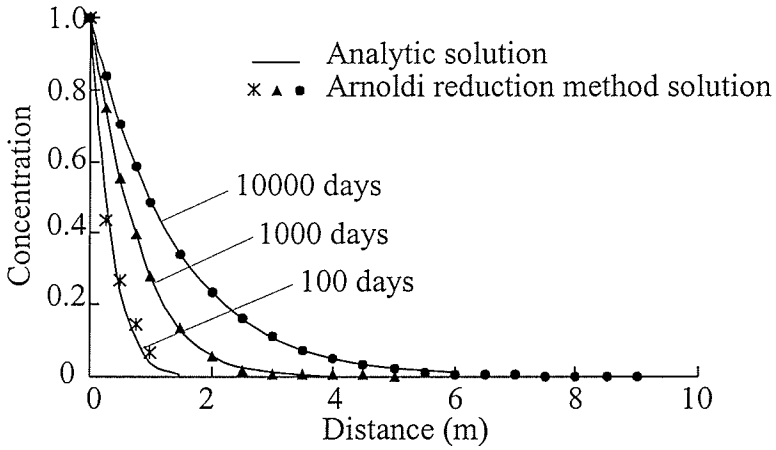

Figure 5-6 Comparison of the Arnoldi reduction method solution with analytical solution (Parallel fracture).

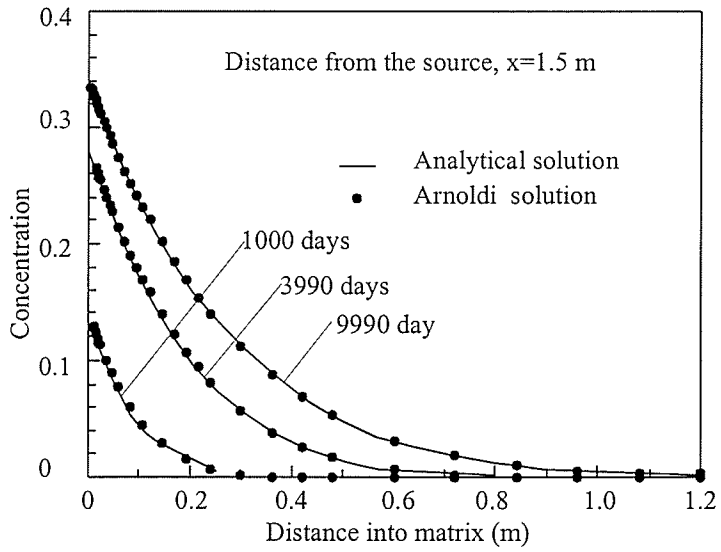

Figure 5-7 Concentration distributions in the matrix blocks, showing comparison of the Arnoldi reduction method solution and analytical solution

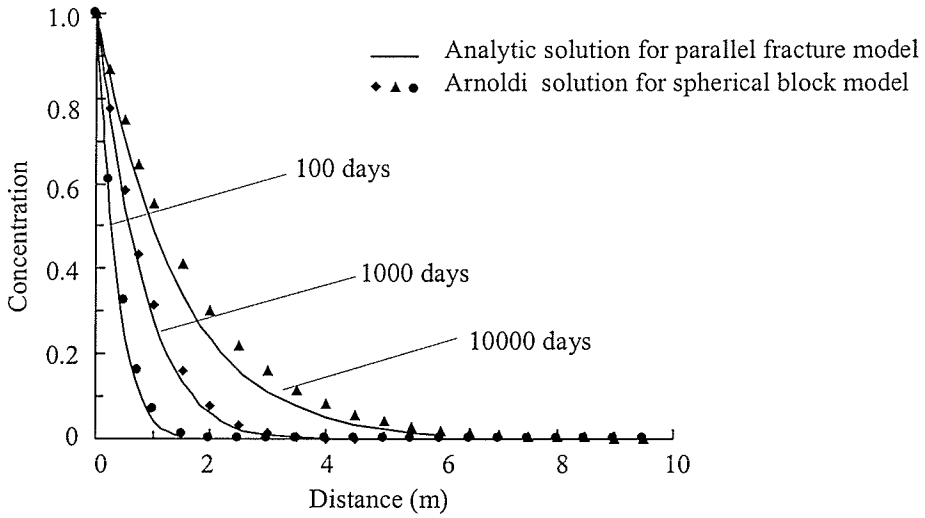

Figure 5-8 Concentration distributions in the fracture by using spherical block model for the verification example 2.

Parameter	Value
Fracture aperture	$2b = 0.0001m$
Fracture spacing	$2a = 2.4m$
Seepage velocity	$v = 0.01m/d$
Secondary porosity	$\phi = 0.000042$
Matrix block porosity	$\phi' = 0.01$
Longitudinal dispersivity	$\alpha_L = 0.5m$
Fracture diffusion coefficient	$D^* = 1.384 \times 10^{-4} m^2/d$
Matrix diffusion coefficient	$D' = 1.384 \times 10^{-7} m^2/d$
Solute decay coefficient	$\lambda = 1.54 \times 10^{-4} d^{-1}$
Retardation factors	$R = R' = 1$

Table 5.2: Parameter values for the verification example 2

Arnoldi vectors or reducing the time step. Note for this example only seven Arnoldi vectors are required. The total solution time (from input data to output data) of this problem for 1000 time steps is less than 1 second on a Pentium II 300 MHz personal computer. Of course, for this small 1-D problem (which has only 79 nodes) the Arnoldi reduction method cannot show its full advantage.

After the computation of the concentrations in the fracture, the concentration distributions in the matrix blocks can be computed using the approach discussed in Chapter 3. Figure 5-7 shows the numerical results together with the analytical solutions [from Huyakorn *et al.*, 1981]. Both solutions are almost identical to each other.

To show the transport behavior for the spherical block model, the same set of parameters are applied to radionuclide transport in a blocky fractured system except that now the parameter a is the radius of the spherical block. The sphere radius is chosen such that the surface-area-to-volume ratio is identical to that for the prismatic slabs. The parallel fracture model of this example has a surface-area-to-volume ratio of 0.833. Therefore 1.8 m is chosen (this equals 1.5 times

of the half-thickness of the slab) for the radius of the spherical block, which ensures the ratio for the both models are the same. The computed concentration distributions along the flow direction in the fracture are shown in Figure 5-8. Due to the fact that no analytical solution for this problem can be found in the literature, the numerical results cannot be directly compared with an exact solution. Comparison of the numerical solutions with the analytical solutions for the parallel fracture model indicates that different matrix block geometries will produce similar concentration distributions in the fracture as long as the surface-area-to-volume ratio remains identical [Rasmuson, 1984; Sudicky, 1990]. The ARM for this problem achieves efficiency similar to the previous example. It should be noted that the **M** matrix for transport equation in the spherical matrix block is a function of r_i^5 (see equation 3.60). Therefore, one may need finer one-dimensional discretization compared to the parallel fracture model to ensure the convergence of the mass exchange terms.

5.3 Three species decay chain transport

This problem illustrates the transport of three species of radionuclides in porous media. Since no analytical solutions to the decay chain transport with rock matrix diffusion are available, an example with no diffusion into the rock matrix is introduced. The effect of the diffusive loss into the rock matrix can be incorporated by a straightforward extention of the present problem. However, in order to carry out a direct comparison with the analytical solution for the system, it has been omitted. Considering the previous example, it is clear that such an assumption does not affect the verification of the whole model. This problem is equivalent to a one-dimensional model for porous media with decay chain. The modeled region can also be viewed as a single fracture with the plane of the fracture parallel to

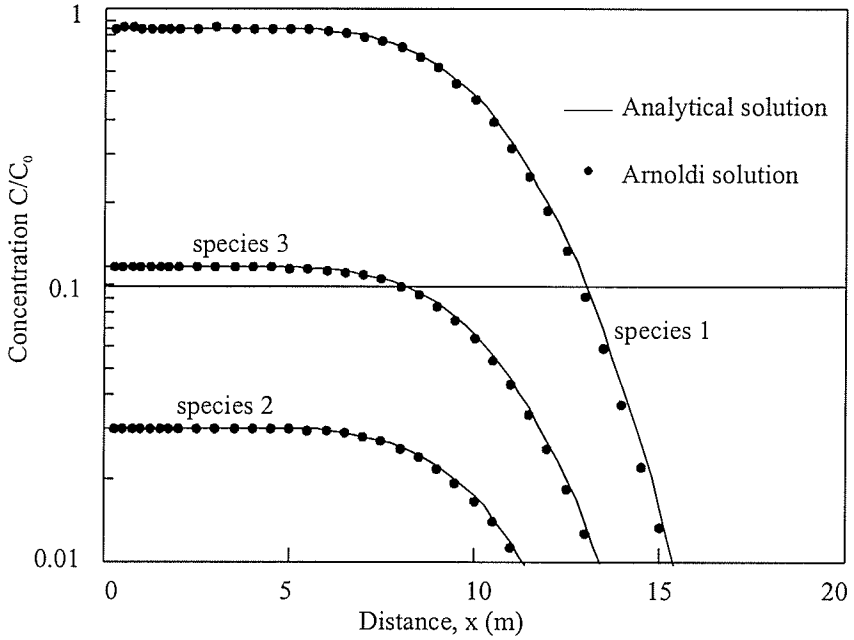

Figure 5-9. Concentration profiles of the three species decay chain transport at 100 years, showing comparison of analytical and the Arnoldi reduction method solutions

the flow plane. A fracture geometry similar to the last example is used. The fracture has unit width and is 20 m in length. Once again the radionuclide source is located at the inflow end (x=0), which forms a first type boundary condition with a transient concentration.

To obtain the numerical solution, the region is discretized into 210 triangular elements with a nodal spacing of 0.25 m in the first two meters and 0.5 m for the remainder. The total number of nodes is 153. The properties of the three radionuclide members and the medium are given in the Table 5.3. For the purpose of comparison, these data are selected to correspond to the data used in a previous study on decay chain transport by Lee *et al.* [1995]. The parent member has an initial concentration of unity at the inlet source. The initial concentrations of the second and third members equal to 0.0 meaning that the source concentrations of all the three species at the inlet point are from the first member of the chain. Decay or ingrowth of three species at the inlet source is governed by equation (3.15) and its solution is given by (3.16).

Parameter	Value
Decay chain	$(1) \rightarrow (2) \rightarrow (3)$
Source initial concentration	
species (1)	$C_1^{B0} = 1.0$
species (2)	$C_2^{B0} = 0.0$
species (3)	$C_3^{B0} = 0.0$
Flow velocity	$v = 10.0m/yr$
Longitudinal dispersivity	$\alpha_L = 0.25m$
Transverse dispersivity	$\alpha_T = 0.0m$
Solute decay coefficient	
species (1)	$\lambda_1 = 0.0016$
species (2)	$\lambda_2 = 0.04620$
species (3)	$\lambda_3 = 0.000106$
Retardation factors	$R_1 = R_2 = R_3 = 100$

Table 5.3: Input data for three decay chain verification example

Computed concentration profiles together with analytical solutions are depicted in Figure 5-9 for the time 100 years. Analytical solutions for this problem can be found in the work by Lester *et al* [1975]. It can be seen from Figure 5-9 that the Arnoldi reduction method yields results that are essentially identical to analytical solutions. In order to test the efficiency of the numerical method, a small time step size of 0.05 year and a large number of time steps are used. For the simulation of 2000 time steps and 8 Arnoldi vectors used, the total solution time is less than 1 second. This example indicates that the ARM can effectively solve the multi-species problem and the proposed schemes for choosing a multiple component common starting vector can be used for the transient first type boundary condition problem.

5.4 Seven species parallel and series reaction transport

The purpose here is to demonstrate the accuracy and efficiency of the Arnoldi reduction method as it applies to the transport of chlorinated solvents in dual-porosity or porous media. To verify the proposed method, a problem involving the transport of seven species, such as the transport of chlorinated solvent tetrachloroethylene (PCE) and its biodegradation products, along a two-dimensional fracture is selected. Groundwater flow is uniform in the domain. Continuous contaminant sources for all seven species, represented as first-type boundary condition, are placed at the upstream end of the aquifer. Since no analytical solutions to this type of transport with rock matrix diffusion are available, an example without diffusion into the rock matrix is introduced. The effects of the diffusive loss into the rock matrix can be incorporated by a straightforward extention of the present problem. However, in order to carry out a direct comparison with the

analytical solution, this has been omitted. Because the application of the Arnoldi reduction method to the radionuclides transport in dual-porosity has been verified in Section 5.2, it is clear that such assumption does not affect the verification of the whole model. The fracture can also be considered as a two-dimensional aquifer system. The accuracy of the ARM for multi-species contaminant transport with parallel and series reaction is demonstrated by comparing reduction method solutions with the one dimensional analytical solutions.

The biodegradation procedure of PCE can be described by a reaction network that includes both serial and parallel reactions, which is the same as TCE biodegradation as discussed in Chapter 4, except the reaction network has one more parent species. Therefore, the model developed for the TCE transport can be used to solve the PCE problem with a minor modification. In this case, PCE will react to produce TCE. TCE can then react to simultaneously produce *cis*-1,2-DCE, *trans*-1,2-DCE, and 1,1-DCE. Subsequently, DCE will react to produce vinyl chloride (VC) and finally to ethene [Skeen *et al.*, 1995; Jain and Criddle, 1995].

The fracture domain is rectangular, with a width equal to 0.4 m and a length equal to 50 m in the direction of flow. The groundwater flow system is two-dimensional with steady and uniform flow in one dimension only. In this way the method can be tested against one-dimensional analytical solutions. To obtain the numerical solution, the region is discretized into 400 triangular elements with a nodal spacing of 1 m in length and 0.1 m in width, giving 255 nodes. The patch pollution source is located at the inflow end (x=0), which forms a first type boundary condition. A constant concentration of species 1 is set to one and the daughter species are zero. Second-type boundary conditions of zero flux are imposed along the remaining three sides of the domain. Groundwater flow velocity

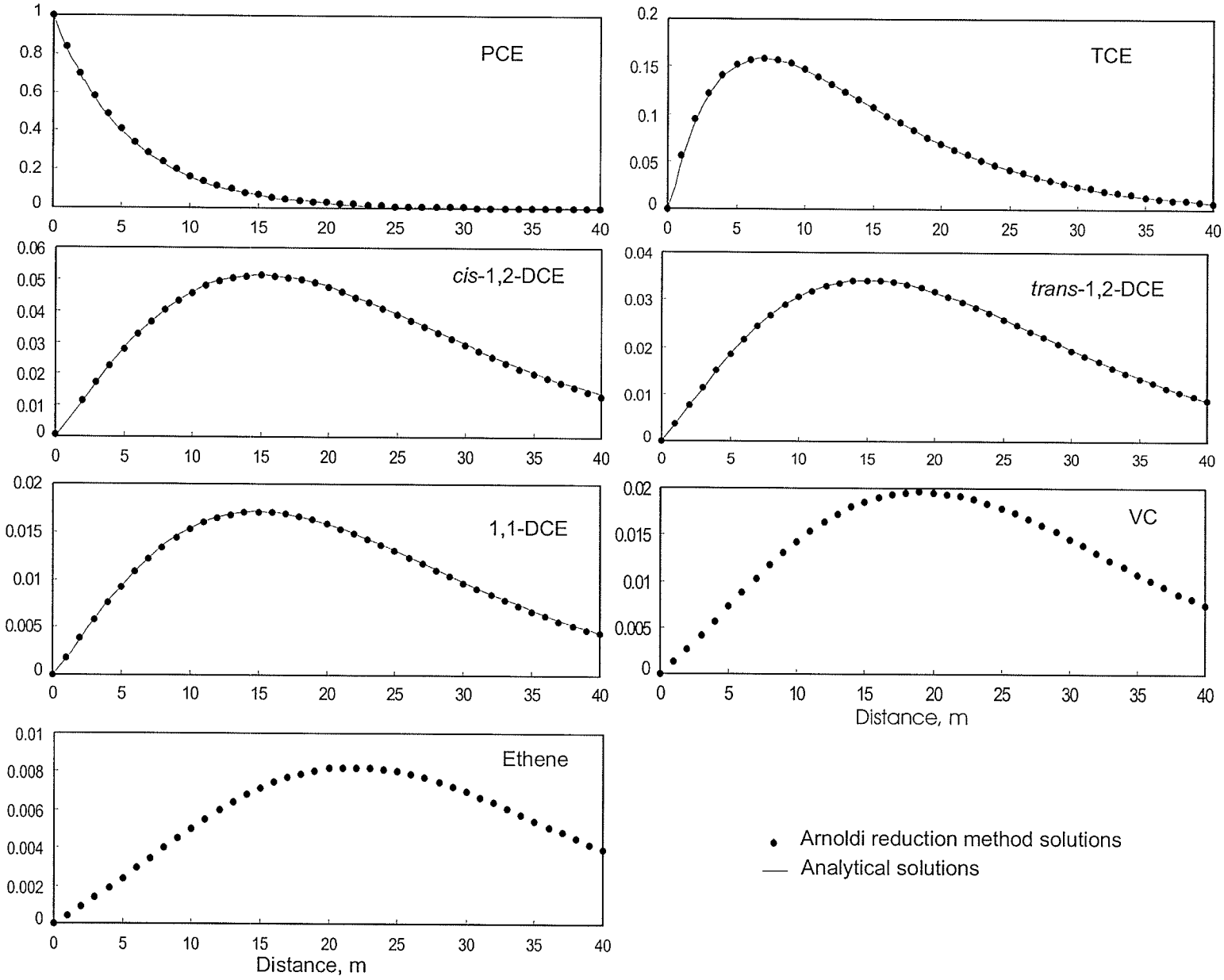

Figure 5-10 Comparison of the Arnoldi reduction method solutions with the analytical solutions.

in the domain equals 0.4 m/d. The longitudinal dispersivity, α_L, is 10 m, and the transverse dispersivity, α_T, is zero. Molecular diffusion is also assumed to be zero. A retardation factor $R = 1$ is used for all the species. Other properties of the contaminants are given in Table 5.4. For the purpose of comparison, these data are selected to correspond to the data used in a previous study for the analytical solutions of a similar problem by Sun *et al.* [1999]. Note that the values of decay coefficient and stoichiometric yield in the table do not reflect the real value of PCE and its daughter products.

Parameter	Value
Solute decay coefficient (d^{-1})	
species (1)	$\lambda_{12} = 0.2$
species (2)	$\lambda_2 = \lambda_{23} + \lambda_{24} + \lambda_{25} = 0.1$
species (3)	$\lambda_{36} = 0.02$
species (4)	$\lambda_{46} = 0.02$
species (5)	$\lambda_{56} = 0.02$
species (6)	$\lambda_{67} = 0.04$
species (7)	$\lambda_{78} = 0.006$
Stoichiometric yield	
species (1)→(2)	$\zeta_{12} = 0.5$
species (2)→(3)	$\zeta_{23} = 0.3$
species (2)→(4)	$\zeta_{24} = 0.2$
species (2)→(5)	$\zeta_{25} = 0.1$
species (3)→(6)	$\zeta_{36} = 1.0$
species (4)→(6)	$\zeta_{46} = 1.0$
species (5)→(6)	$\zeta_{56} = 1.0$
species (6)→(7)	$\zeta_{67} = 1.0$

Table 5.4: Parameters for the 7 species transport verification problem

The stoichiometric yield factor ζ in Table 5.4 describes the fraction of parent component transforming into daughter component. The theoretical development in this research does not consider the influence of this parameter. However it can be easily incorporated into the model by substituting λ with $\lambda \times \zeta$ for each

corresponding daughter species.

Numerical solutions for the problem are compared with the analytical solutions provided by Sun [personal communication, see also Sun *et al.*, 1999]. There are no analytical solutions available for species six and seven. Figure 5-10 shows concentration profiles computed by the Arnoldi reduction method compared to analytical solutions for 40 days after the release of pollution. The concentration distributions predicted by the Arnoldi method are identical to analytical solutions. In order to get the numerical solutions for 40 days, a constant time step size of two days is used for a total of 20 time steps. For this problem, only 10 Arnoldi vectors are needed. The total CPU time for 20 time steps is less than one second using a Pentium 333 MHz personal computer. According to the report of Sun *et al.* [1999], on a Pentium 100 MHz computer, the total solution time for the first five species of this problem is 13 seconds using the analytical method and 112 seconds by using the RT3D model [Clement *et al.*, 1998]. Even for this small problem, the Arnoldi reduction method has shown its efficiency.

5.5 Flow in discretely fractured media

The extension of Lanczos reduction method to the simulation of groundwater flow in fractured porous media using a discrete fracture approach is verified by comparison with the solutions of the dual-porosity approach. The dual-porosity approach for the simulation of groundwater flow in fractured porous media was discussed in previous sections and it has been verified.

The problem considered here consists of a two-dimensional cross-section domain with a single horizontal fracture distributed across the domain center. The thickness of the layer is one meter and the domain has a length of 200 meters. The fracture has a uniform aperture of 1×10^{-4} m. Water was pumped from

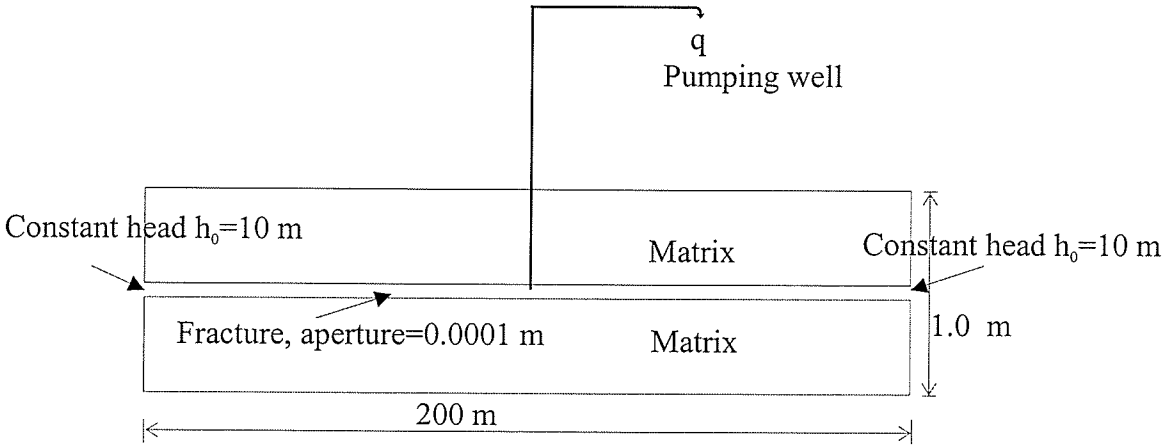

Figure 5-11 The physical system for the discrete fracture flow verification problem

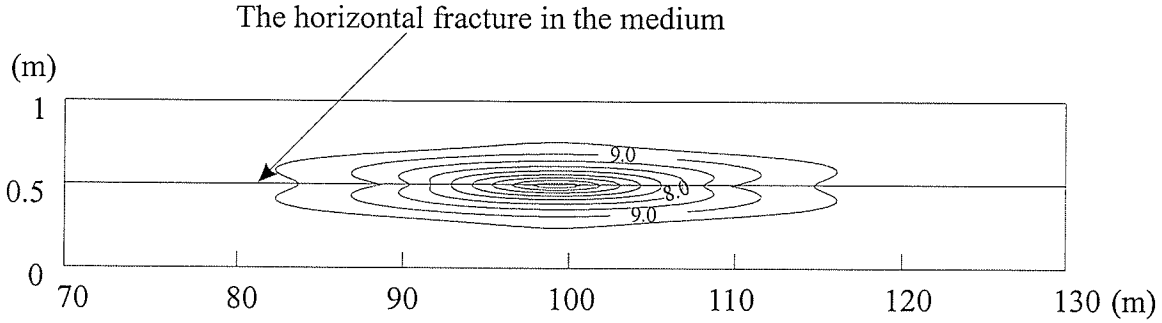

Figure 5-12 Hydraulic head distribution in the discretely fractured medium after 10 day's pumping

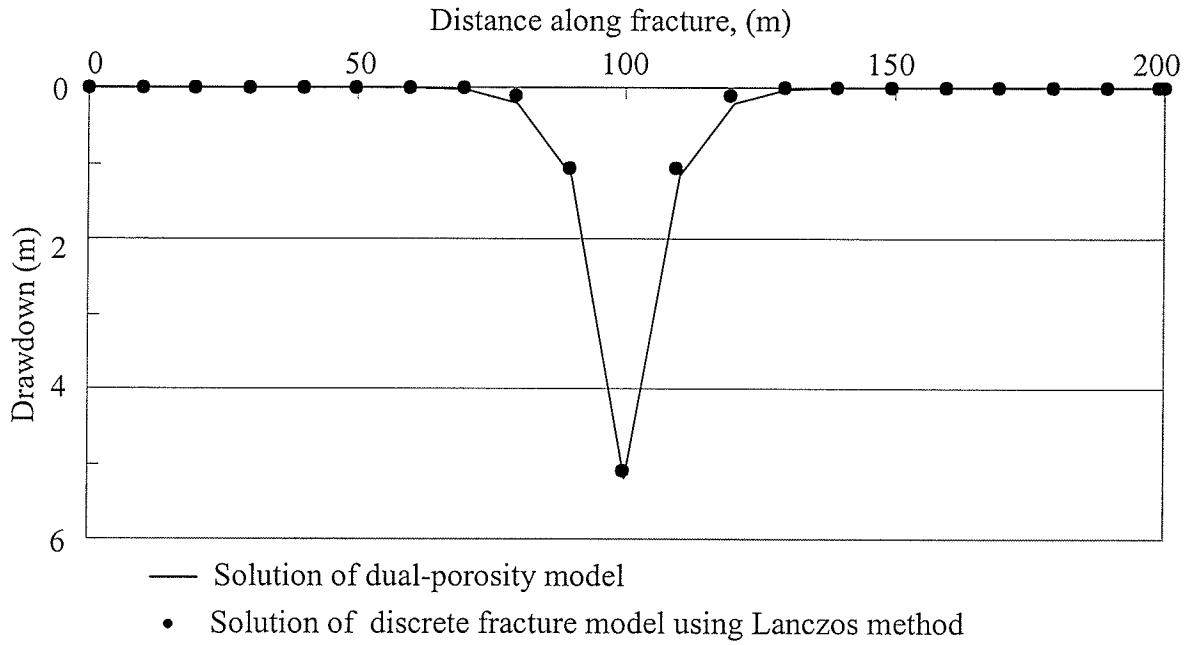

Figure 5-13 Comparison of the computed drawdowns by the dual-porosity model and the discrete fracture model using the Lanczos reduction method.

the center of the fracture with a constant pumping rate of 0.1 m^3/d (see Figure 5-11). The two ends of the fracture in the domain are considered as constant head boundaries. Values of various parameters used in the simulation are given in Table 5.5. The hydraulic conductivity of the fracture can be calculated based on equation (3.8) using the given parameters in table 5.5.

Parameter	Value
Matrix transmissivity T'_x, T'_y	0.0001 m^2/d
Matrix storage coefficient, S'	0.05
Fracture specific storage, S_s	0.0002 m^{-1}
Thickness of the flow system, H	1 m
Fluid density, ρ	1000 kg/m^3
Fluid viscosity, μ	86.4 kg/m.d
Gravity constant, g	7.3223×10^{10} m/d^2

Table 5.5: Parameter values for the discrete fracture flow verification problem

The domain was discretized into 80 rectangular elements and 105 nodes. A uniform nodal spacing of 10 and 0.25 m was used in the horizontal and vertical directions respectively. The one-dimensional linear elements for the fracture have a constant length of 10 m with total 20 elements. In the simulation, a constant time step size of 0.1 day was used for a total of 100 time steps. Convergence tolerance used in the PCG solver equaled 1×10^{-8}. A total 15 Lanczos vectors were used for the simulation. The computed hydraulic head distribution at time equal to 10 days is shown in Figure 5-12. It is clear that the fracture influences the head distribution significantly.

The same problem is solved by a one-dimensional dual-porosity model. Figure 5-13 shows the comparison of hydraulic head solutions along the fracture at the end of the 10th day by both the dual-porosity and discrete fracture models using the LRM. The agreement between the solutions of the two methods is quite good,

despite the fact that both models have different assumptions.

5.6 Single species contaminant transport in discretely fractured porous media

A problem involving solute transport through a single fracture (or a system comprised of closely spaced and parallel fractures) was selected to verify the application of the Arnoldi reduction method to discrete fracture approach. The analytical solution for this problem is provided by Sudicky and Frind [1982].

The input parameters and values for the problem are shown in Table 5.6. In order to compare with the exact analytical solution, the groundwater velocity in the matrix is set equal to 0. Movement of contaminant into the matrix blocks is governed solely by molecular diffusion. The domain is 200 m long in the x-direction and 0.1 m in the z direction. A uniform nodal spacing of 10 and 0.025 m was applied in the x- and z-directions respectively. Using this discretization scheme, a total of 105 nodes and 80 rectangular elements are formed. The discretized nodes include 21 fracture nodes which are connected by 20 one-dimensional linear elements for the fracture. A constant concentration of 1.0 was specified at the upstream end of the fracture. The problem with the same data set has been solved for verifications of different numerical methods [Sudicky 1989; Sudicky and McLaren].

The second scheme which requires two Arnoldi processes is used to solve the problem. A constant time step of 100 days is applied. To reach 20,000 days, 200 time steps are required. A total of 15 Arnoldi vectors are used in both Arnoldi processes. Concentration distributions in the fracture for times equal to 10,000 and 20,000 days are compared to the analytical solutions in Figure 5-14. Good agreement between the analytical and Arnoldi method results can be seen, despite

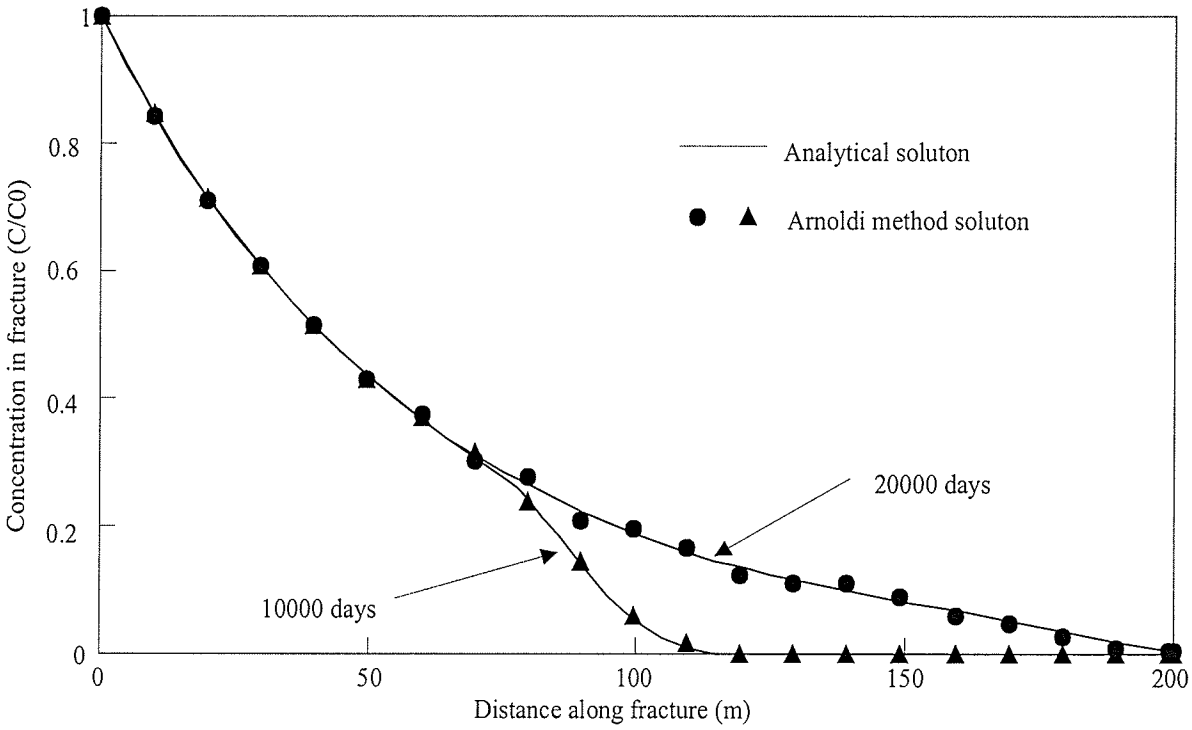

Figure 5-14 Comparison of the Arnoldi method solution with the analytical solution using the discrete fracture model

Parameter	Value
velocity in fracture (m/d)	0.1
Fracture longitudinal dispersivity (m)	0.1
Fracture aperture (m)	1.0×10^{-4}
Fracture separation (m)	0.1
Fracture diffusion coefficient m^2/d	1.38×10^{-4}
Matrix porosity	0.01
Matrix dispersivity	0.0
Matrix diffusion coefficient m^2/d	1.38×10^{-5}
Solute decay coefficient, d^{-1}	1.5377×10^{-4}
Fracture and matrix Retardation factor	1.0

Table 5.6: Parameter values for the discrete fracture transport verification problem

the fact that the numerical solution was obtained by using relatively coarse spatial and time discretizations. For the 20,000 day solution, the numerical results show a slight fluctuation for the part a little far away from the comtaminant source. This circumstance can be eliminated by using more Arnoldi vectors for the solution. It is interesting to note that the problem has a Peclet number of 100 in the direction of flow along the axis of the fracture. If one solves this problem directly based on the original conductivity matrix $\mathbf{K}$, for each Arnoldi reduction solution step more than 200 iterations are required to achieve the 1×10^{-8} convergence criterion. It is difficult to get a convergence solution for this problem due to the large Peclet number. By using the "shift" technique, the problem can be successfully solved (see Chapter 3). After application of a shift factor of 0.002 to the problem, each step in the reduction process requires only 12 iterations on average. The total CPU time for 200 time steps on a Pentium II 333 MHz PC is less than 1 second. The result indicates that the $\mathbf{K}$ matrix with a little "shift" can not only greatly enhance the iterative convergence speed in the ORTHOMIN solution process, but also improve its capacity for problems with large Peclet number.

Chapter 6

Illustrative Examples

Six illustrative generic examples concerning groundwater flow and multi-species contaminant transport in dual-porosity media and discretely fractured media are presented in this chapter. The first problem involves application of the LRM to the modeling of groundwater flow in a dual-porosity aquifer with multiple wells. The second and third examples show the ARM for the simulation of three species decay chain transport and 6 species TCE transport in dual-porosity media, respectively. The fourth example investigates the application of LRM to the discrete fracture flow problem and the last two examples show the application of ARM to 8 species decay chain and 7 species biodegradation transport in discretely fractured media respectively.

6.1 Groundwater flow in dual-porosity aquifer

In order to investigate the efficiency and robustness of the Lanczos method for multiple well system with different time history, a relatively large confined dual-porosity aquifer problem has been solved. Figure 6-1 shows the synthetic aquifer system. The selected domain is a dual-porosity version of the example given in the work of Townley and Wilson [1980]. The example is chosen to include sev-

eral of the commonly occurring complexities in groundwater analysis. It includes Dirichlet boundary conditions and two groups of time-dependent sources with different pumping histories. The fractured rock aquifer system is heterogeneous and anisotropic with respect to the fracture transmissivity. The model parameters are given in Table 6.1.

Parameter	Value
Dimension of aquifer	2000 m
Fracture Transmissivity T_x, T_y	
area 1	10, 10 m^2/d
area 2	100, 30 m^2/d
Pumping rate,	
q_1: ($1 \geq$ t>0 day)	150 m^3/d
($2 \geq$ t>1 days)	100 m^3/d
(t $\geq$ 2 days)	0
q_2: ($1 \geq$ t>0 day)	100 m^3/d
q_3: ($1 \geq$ t>0 day)	250 m^3/d
q_2, q_3: (t $\geq$ 1 days)	0
Fracture storage coefficient, S	0.002
Hydraulic conductivity of matrix, K'	0.0005 m/d
Specific storage of matrix, S'_s	0.005 m^{-1}
Thickness of matrix block, $2a$	5.0 m
Fracture aperture, $2b$	0.01 m
Total thickness of the aquifer	20.04 m

Table 6.1: Synthetic aquifer model parameters

To obtain the numerical solution for the problem, the flow domain was discretized into 10,085 triangular elements and 5,120 nodes. The elements have a size of 10 m near the pumping wells and 100 m in the boundary area. The initial hydraulic head in the fractures is 60 m. A fully penetrating river flows through the area and it is considered to be a first type boundary with a constant head of 60 m. Three pumping wells with different pumping rate are distributed in the area (see Figure 6-1). Well 2 and 3 have the same time-dependent pumping his-

tories, so the three wells and constant heads can be grouped into two groups of time-dependent boundary conditions for the Lanczos method.

Table 6.2 shows the comparison of performance behavior of the Lanczos and direct solution methods. The maximum error, which is defined as the maximum difference between the two solution methods at each time level, is expected to occur at one of the pumping wells. The root-mean-square (RMS) in the table is computed based on the drawdown data at the three wells for all 3,000 time steps. The maximum computed drawdown difference between the two methods is 0.039 m and occurs at well 3 at the first time step. The results of the comparison are very encouraging. For the case of 3,000 time steps and 80 Lanczos vectors used, the Lanczos method is approximately 18 times faster than the direct solution method and the accuracy is almost the same. Even higher efficiency can be achieved if the problem requires more time steps. In addition, if the wells have the same pumping history, only one Lanczos process is needed. The solution time for this problem is still reduced by about 45% compared to the solution time for the original problem which requires two Lanczos processes. The Lanczos method also shows great saving in computer memory. Through the operating system, It was found that the peak computer memory requirement of Lanczos method for this example is about 60% of the memory requirement for solving the original system.

The number of Lanczos vectors determines the accuracy of the method. The maximum error always occurs in the first several time steps or the moment of pumping rate change at a particular well. Figure 6-2 shows maximum errors in the first 10 time steps compared to the number of Lanczos vectors for both homogeneous and heterogeneous situations. For a problem of homogeneous and isotropic hydraulic properties and simple boundary conditions, less Lanczos vectors may be required. Figure 6-2 indicates that if the domain is homogeneous, less

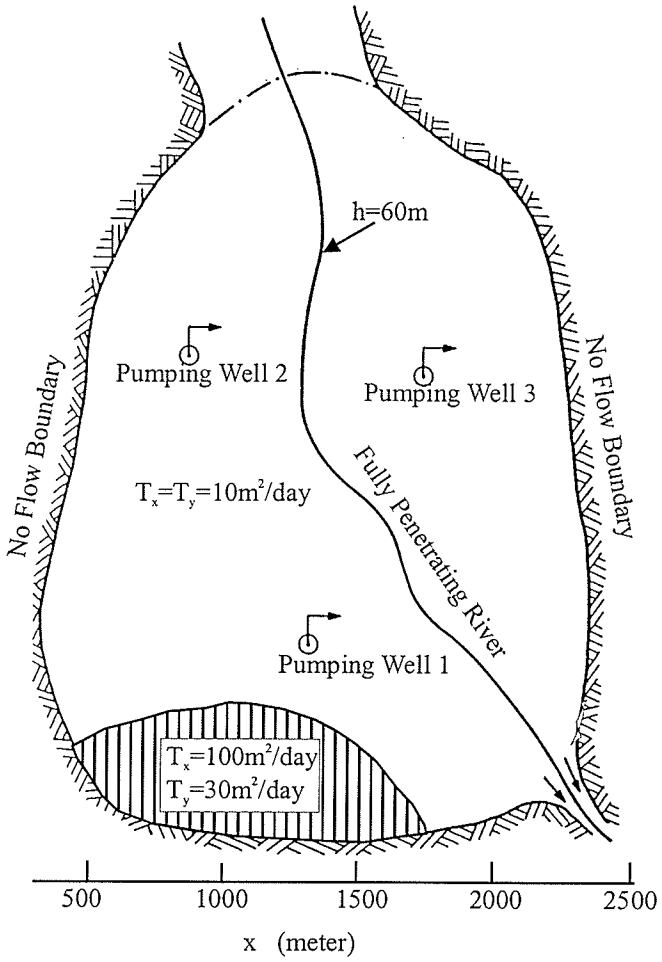

Figure 6-1 Synthetic dual-porosity aquifer system

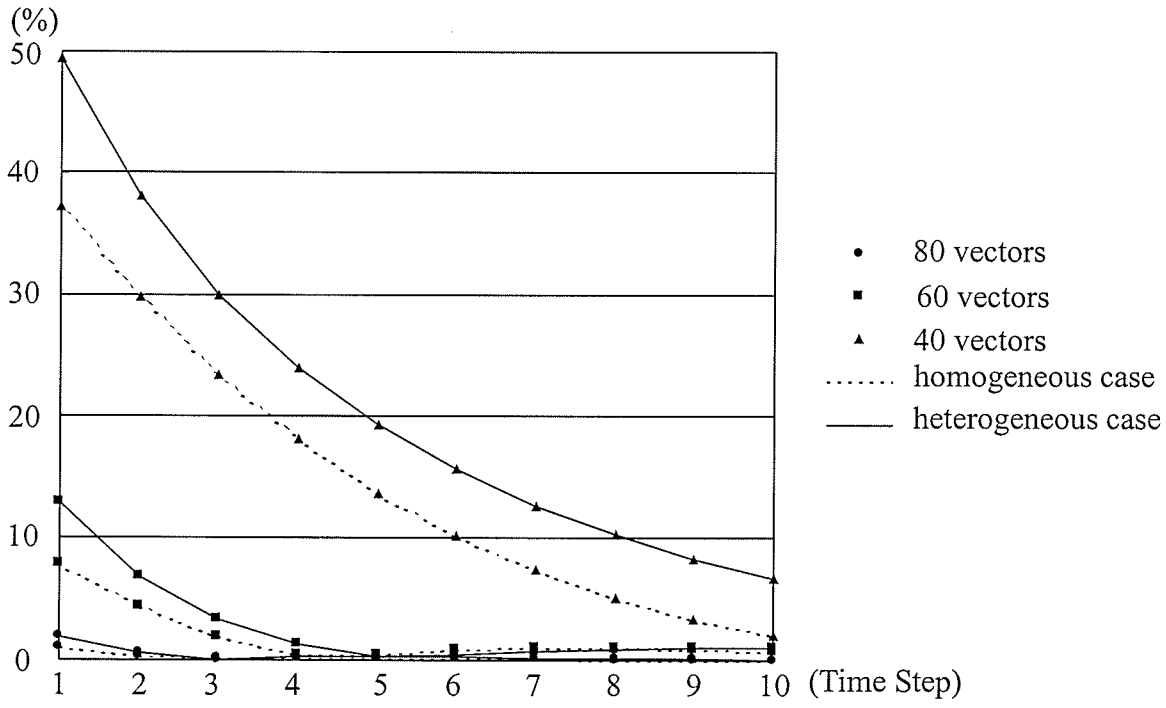

Figure 6-2 The maximum drawdown differences between the Lanczos and direct solution method for homogeneous and heterogeneous cases using different Lanczos vectors up to 10 time steps.

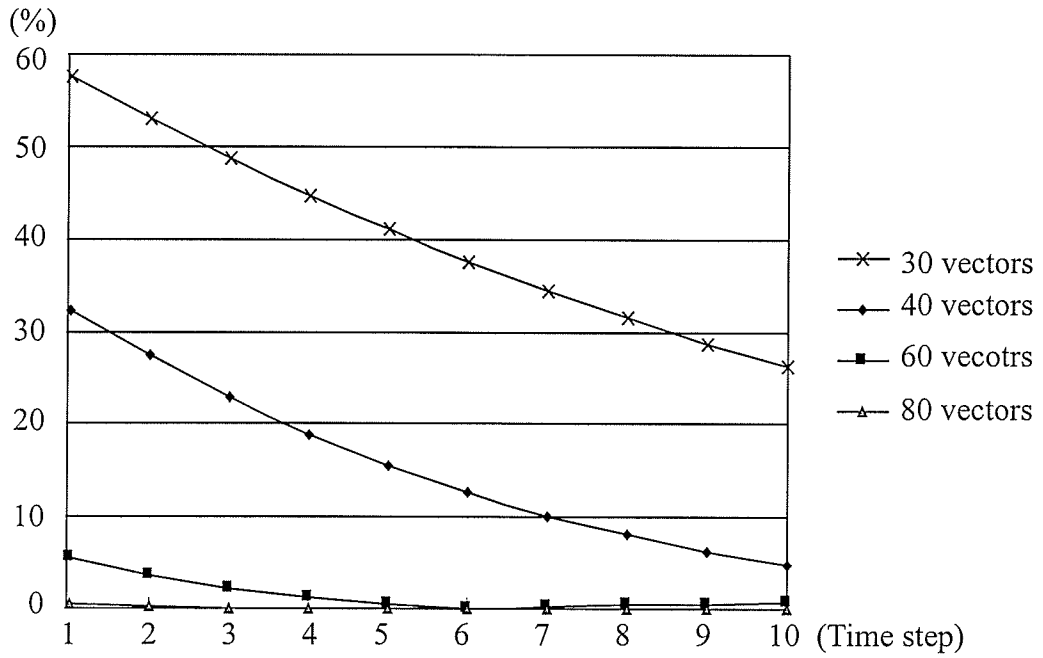

Figure 6-3 The maximum drawdown differences between the Lanczos and direct solution method for the case without a partial grid refinement near pumping wells by using different vectors for the first 10 time steps

Items	Direct solution	Lanczos
Time step size	0.001 day	0.001 day
Time step number	3000	3000
Equation matrix size (n, m)	n=5120	m=80
Total solution time	92 min 34 sec	5 min 12 sec
Maximum drawdown difference		
between the two methods		0.039 m
(in percentage)		1.9 %
RSM error		7.74×10^{-4} m

Table 6.2: Comparison between the Lanczos and direct solution method, a Pentium II 333 MHz CPU with 128M memory personal computer was used for the simulation.

Lanczos vectors are needed to achieve a similar accuracy. In addition, if the heads of the first several time steps are not important for a problem, one can use less Lanczos vectors. For the example, less than 1% drawdown difference (or 0.018 m) will occur by using only 60 vectors after 10 time steps, or 7% for 40 vectors. The time needed to solve the problem is 3 minutes, 32 seconds using 40 vectors and 4 minutes, 20 seconds using 60 vectors.

In order to show the influence of domain discretization on the number of Lanczos vectors, a different discretization scheme was used. The example domain was discretized into 28,514 triangular elements and 14,456 nodes without a refinement near the pumping wells. The new equation system has about 3 times the nodes as the first scheme. However, it requires even less Lanczos vectors to achieve the similar accuracy as the first scheme (see Figure 6-3). Using 60 vectors, a maximum error of 0.074 m and RSM of 2.16×10^{-3} m is reached. The total solution time for 3000 time steps is about 6.7 minutes. This result indicates that the discretization scheme is one of the most important factors in determining the number of Lanczos vectors required.

6.2 Decay chain transport in dual-porosity media

In order to investigate the efficiency and robustness of the proposed approach, the Arnoldi technique is applied to a three species decay chain transport problem which is loosely based on the McClean Lake project in Saskatchewan as shown on Figure 6-4. At the center of study area is a pit which is proposed to accommodate the disposal of uranium tailings generated from several ore bodies. Surrounding the pit is a three meter buffer zone. Because the pit has a funnel shape, the simulated pollution source is smaller than the pit shown on Figure 6-4. Solute transport analyses are required to predict the long term environmental loadings from the tailings. In this example, the computed concentration field is compared to the results computed from a Crank-Nicolson (CN) scheme using a direct solution method. For comparison purposes, two definitions [Woodbury, *et al.* 1990] are used: the maximum error and root-mean-square(RMS) error.

The main radioactive component in the tailings is radium-226. All of the decay products of ^{226}Ra and their half-life are given as: $^{226}Ra \xrightarrow{1600yr} {}^{222}Rn \xrightarrow{3.8day} {}^{218}Po \xrightarrow{3min} {}^{214}Pb \xrightarrow{27min} {}^{214}Bi \xrightarrow{20min} {}^{214}Po \xrightarrow{0.16sec} {}^{210}Pb \xrightarrow{22yr} {}^{210}Bi \xrightarrow{5day} {}^{210}Po \xrightarrow{138day} {}^{206}Pb$. Compared with radium-226 and lead-210, all other components have relatively short half-lives. If the influence of mass loss due to any physical or chemical processes is neglected for all other species, the decay chain may be simplified as $^{226}Ra \rightarrow {}^{210}Pb \rightarrow {}^{206}Pb$, which will predict the worst case of decay of final products. Lead-206, the last element on the list, is not radioactive.

The steady-state groundwater flow in the area is simulated by a two-dimensional single-porosity model. For the steady-state flow, the dual-porosity properties do not affect the groundwater flow behavior. This is because at steady-state there is no fluid exchange between the matrix blocks and fractures. Therefore, the single-

porosity model can be used for the simulation. The average velocities for both the buffer zone and outside zone given by the flow problem solution are used as input data for the three-species decay chain transport problem.

Figure 6-5 shows the finite element grid used for the transport model; a total of 9,308 nodes and triangular 18,094 elements are used. A partial refinement is made near the contaminant source area. A five year time step size is used for the simulation. All the grid Peclet numbers are less than 2. Boundary conditions for the transport model are also shown on Figure 6-5. The contaminant sources are introduced instantaneously at time zero in the pit. The initial concentration within the pit is normalized to one for ^{226}Ra and zero for ^{210}Pb and ^{206}Pb. Note the decaying source concentrations satisfy the Bateman equation and their solutions are given by equation (3.16). The fracture longitudinal dispersivity is set to 10 m and transverse dispersivity is 1.0 m. The molecular diffusion coefficient in the fracture is set at 2.2075×10^{-3} m^2/yr for all the three species. Due to lack of field data, retardation factors in the fractures are assumed to be the same for all the three species. The fracture density in the area is about 30.4 fractures/10 m. Based on this information, the thickness of the parallel slab used in the dual-porosity model can be determined. All the parameters for this example are given in Table 6.3.

The concentration distribution of the three species, after various time periods, are shown in Figure 6-6, Figure 6-7 and Figure 6-8. Figure 6-9 shows the breakthrough curves for a point (x=387.01 m, y=381.77 m) between the pit and Fox Lake. The spreading patterns of these three species are similar and have a physically reasonable concentration distribution. In the period of 10,000 years, most of the radioactive materials will decay to lead-206, which is not a radioactive material. This is because the half-life times of both parent species are much

Parameter	Value
Fracture aperture	$2b = 0.00007m$
Fracture spacing	$2a = 0.35m$
Seepage velocity	
Buffer zone	$v = 2.0m/yr$
Other area	$v = 20.0m/yr$
Secondary porosity	$\phi = 0.0002$
Matrix block porosity	$\phi' = 0.02$
Dispersivity	$\alpha_L = 10.0m, \alpha_T = 1.0m$
Fracture diffusion coefficient	$D^* = 2.2075 \times 10^{-3} m^2/yr$
Matrix diffusion coefficient	$D' = 2.2075 \times 10^{-4} m^2/yr$
Source initial concentration	
^{226}Ra	$C_1^{B0} = 1.0$
^{210}Pb	$C_2^{B0} = 0.0$
^{206}Pb	$C_3^{B0} = 0.0$
Solute decay coefficient	
^{226}Ra	$\lambda_1 = 0.0004332$
^{210}Pb	$\lambda_2 = 0.0315$
^{206}Pb	$\lambda_3 = 0.0$
Retardation factors	
In fracture	$R_1 = R_2 = R_3 = 349.33$
In matrix block	$R_1' = R_2' = R_3' = 1.0$

Table 6.3: Parameter values for the decay chain transport in dual-porosity media case study problem

less than 10,000 years. The speed of transformation from ^{226}Ra to ^{210}Pb is much slower than that from ^{210}Pb to ^{206}Pb. This behavior results from the half-life of ^{226}Ra being much longer than that of ^{210}Pb.

The execution time required for the solution of the three species decay-chain transport problem for 2,000 time steps is about 5.12 minutes by using two Arnoldi processes (using scheme two for a starting vector), and about 3.53 minutes by using single Arnoldi process (using scheme one for starting vector with an average η value) on a Pentium II 350 MHz personal computer. Sixty Arnoldi vectors were used for the solution. The traditional direct solution method on the same

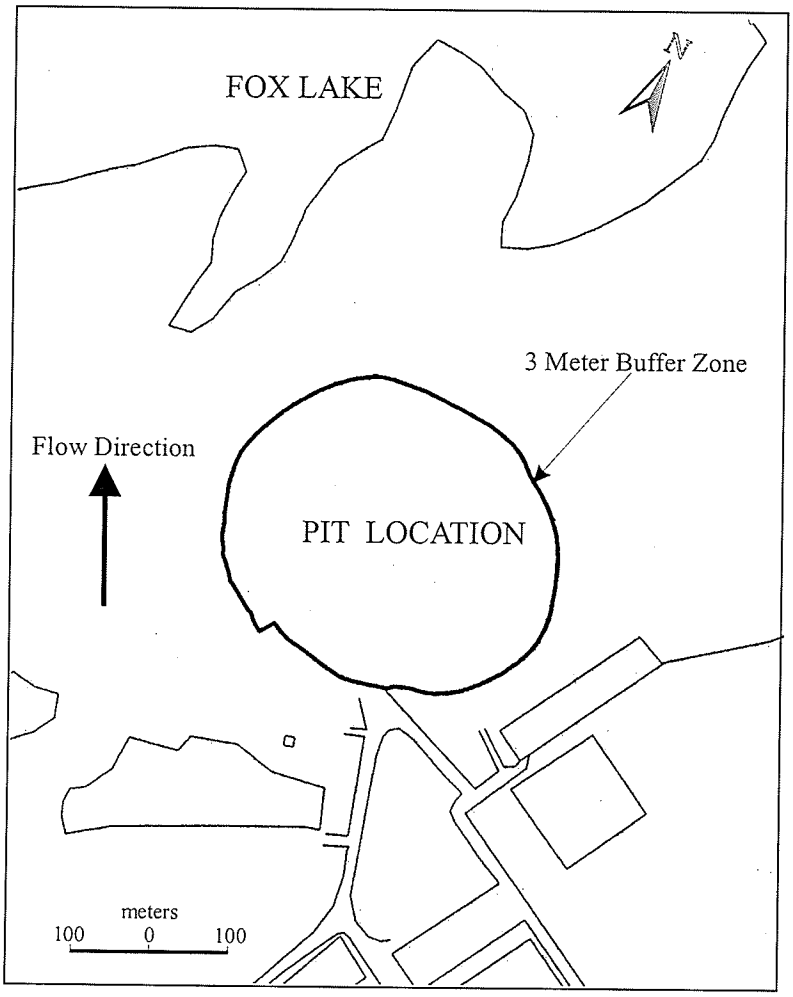

Figure 6-4 Plan view of the simulation area

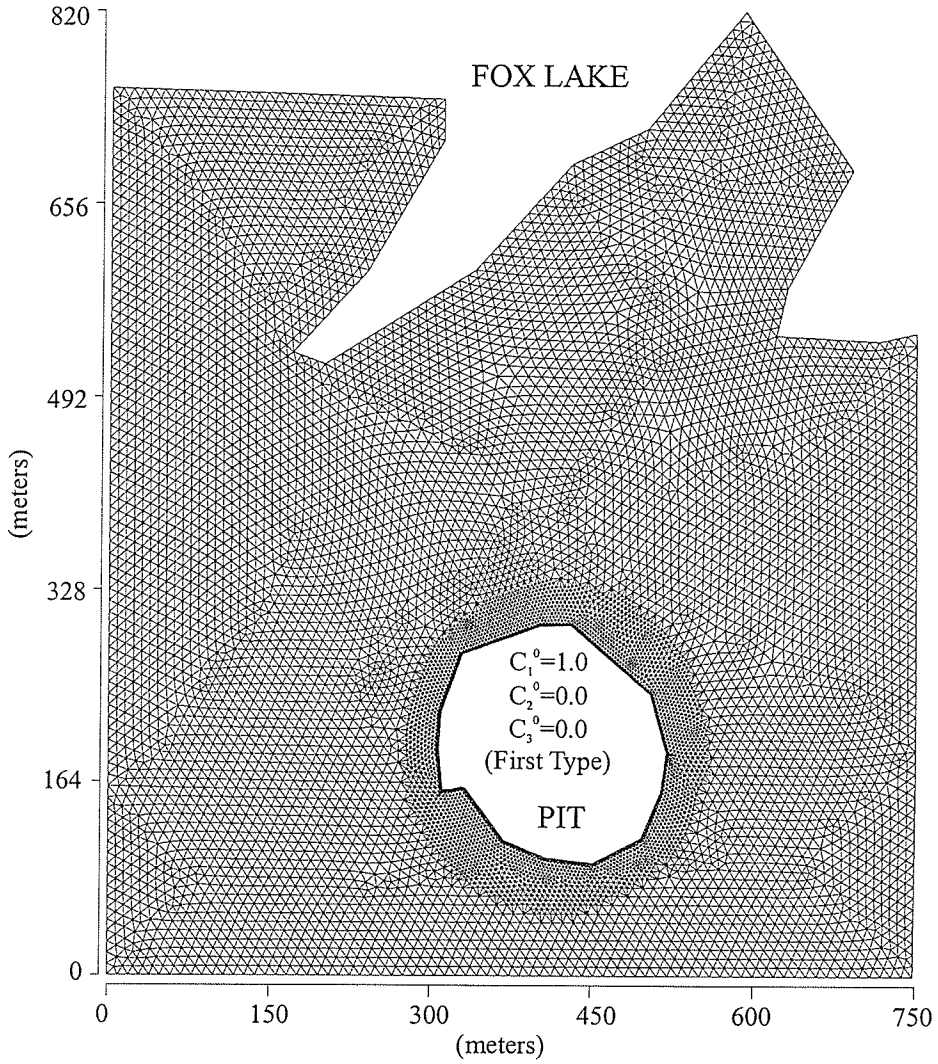

Figure 6-5 Finite element grid used for the example of multi-species decay transport; total 9,308 nodes and 18,094 elements

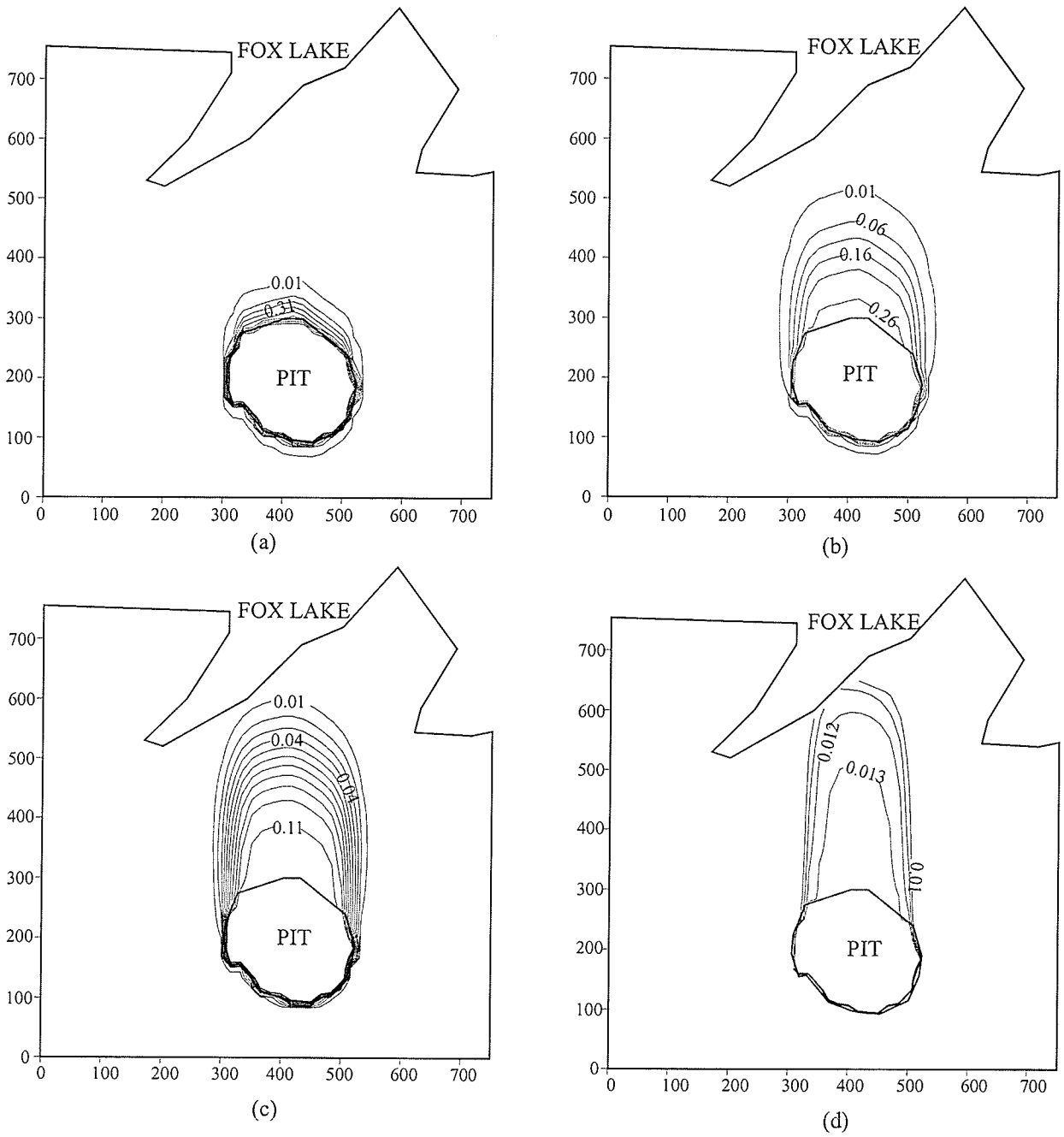

Figure 6-6. Concentration distribution of ^{226}Ra at different time period, (a) 500 years, (b) 3000 years, (c) 5000 years, (d) 10000 years

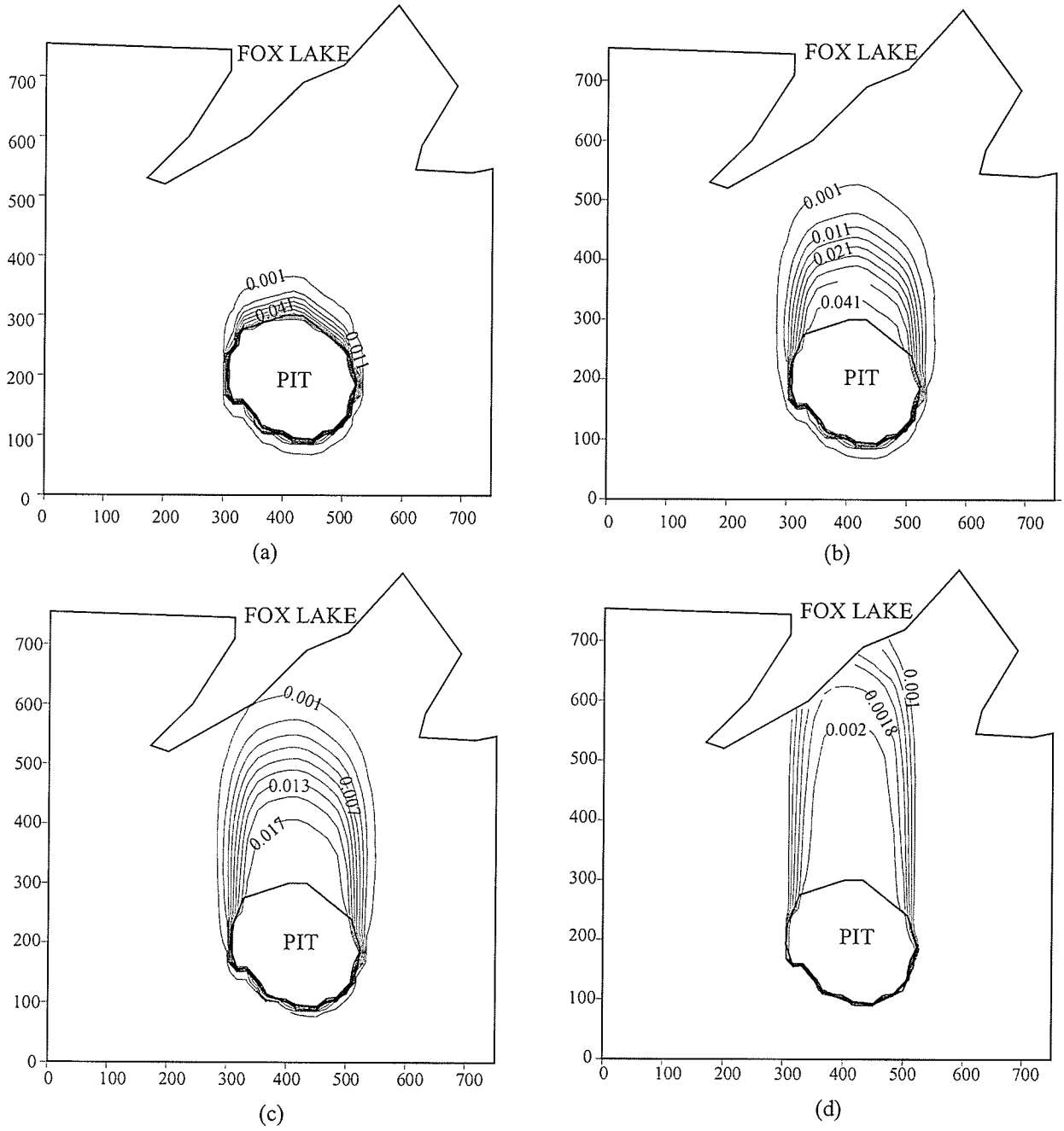

Figure 6-7 Concentration distribution of ^{210}Pb at different time period, (a) 500 years, (b) 3000 years, (c) 5000 years, (d) 10000 years

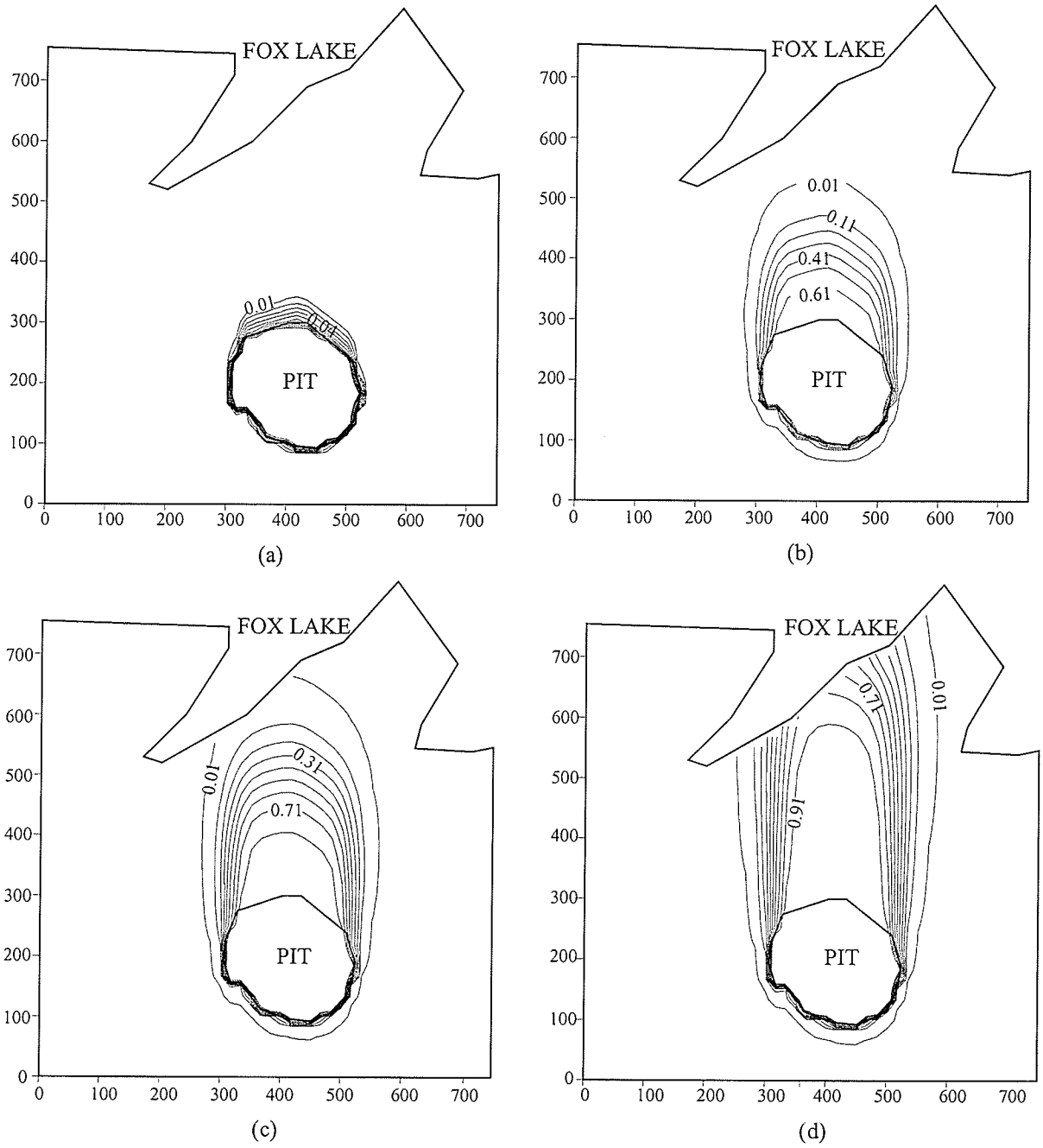

Figure 6-8 Concentration distribution of ^{206}Pb at different time period, (a) 500 years, (b) 3000 years, (c) 5000 years, (d) 10000 years

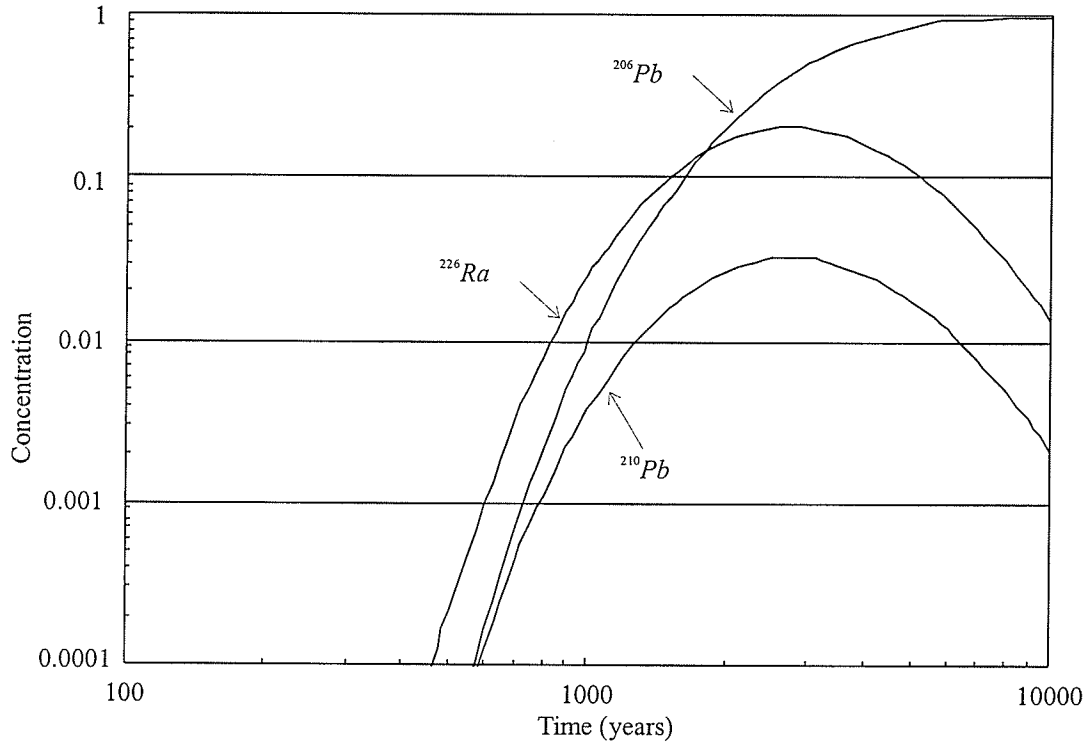

Figure 6-9 Breakthrough curves of the three species predicted by the Arnoldi method at the location x=387.01m, y=381.77m

computer requires about 5.4 hours. The original equation system has a bandwidth of 142. For this problem, the Arnoldi method needs only about 1.1% of the execution time of the classic Crank-Nicolson solver. For problems with more time steps, even higher efficiency in execution time can be reached. Table 6.4 lists error comparisons with respect to the solution by the traditional method. The table shows that the RMS error is of the order of 10^{-4} and the maximum error is of the order of 10^{-3}. Even though the third species has relatively high maximum errors, the maximum error in percentage is less than 3% (the percentage error is defined by dividing maximum error by the concentration of that point). These data indicate that 60 vectors is enough to produce good approximations to the solution by the classic method. Note, however, that the percentage of Arnoldi vectors to the total number of nodes is different in each case. Therefore even for extremely large grids in three dimensions only a small number of vectors will be required to solve a problem [Woodbury *et al.*, 1990].

Through the Task Manager of Windows NT^{TM} system, it is found that the peak memory requirement to solve this problem by the Arnoldi method is about 25% of the peak memory requirement of the direct solution method. A personal computer with 64 MB memory can be used to solve this problem by the Arnoldi method without extensive use of virtual memory. The great saving in computer memory makes it possible to use a personal computer to solve large contaminant transport problems. It is interesting to note for more species only very little additional memory and computing time are required. This is due to the fact that for each additional species, the additional required storage space and computing time are for storing and solving an additional reduced equation system, which is much smaller compared to the original system. An estimation is made for this example that for each additional species, less than 0.5 MB additional memory and

Time	^{266}Ra	^{210}Pb	^{206}Pb
One Arnoldi Process:			
RMS error			
500 years	0.139E-2	0.356E-3	0.208E-3
3000 years	0.210E-2	0.955E-3	0.389E-2
5000 years	0.126E-2	0.470E-3	0.437E-2
10000 years	0.238E-3	0.664E-4	0.405E-2
Maximum error	0.203E-1	0.346E-2	0.228E-1
Maximum error in Percentage	6.0%	8.3%	2.8%
Two Arnoldi Process:			
RMS error			
500 years	0.114E-2	0.257E-3	0.129E-3
3000 years	0.206E-2	0.906E-3	0.376E-2
5000 years	0.125E-2	0.468E-3	0.425E-2
10000 years	0.238E-3	0.663E-4	0.398E-2
Maximum error	0.151E-1	0.345E-2	0.221E-1
Maximum error in Percentage	4.5%	8.2%	2.7%

Table 6.4: RMS errors and maximum errors of the Arnoldi method with respect to classic CN solver

less than 1 minute additional solution time are required. It is estimated that a 50 species contaminant transport problem with 10,000 nodes can be solved on a 96 MB PC computer by using the Arnoldi reduction method.

6.3 TCE transport in dual-porosity media

This problem involves the transport of TCE and its degradation products from three point pollution sources in a dual-porosity aquifer. The presence of volatile organic compounds, including TCE, were identified in well water samples from an industrial site in Manitoba. The industrial site has been in operation for approximately 30 years and used chlorinated solvents TCE and TCA as a metal cleaning fluid. The regional groundwater system, pollution sources and modeling domain are shown in Figure 6-10 [Song and Woodbury, 1998]. It must be emphasized

that only a semi-quantitative analysis of the case study is possible at this time, and this simulation is intended to show the generic modeling capabilities of the proposed method. Consequently, a detailed calibration to observed data is not possible at this site.

The major aquifer underlying the site is a fractured carbonate aquifer which is confined by glacial drift. The fractures observed in drill core are mainly horizonal to sub-horizontal. Discrete packer sampling from boreholes indicates that the concentrations of contaminants are distributed in layers. Therefore, the aquifer system can be regarded as a typical dual-porosity medium. Also based on the packer sampling results, it is assumed that the matrix slab has a thickness of $2a = 10$ m and the fractures have a constant aperture of $2b = 5 \times 10^{-4}$ m, which gives a secondary porosity of 5×10^{-5}. According to the regional groundwater flow condition (Figure 6-10), boundary conditions for groundwater flow are constant head on the east and west sides of the domain, and no-flow boundaries on the north and south sides, resulting in fluid flow from west to east with an approximately uniform velocity. The average flow velocity of 1.0 m/d in the W-E direction and 0.1m/d in the N-S direction are applied to the simulation. The study domain covers a range of 3,200 m by 2,000 m and the Galerkin finite element method is used to discretize the problem, with uniform linear triangular elements. The maximum nodal spacing is about 20 m and is decreased to about 10 m near the contaminant source areas. Discretization of the fracture domain results in 20,981 nodes and 41,440 elements. Each one-dimensional matrix block is discretized into 55 nodes. Using this discretization scheme, a total of $55 \times 20,981 \times 6 = 6,923,730$ unknowns are needed to be solved at each time step. A constant time step size of 10 days is used for all transport simulations. The simulation is terminated at 30 years with a total of 1,095 time steps.

Transforming	Half-life
TCE→ cis-1,2 DCE (λ_{12})	200 days
TCE→ tran-1,2 DCE (λ_{12})	300 days
TCE→ 1,1 DCE (λ_{13})	300 days
cis 1,2-DCE→ VC (λ_{25})	140 days
tran 1,2-DCE→ VC (λ_{35})	20 days
1,1-DCE→ VC (λ_{45})	70 days
VC→ Ethene (λ_{56})	1 year
Ethene→ (λ_{67})	10 years

Table 6.5: Half-life of TCE and its biodegradation products

Chlorinated solvents undergo chemical reactions with half-lives ranging from several days to years. Table 6.5 lists typical half-life data [Woodbury and Li, 1998] which are used in the simulations. A constant retardation factor of 1.0 is applied to all six species. The pollution sources in the fractured medium are treated as the internal Dirichlet conditions in which the concentrations are prescribed as constant values. The concentrations of TCE at the three point sources are set to 120,000, 20,000 and 15,000 ppb respectively, and the degradation species, DCEs, VC and ethene are set to zero for all time. Other parameter values used in the simulation are listed in Table 6.6 [Song and Woodbury, 1998].

Parameter	Value
Porosity of the matrix blocks	0.01
Secondary porosity	5×10^{-5}
Fracture diffusion coefficient	7.29×10^{-5} (m^2/d)
Matrix diffusion coefficient	7.29×10^{-6} (m^2/d)
Longitudinal dispersivity	25 m
Transverse dispersivity	7 m

Table 6.6: Parameters for TCE transport in dual-porosity media

The concentration distributions in the fracture for the first species (TCE) and sixth species (ethene) at the time of 30 year are shown on Figure 6-11. Also

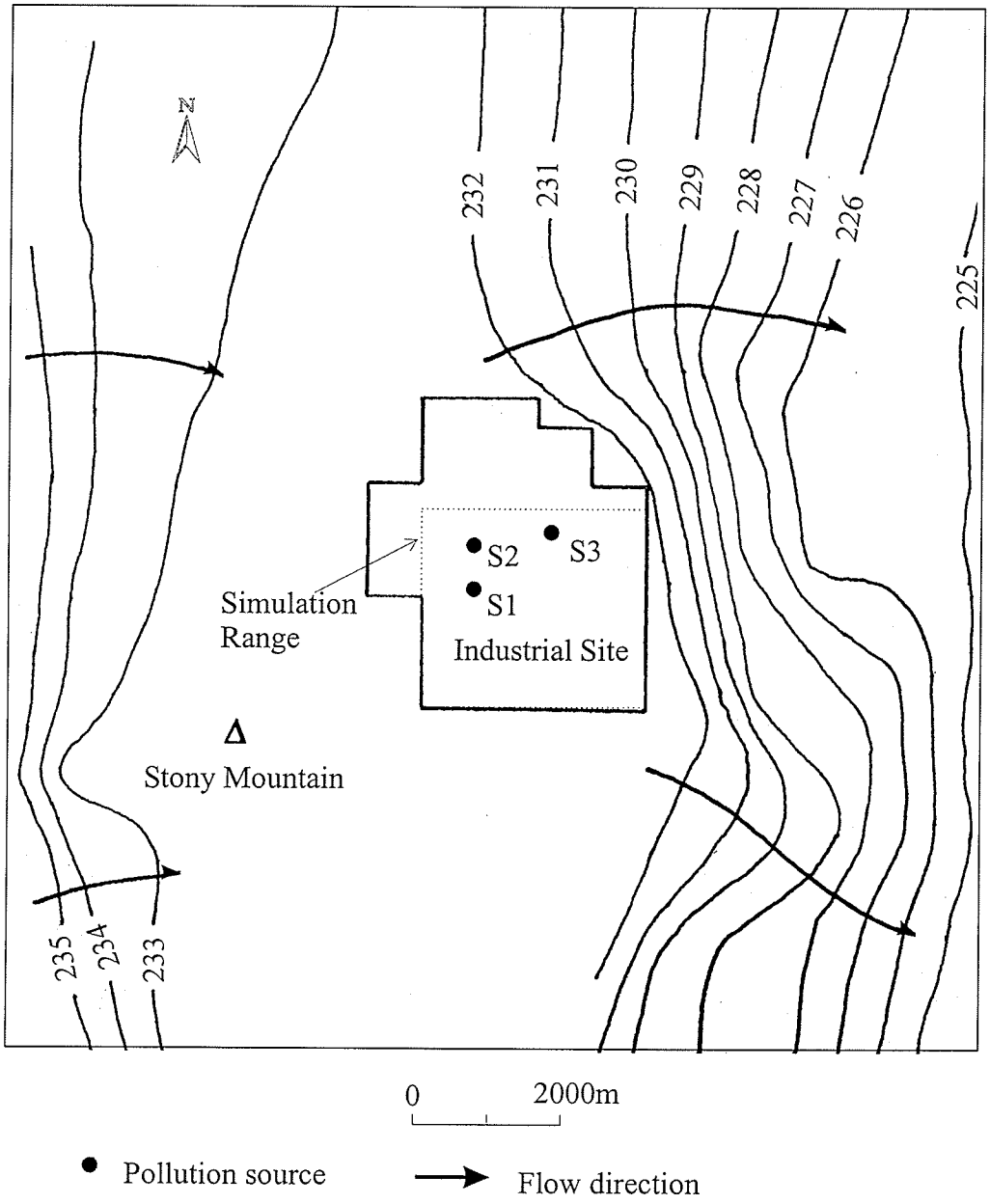

Figure 6-10 Regional groundwater flow system and pollution sources in the area. The contour lines are the hydraulic head distributions (Song and Woodbury, 1998)

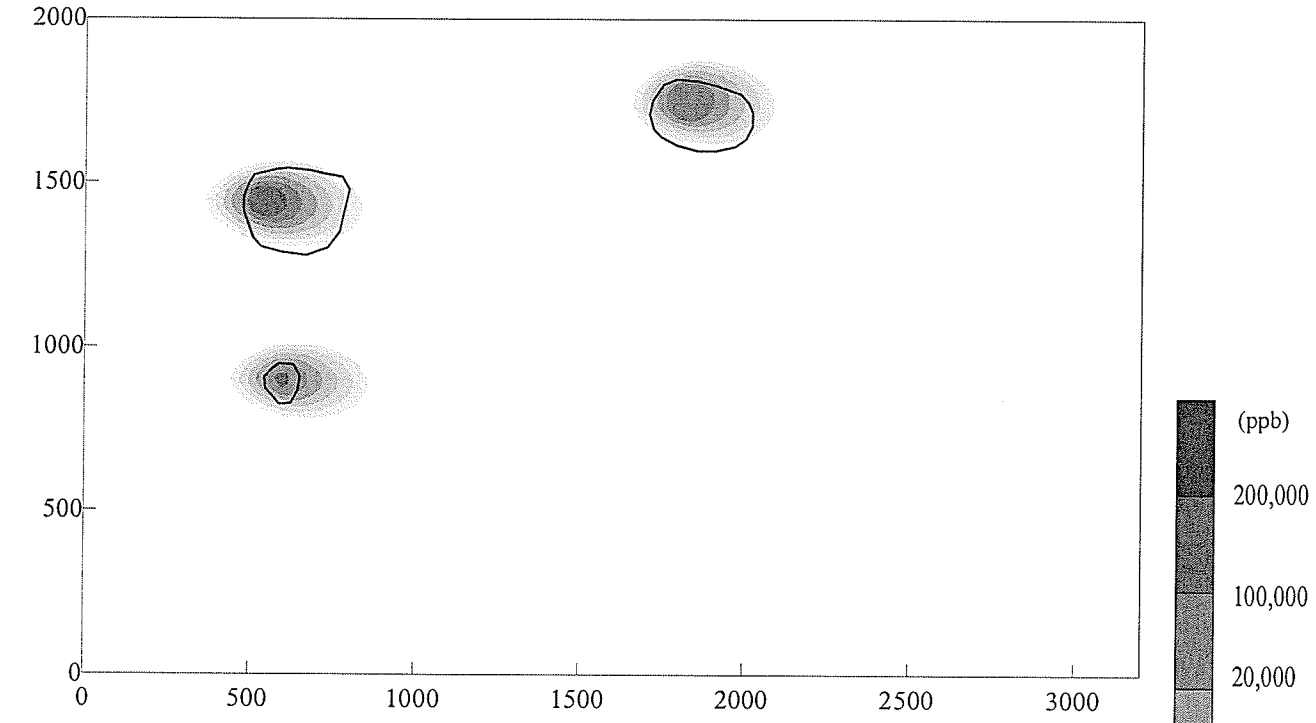

(a) Species 1 (TCE)

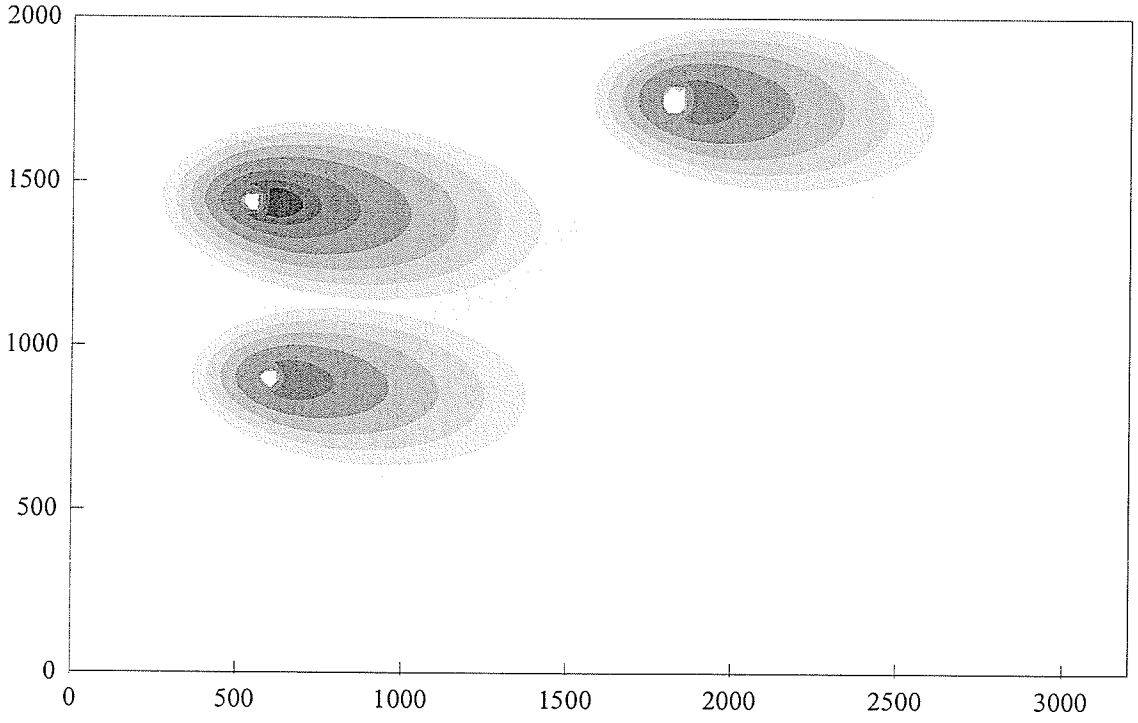

(b) Species 6 (ethene)

Figure 6-11 The concentration distributions of species 1 (TCE) and species 6 (ethene) in the fracture after 30 year release of pollution sources. ⬭: Measured 1.0 ppb pollution plume

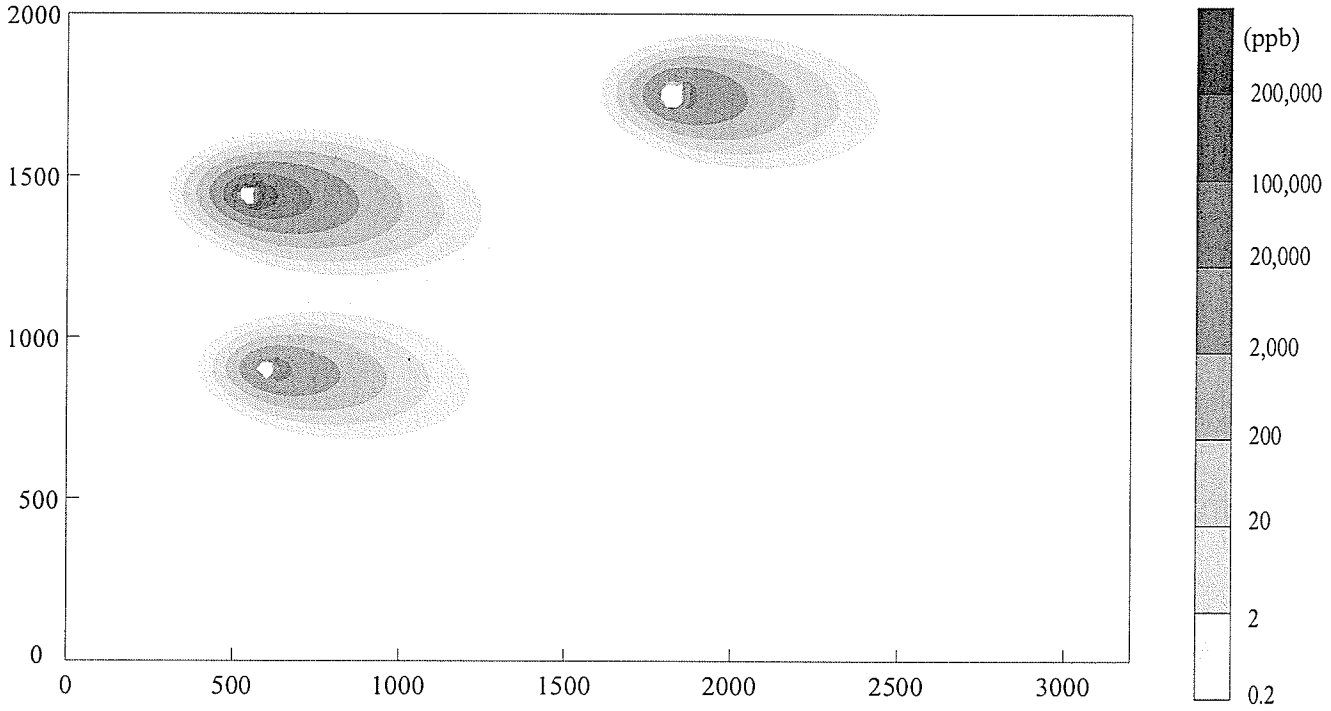

Figure 6-12 The concentration distribution of species 6 in the matrix with 3 m away from fracture after 30 year release of pollution source.

shown on Figure 6-11(a) is the measured 1.0 ppb TCE plume after about 30 years. Unfortunately these were the only data available for comparison. In addition, no measurements of biodegradation products are available for analysis. Nevertheless, it is felt that the numerical scheme could be used at a site where such data is available and are looking forward to incorporating the model in a well documented area. TCE has a smaller contamination plume size compared to the plume size of ethene. This is due to the fact that the ethene has a longer half-life than TCE. The other four species have similar plume shapes but different sizes. Figure 6-12 shows the concentration distribution of species six in the matrix medium (3.0 m away from fracture). It is clear that the concentration decreases rapidly into the porous matrix.

In this example, 200 Arnoldi vectors are used. The number of Arnoldi vectors is one of the most important parameters determining the accuracy and efficiency of the Arnoldi reduction method. Based on the convergence criteria, the number of Arnoldi vectors can be determined during the process. In addition, the problem has been tested with 250 Arnoldi vectors and found almost the same results as the 200 vector solution case. It is interesting to note that the number of Arnoldi vectors required for a problem is dramatically reduced if the simulation domain is discretized into a homogeneous grid size.

Due to the large number of degrees of freedom of the original equation systems, it is difficult to compare solution times for a classic time marching solution of (4.24)-(4.27) to that of the Arnoldi method for (4.33)-(4.36). However, the computation loads for the example for both the Arnoldi method and traditional method with Crank-Nicolson scheme can be qualitatively estimated. Table 6.7 shows the comparison of computational effort for the different methods. It is clear that the Arnoldi method is more efficient than classic time marching.

Traditional method	Arnoldi reduction method
• Solve the original equation system of size $20981 \times n_b$ for 1095×6 times.	• Solve the original equation system of size $20981 \times n_b$ for 200 times[(1)].
• Solve the equation system for matrix block of size 55×3 for $20981 \times 1095 \times 6$ times.	• Solve the reduced equation system of size 200×200 for 1095×6 times[(2)].
	• Solve the equation system for matrix block of size 55×3 for $200 \times 1095 \times 6$ times.

Table 6.7: The computation work need to be done for both the Arnoldi and traditional methods for the example, n_b is full band width of the original equation system. (1) The Arnoldi process requires (as a principal computation overhead) approximately m (=200)forward solutions of original equation system. (2) The reduction method needs a little additional computation effort to transform the reduced space solution to original solution at any desired time step or location.

For this problem, the total solution time for 1095 time steps is about 23.4 minutes on a Pentium II 350 MHz personal computer. Note that the total time for the solution procedure is dominated by the reduction process. If the reduction process is performed by a more efficient numerical solution method, such as ORTHORMIN iterative solver [Vinsome, 1976], even higher efficiency can be reached by the reduction method.

6.4 Flow in discretely fractured media

Groundwater transient flow in a two-dimensional saturated porous matrix containing a randomly distributed and fully penetrated fracture network is used to demonstrate the efficiency and accuracy of the discrete fracture flow model. A comparison is made with the classic Crank-Nicolson method using a PCG solver. The domain is 200 m in length and 100 m in width with a constant thickness of 10

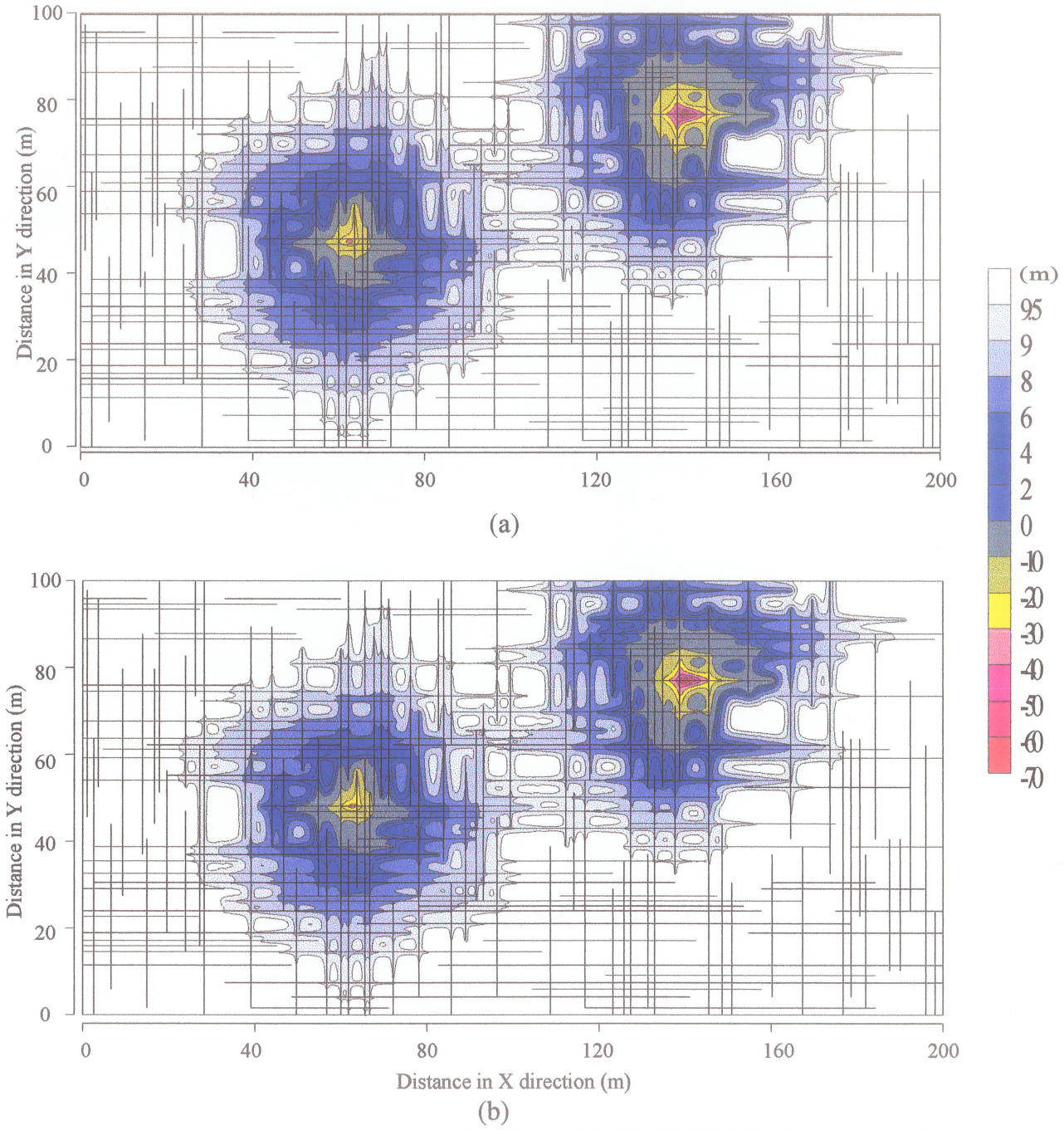

Figure 6-13 Groundwater head distribution after 3 year pumping, (a) Solution of the Lanczos method, (b) Solution of classical time-marching PCG method.

m (see Figure 6-13). The fractures are generated randomly in the two-dimensional plane. The fractures can be distributed in any direction. Consistent with Sudicky and Mclaren [1992], in this study two orthogonal sets of fractures are used, one set being parallel to the x direction and the other parallel to the y direction. The fractures have a constant aperture equal to 3.0×10^{-5} m. Two pumping wells are located inside the domain. The first at x=139.89 m, y=77 m has a constant pumping rate of 200 m^3/y, and the second at x=62.68, y=48.17 m has a constant pumping rate of 150 m^3/y.

The transmissivity and storage coefficient for the matrix blocks are 3.1536×10^{-2} m^2/y and 0.03, respectively. The fractures have a specific storage of 0.001 m^{-1}. Their conductivity can be computed by equation (3.8) using the constants given in Table 5.5. The boundary conditions for the problem consist of a specified hydraulic head equal to 10 m along the right-hand boundary and the lower half part of the left-hand side boundary (y=0-50 m).

The program PREFRAC [Sudicky and McLaren, 1998] is used for the domain discretization. The generated mesh contains a total of 121,408 nodes, including 404 first type boundary nodes. The fractured porous medium is represented by 120,690 rectangular elements, 10,445 horizontal fracture elements, and 10,140 vertical fracture elements. The convergence criterion used in the PCG iteration solver is 1×10^{-8} m for both classic time-marching solution and Lanczos reduction process. For the reduction method, a shift factor equal to 30.0 is used. Figure 6-13(a) and (b) show the solutions of hydraulic head distribution in the domain after 3-year pumping using Lanczos method and PCG method, respectively. The comparison indicated that both methods yield nearly identical results.

The total CPU time for 3000 time steps using the classic method is about 5.93 hours, and the Lanczos method is about 0.95 hours on a Pentium II 350

MHz personal computer. A total of 500 Lanczos vectors are required for this problem. The classic method requires an average of 32 iterations for each solution step. In the reduction process only about seven iterations are required for each recursion step when the "shift" technique is applied. It is interesting to note that solving the problem for 30,000 time steps using the Lanczos method requires only about 50 seconds more time compared to solving 3000 time steps. However, for a traditional time-marching method the solution time for 30,000 time steps can be 10 times the solution time for 3000 time steps. Therefore, the reduction method is extremely efficient for large scale and long time simulations.

6.5 Decay chain transport in a complex fracture network

The transient migration of an eight component decay chain transport in a two-dimensional saturated porous matrix containing a complex fracture network is used to demonstrate the performance of ARM for the simulation of decay chain problems using the discrete fracture approach. A comparison with the Laplace Transform Galerkin (LTG) method described by Sudicky [1989] is made. Implementation of the LTG method using the commercial software FRACTRAN can only handle single species problems. Therefore the comparison for both efficiency and accuracy is limited to the first species.

The geometry of the problem is a rectangular cross section of length 200 m with a thickness of 30 m. The radioactive pollution source is located on the left top (x=15-30 m, y=27-30 m) of the cross section. The physical properties of the waste zone, porous matrix and fracture are given in Table 6-8. The conductivity of fractures can be computed based on equation (3.8) using the values of fluid density, viscosity and gravity constant presented in Table 5.5. The fracture distribution

is shown in Figure 6-14. The fracture distributions are idealized horizontally and vertically. Densities of horizontal and vertical fracture decrease with the depth. All the fractures have a constant aperture of 5.0×10^{-5}m.

Parameter	Porous matrix	Waste Zone	Fractures
Hydraulic conductivity, m/y	0.31536	31.536	-
Porosity	0.3	0.3	1.0
Longitudinal dispersity, m	0.1	0.1	0.1
Transverse dispersivity, m	0.05	0.05	-
Diffusion coefficient, m^2/y	0.0028	0.0028	0.0568
Retardation factor for all species	1.0	1.0	1.0

Table 6.8: Physical properties of 8 species decay chain transport in discrete fracture media

The main radioactive component in the pollution source is considered to be radium-226. The decay products of ^{226}Ra and their half-lives are given as: $^{226}Ra \xrightarrow{1600yr} {}^{222}Rn \xrightarrow{3.8day} {}^{218}Po \xrightarrow{3min} {}^{214}Pb \xrightarrow{27min} {}^{214}Bi \xrightarrow{20min} {}^{214}Po \xrightarrow{0.16sec} {}^{210}Pb \xrightarrow{22yr} {}^{210}Bi \xrightarrow{5day} {}^{210}Po \xrightarrow{138day} {}^{206}Pb$. Half-life times of the radionuclides are greatly different from species to species. Due to the extremely short half-life time of Polonium-218 and Polonium-214, these two components are neglected in the simulation. This study focuses on the other eight species of the decay chain.

The flow velocities for both matrix blocks and fractures are determined by solving the steady state flow problem of the domain. All sides of the domain represent constant head boundaries except the bottom which is an impermeable boundary. The left and right side have a constant hydraulic head of 31 m and 30 m, respectively. Along the top, the head decreases linearly from 31 m on the left to 30 m on the right. These boundary conditions cause groundwater to move through the domain primarily in the horizontal direction from left to right. The waste zone represents a contaminant source with a unity concentration for the first component (^{226}Ra) and 0.0 concentration for all other species at all the time.

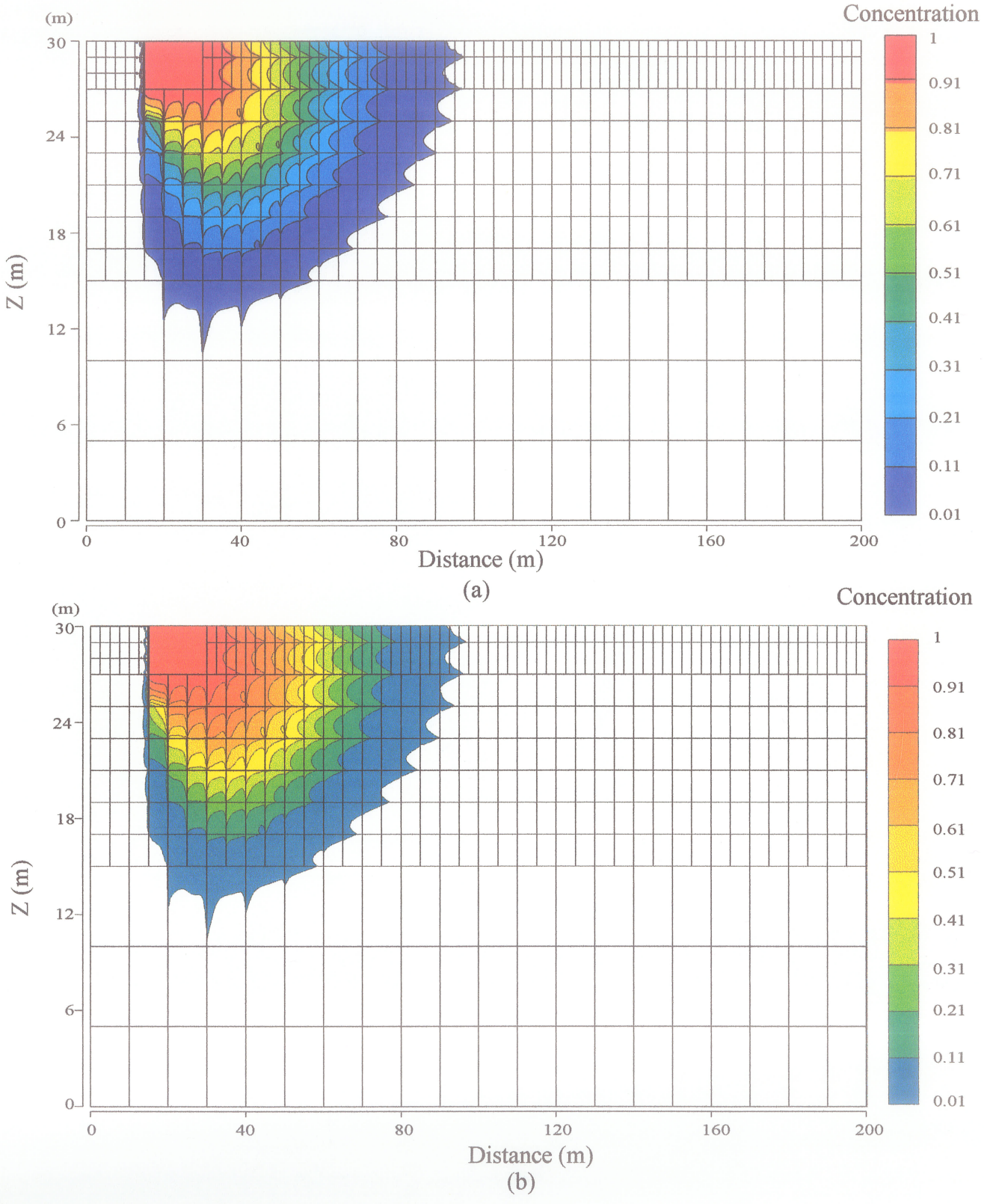

Figure 6-14 Concentration distribution of the first species of decay chain transport in discrete fractures 1000 year after release of pollution source, (a) by LTG method, (b) by Arnoldi method

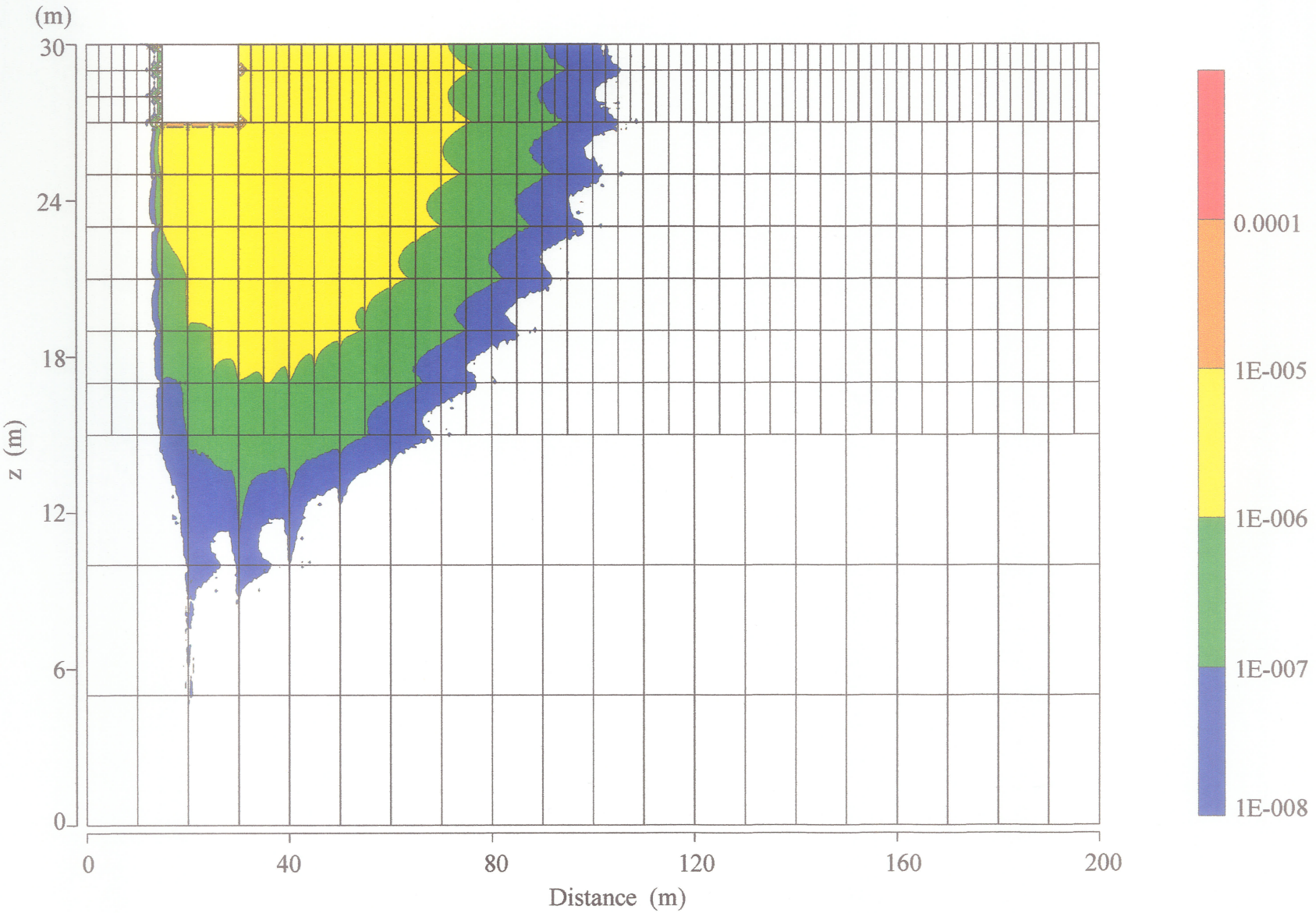

Figure 6-15 Concentration distribution of the 2nd species of decay chain transport in discrete fracture media 1000 year after release of pollution source (by Arnoldi method).

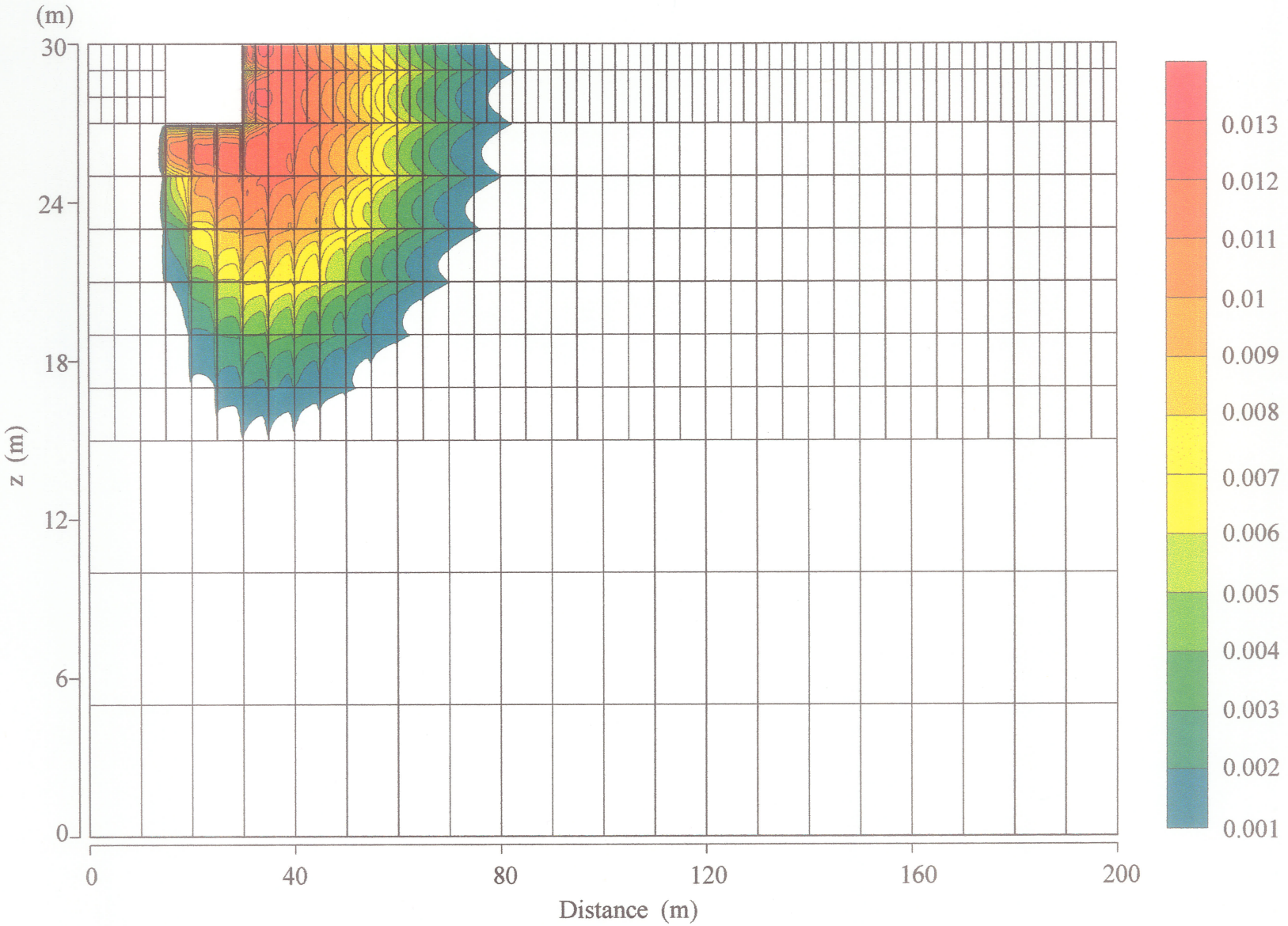

Figure 6-16 Concentration distribution of the fifth species of decay chain transport in discrete fracture media 1000 year after release of pollution source (by Arnoldi method).

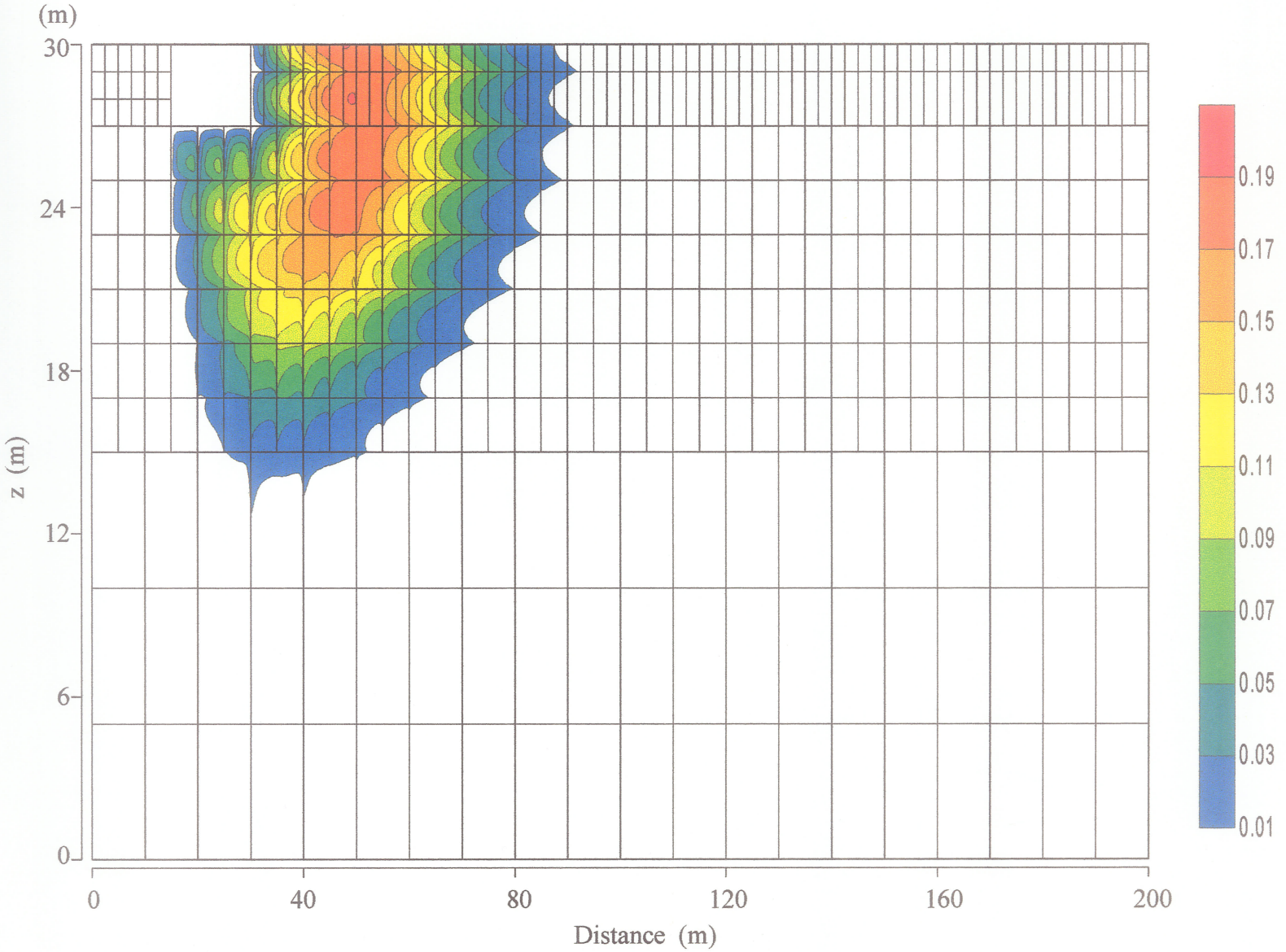

Figure 6-17 Concentration distribution of the 8th species of decay chain transport in discrete fracture media 1000 year after release of pollution source (by Arnoldi method).

The domain was discretized into 120,701 nodes with 120,000 rectangular elements representing the porous matrix, 4,430 horizontal fracture elements and 10,350 vertical fracture elements. With this discretization scheme, the waste zone contains 961 constant concentrations nodes. The convergence criterion used in ORTHOMIN for the Arnoldi reduction process equals 1×10^{-8}. A constant time stepping with a size of 1 year was used to march the solution to 1000 years for the ARM solution. A shift factor of 0.4 is used.

The same data set were applied to the LTG method. Figure 6-14(a) and (b) shows the concentration solutions for the first species (^{226}Ra) of the decay chain by ARM and LTG method, respectively. Comparison of the two computed concentrations indicates that the both methods yield nearly identical results. For this problem the LTG method requires 21 ORTHOMIN iterations on average for each of the 11 p space solutions. The solution for each Arnoldi vector in the reduction process requires about 5 ORTHOMIN iterations. A total of 71 Arnoldi vectors are required for this problem. The size of the reduced equation is only 1/1700 of the original equation system. For the solution of t=1000 years, the total CPU time for single species using the LTG method is 4.72 minutes on a Pentium II 350 personal computer. The total CPU time for 8 species using the ARM is 4.63 minutes on the same computer. Solving all the 8 species with 30,000 time steps using the ARM for this problem (30,000-year simulation) requires about 17 minute CPU time. The simulation results indicate that the ARM is extremely efficient for large problems and long time simulation.

Figure 6-15, 6-16 and 6-17 show the concentration distribution of species 2 (^{222}Rn), 5 (^{210}Pb) and 8 (^{206}Pb), respectively. The rapid advance of the plume front in the fractures and the smoothing effect of diffusion in the matrix are quite apparent for all the species. All the 8 species have similar pollution plume pat-

tern. However their concentration values are tremendously different from species to species. This is due to the large difference of half-life times for the different species. The 8th species *Pb*-206 is a stable component and does not decay to other materials. Due to this fact, the species has the highest concentration plume compared to other daughter products. The zone of its peak concentration has shifted to approximately 20 m down gradient from the waste zone after 1000 years. The problem has been tested with different hydraulic conductivities and diffusion coefficients for the matrix block. The results indicate that these two parameters control the regularity of concentration distributions. Detailed discussion of factors controlling concentration distribution can be found in the work of Harrison *et al.* [1992]. From this example, it can be concluded that the decay chain transport is not only controlled by advection, dispersion and diffusion but also greatly influenced by the half-lives of the chain components.

6.6 Seven species PCE transport in discretely fractured aquitard with an underlying aquifer

This example deals with the transport of PCE and its biodegradation products in a two-dimensional cross section comprised of a low-permeability clay aquitard overlying a sandy aquifer. A similar aquitard-aquifer system has been used in many examples for demonstration of different discrete fracture models [Sudicky and McLaren, 1992, Harrison, 1992; Therrien and Sudicky, 1996]. Surficial clayey deposits overlying sand, gravel and bedrock aquifers are common aquifer-aquitard systems. Because of the their low permeability, many clayey deposits are used for waste burial. The clayey layer may protect the underlying aquifers from contamination. The amount of aquifer protection depends on the thickness, hydraulic gradient, and diffusion properties of the aquitard, as well as the distribution and

the hydraulic properties of any fractures that may exist in the aquitard.

In this example, the top clay aquitard has a thickness of 10 m and the underlying sandy aquifer has a thickness also equal to 10 m (see Figure 6-18). The aquitard contains randomly distributed vertical and horizontal fractures. The downward migration of contaminants of different species from a pollution source located on the surface and into the underlying aquifer will be examined. The aquifer is considered to be a homogeneous porous medium. The rectangular cross section has a length of 200 m and total thickness of 20 m. The physical system is assumed to be entirely saturated. A typical set of hydraulic properties of aquitard and the aquifer are used. A list of the physical properties characterizing the system under consideration is presented in Table 6.9. The permeability contrast between the aquifer and the clayey aquitard is six orders of magnitude. All the seven species are assumed to have the same effective diffusion coefficient in aquitard and the aquifer.

Parameter	Aquifer	Aquitard	Fractures
Hydraulic conductivity, m/y	3.1536×10^{3}	3.1536×10^{-3}	-
Porosity	0.3	0.3	1.0
Longitudinal dispersity, m	0.1	0.1	0.1
Transverse dispersivity, m	0.01	0.01	-
Diffusion coefficient, m^2/y	0.0227	0.0227	0.0568
Retardation factor for all species	1.0	1.0	1.0

Table 6.9: Physical properties of 7 species PCE biodegradation transport in discrete fracture media

This generic multi-species contaminant transport model has properties representative of commonly encountered chlorinated organic contaminants such as the tetrachloroethylene (PCE) and its biodegradation products. The solubility of such organics is generally in the range of several hundreds to several thousands milligrams per liter. Because the permissible levels of groundwater contamina-

tion by these compounds are low (typical allowable drinking water limits is 1-50 μg/l), it is important to understand the transport behavior of the these organic contaminants. In numerical studies, it is common to neglect the transport of biodegradation products. In this example, PCE and its biodegradation products will be simulated at the same time. In anaerobic conditions, PCE biodegradation will produce 6 products, including TCE, 1,1-DCE, *cis*-1,2-DCE, *trans*-1,2-DCE, VC and ethene. A detailed discussion of the degradation procedure can be found in section 3 of this chapter. All the biodegradation procedures in this example are simplified to first order decays. A half-life of 100 days is used for PCE. the same half-life data as presented in Table 6.5 are used for other components.

In the aquitard, the fractures are generated randomly in the two-dimensional section. In this example two orthogonal sets of fractures are considered, one set being parallel to the x-axis and the other parallel to the z-axis. In addition, a single vertical fracture runs through the pollution source from the top of the aquitard to the bottom. The fractures have a constant aperture equal to 3×10^{-5} m. The domain is discretized with rectangular elements and the fractures are discretized with linear 1-D elements using the program PREFRAC [Sudicky and McLaren, 1998]. The mesh is refined where necessary to ensure that there is a minimum of three nodes between adjacent fractures in each of the orthogonal sets. The generated mesh contains 131,631 nodes. The aquifer and porous matrix blocks in the aquitard are represented by 130,872 rectangular elements. The fractures are discretized into 3824 horizontal fracture elements and 1842 vertical fracture elements.

The groundwater system is supposed to be steady state. The aquifer has two constant head boundaries, one at the left end of the aquifer with a hydraulic head of 17 m, the other at the right end of the aquifer with a hydraulic head of 16 m.

Along the top of the domain, the head decreases linearly from 21 m on the left to 20 m on the right. All other portions of the domain boundaries consist of impermeable boundary conditions for flow. With these boundary conditions, the flow is predominantly downward through the aquitard to the aquifer. In the aquifer, the groundwater flow direction is from left to right. The discrete fracture flow system was solved first and then the solution results of flow velocity were applied to the contaminant transport model. The boundary conditions for the transport model consist of zero dispersive flux everywhere, except the pollution source on the top of the aquitard between 30-50 m is a first type boundary. The constant concentration is 1 for PCE and 0 for all other species. At the beginning of the simulation, all contamination is confined to the pollution source. The contaminants are assumed to be present in the dissolved phase. Thus, uncontaminated groundwater enters the aquifer from the left side and mixes with contaminated water leaking from the overlying aquitard and then exits from the aquifer at the right side.

The convergence criterion used in the ORTHOMIN solver for the Arnoldi reduction process is 1×10^{-6}. A total of 135 Arnoldi vectors are used for this problem. On average, six ORTHOMIN iterations are required to get an Arnoldi vector. For a 200-year simulation with a time step size of 1 year, 11.5 minute CPU time is needed for all of the 7 species solutions. The problem with the same data set and same convergence criterion is also solved by LTG method. Because the program FRACTRAN [Sudicky and McLaren, 1998] for the LTG method solution is for single species problem, only the first species is solved for this problem. The total CPU time to get the solution for the first species is 2.5 minutes. Each of the 11 p space solutions on average requires eight ORTHOMIN iterations. Comparison of the first species computed concentrations with the two different methods in-

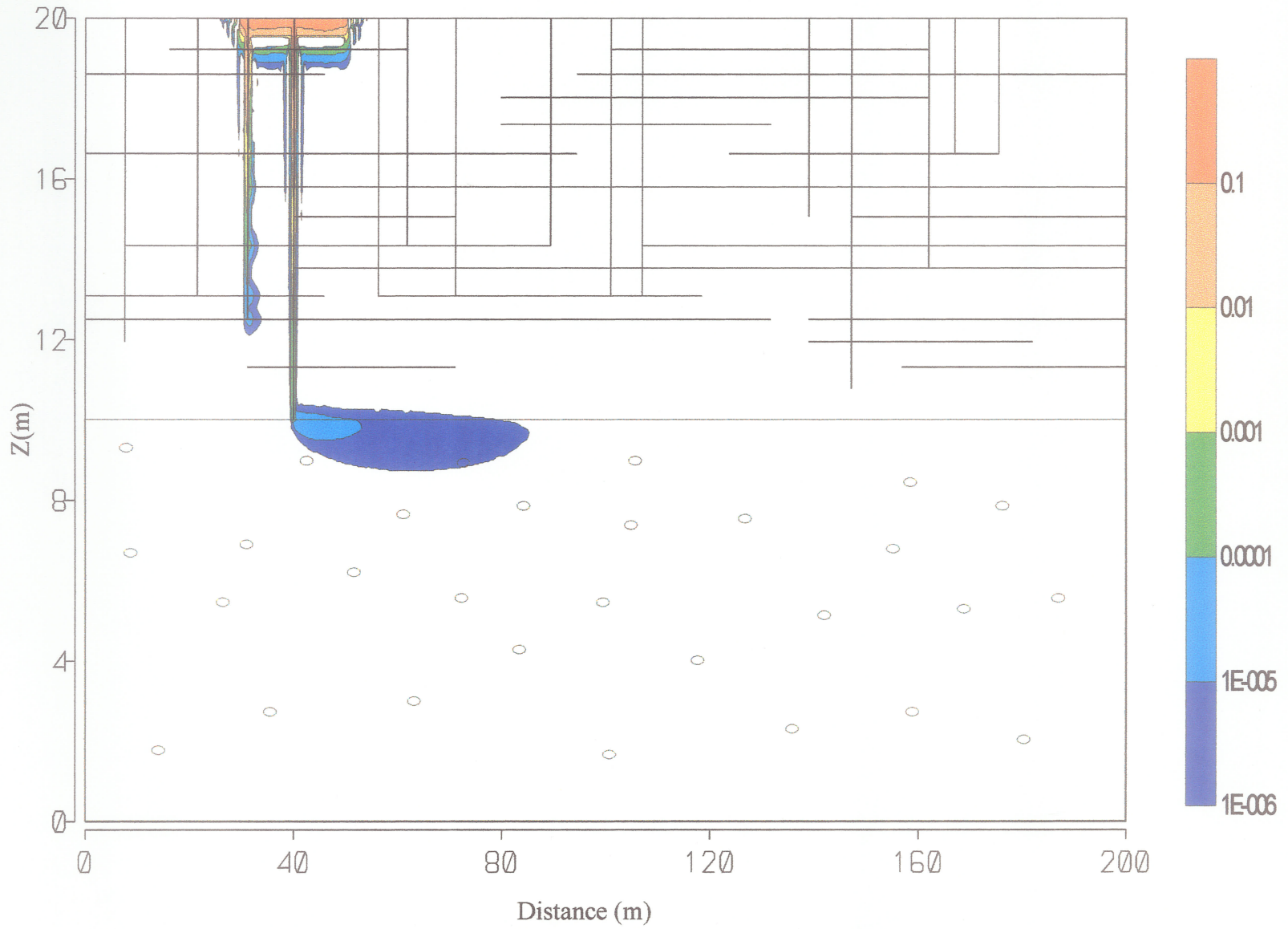

Figure 6-18 Concentration distribution of PCE transport in discrete fracture media 50 year after release of pollution source (by Arnoldi method).

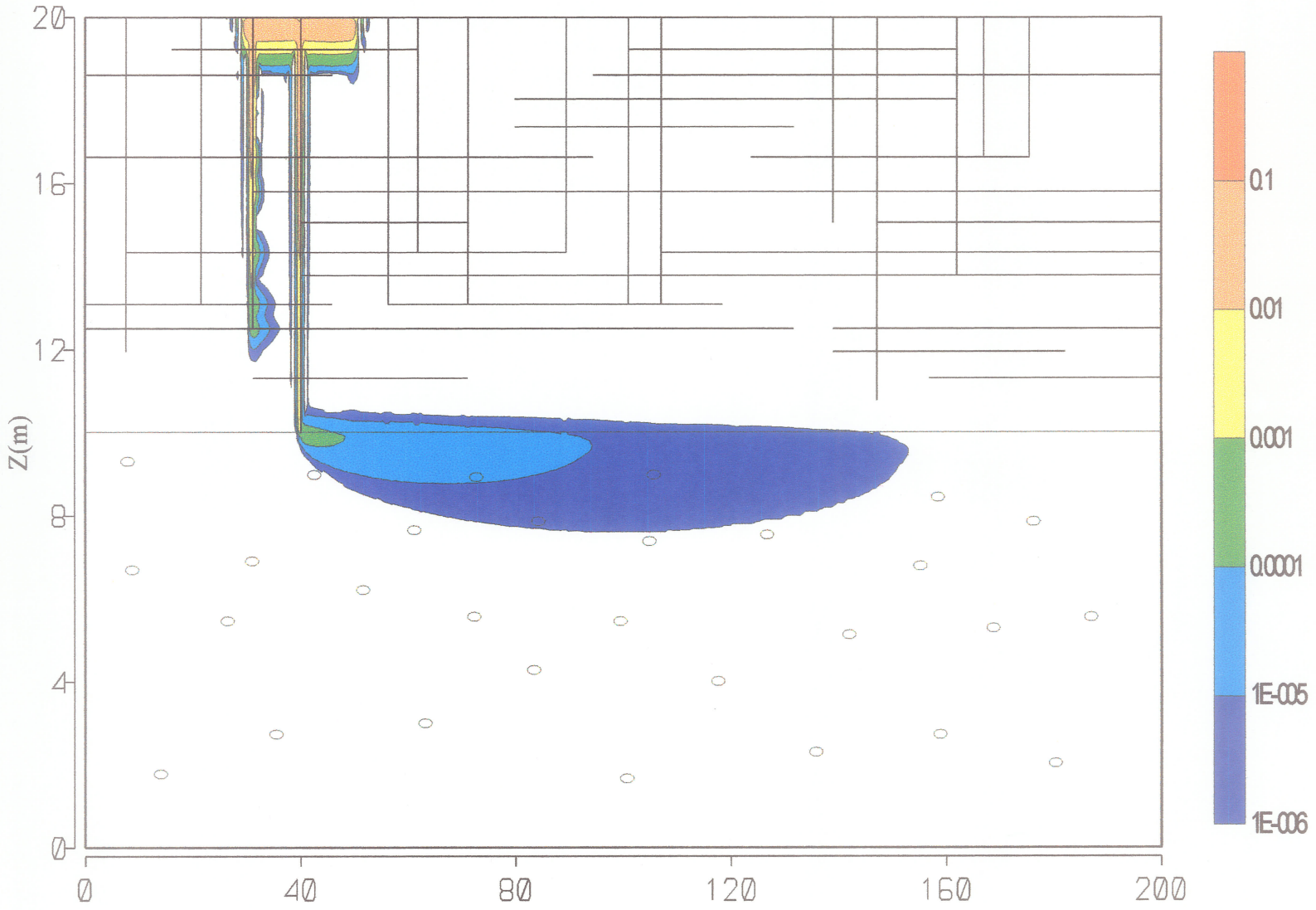

Figure 6-19 Concentration distribution of cis-1,2 DCE transport in discrete fracture media 50 year after release of pollution source (by Arnoldi method).

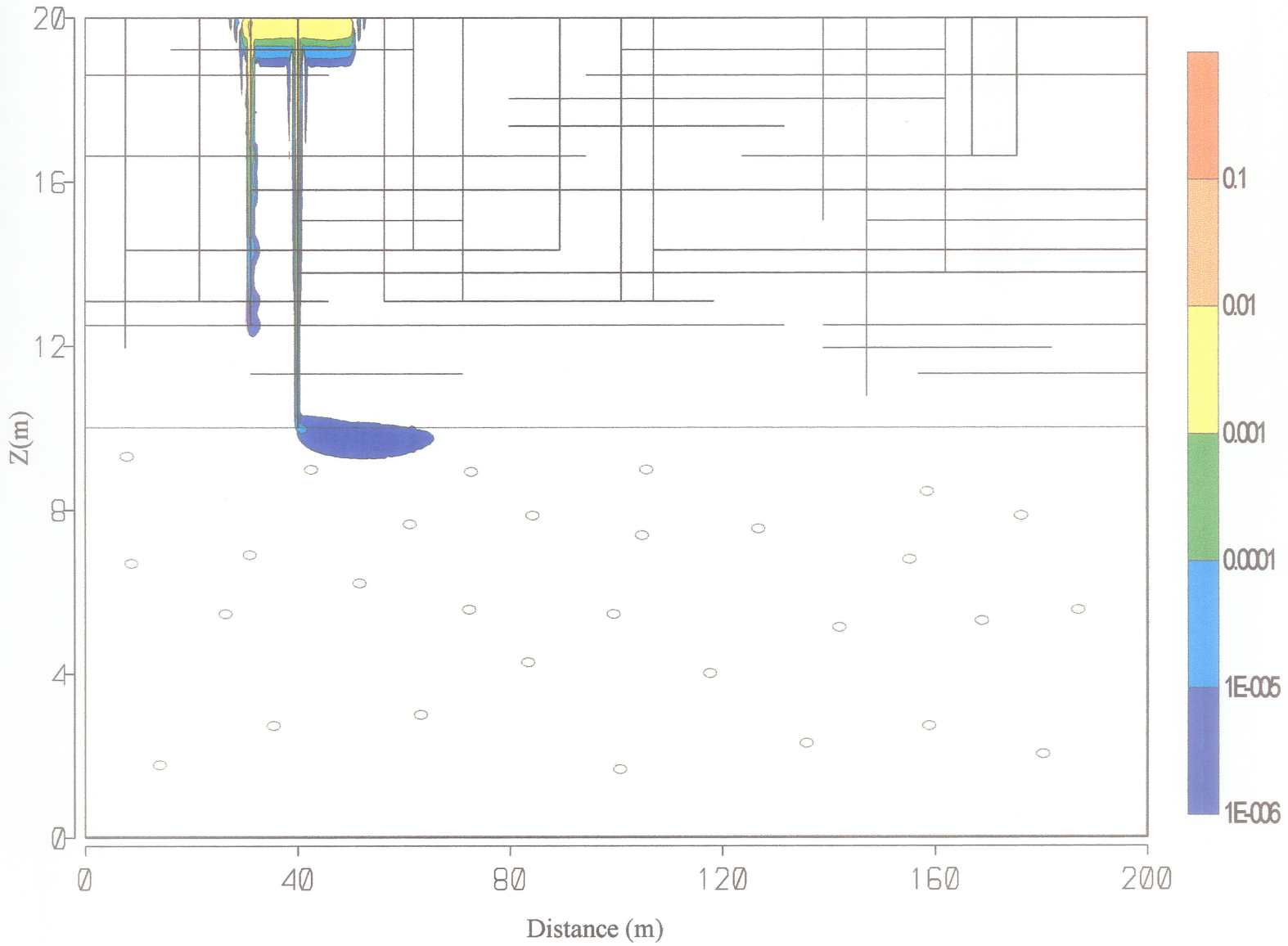

Figure 6-20 Concentration distribution of tran-1,2 DCE transport in discrete fracture media 50 year after release of pollution source (by Arnoldi method).

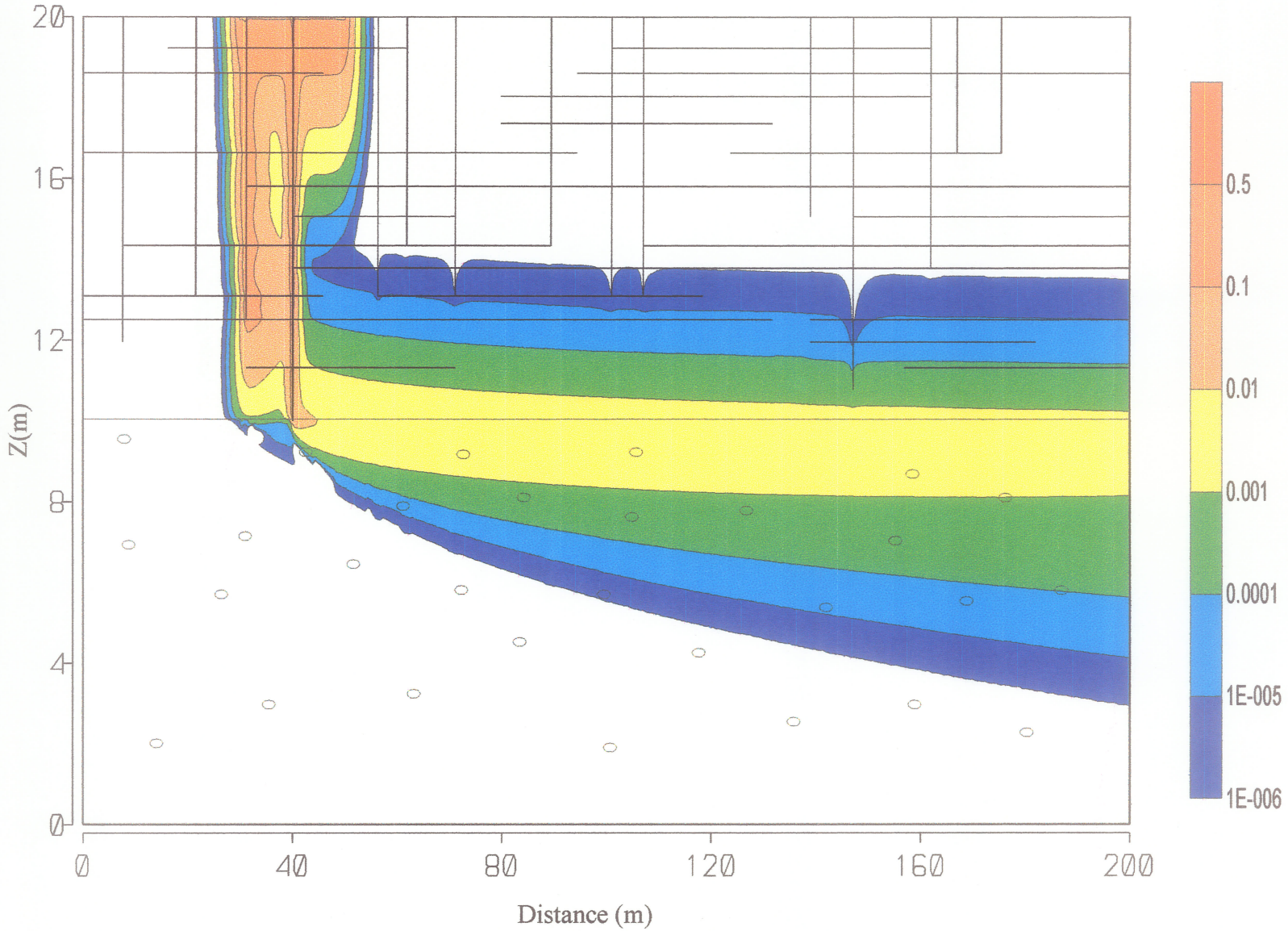

Figure 6-21 Concentration distribution of ethene transport in discrete fracture media 50 year after release of pollution source (by Arnoldi method).

dicated that both methods yielded almost the same results. Therefore only the results obtained with the ARM are shown.

Figures 6-18 to 6-21 show the concentration distribution at 50 years for PCE,*cis*-1,2 DCE, *tran*-1,2 DCE and ethene, respectively. It is clear that the pollution plumes of all the components move rapidly down through the fractures and are deflected laterally by the flow in the aquifer. As the contaminants move through the aquifer, some diffusion up into the aquitard occurs. The fractures clearly act as the controlling pathways for contaminant migration from the pollution source to the underlying aquifer. Due to the low hydraulic conductivity of the matrix block in the aquitard, contaminant transport in matrix blocks are mainly controlled by diffusion. The strength of the advective transport process along vertical fractures in the aquitard is evidenced by much higher groundwater velocities compared to velocities in the aquitard matrix. For the short half-life species, contaminant transport is dominated by advection. This is because before the contaminants effectively diffused into the matrix block, it had already been dramatically diminished. This property is clear for PCE and DCE isomers. However, because of matrix diffusion, the rate of contaminant migration along the fractures is reduced and the contaminant front advances with a slower velocity than the groundwater velocity in the fracture. It is important to note that the biodegradation products of an organic contaminant species can have much higher concentration distribution and larger plumes than the species itself, such as VC and ethene in this example which have about 1000 times higher concentration than PCE in the aquifer. Therefore, simultaneous simulation of multi-species chlorinated organic contaminants transport and biodegradation is important for the evaluation of these type contamination to groundwater.

Chapter 7

Conclusions and Suggestions for Future Work

7.1 Conclusions

In this thesis, in-depth discussions for application of the two reduction methods have been presented. Several very efficient two-dimensional numerical models based on the reduction methods have been developed to solve problems of groundwater flow and multi-species contaminant transport in fractured media. The developed models include a dual-porosity groundwater flow model, dual-porosity decay chain transport model, dual-porosity TCE biodegradation transport model, discrete fracture flow model, and a discrete fracture multi-species contaminant transport model. These models are suitable for solving flow and transport problems using the most popular three approaches (continuum, dual-porosity and discrete fracture approach) for the fractured porous media. Because of the large number of unknowns that can be expected for field-scale multi-species transport problems and because of the high contrast in material properties between the fractures and matrix, selecting an efficient and robust numerical technique is necessary. The research has demonstrated that both the Arnoldi and Lanczos reduction method are the suitable choices for this type problems. The numerical results have shown

that the reduction methods can result in large computational savings for long term prediction. In addition, the storage saving is also significant. The following is the summary of the conclusions of this research.

1. The LRM has been successfully developed for the solution of problems involving groundwater flow in heterogeneous and anisotropic dual-porosity media. The main advantages of the method are twofold: (1) the equation system is solved in a reduced space, which is much smaller than the original system, (2) The fluid leakage terms are calculated by a recursion scheme in the reduced space. The solution time for the Crank-Nicolson scheme with a direct solution method is proportional to $n \times n_b$, where n is the total unknowns of the original equation system and n_b is the half bandwidth of the matrices $\mathbf{K}$ and $\mathbf{M}$, however solution of the reduced tridiagonal system is only proportional to m, which is the unknown number of the reduced equation system. In addition, the Lanczos method efficiency is such that a dual-porosity solution presents a negligible additional computational burden compared to that for a single-continuum simulation. Consequently, the decrease in solution effort is pronounced, particularly on large problems or problems required more time steps.

2. Comparisons with exact analytical solutions have indicated that the LRM is capable of yielding a highly accurate solution even when relatively less Lanczos vectors are employed. The example simulation for the case of multiple wells with different pumping time histories indicates that the reduction method is very robust. Examples have shown that only a small number of Lanczos vectors were required to accurately match the drawdown computed by direct solution method. For the homogeneous problems, experiments have shown the ratio of n to m can be as high as 200. However, m is not a

function of n. For a problem with a large n, the ratio is expected to be larger. Experiences indicate that the aquifer hydraulic properties and domain discretization scheme are among the most important factors in determining m.

3. Multiple well systems with different pumping time histories or time-dependent boundary conditions have been implemented in the reduction method using a superposition principle. The results of the field-scale example have verified that the implementation method is correct and efficient. It is noted that the reduction method could be applied to any realistic single, dual-porosity or discrete fracture groundwater flow or contaminant transport model. The Lanczos algorithm performs the reduction process based on the matrix $\mathbf{K}$ and $\mathbf{M}$, and the starting vector. No matter what dimensionality of the problem, the properties of these matrices and vectors are the same. Therefore, the theory developed in this thesis is readily applicable for a fully three-dimensional groundwater flow problem.

4. The LRM is also successfully extended to the modeling of groundwater flow in discretely fractured porous media. An iterative version of the Lanczos algorithm has been developed and the "shift" technique has been introduced to the discrete fracture flow model. The model is verified by comparison with dual-porosity approach. The efficiency and accuracy of the method are demonstrated on a field scale problem and compared to the performance of classic time marching using a PCG iterative solver on the original system.

5. By using the "shift" technique, the diagonal dominant property of the matrix to be solved is improved. This property greatly enhances the iterative solution convergence rate. Equally important, the "shift" technique can also

increase the convergence rate for the Lanczos or Arnoldi reduction recursion processes which means less Lanczos or Arnoldi vectors are required compared to the case without using this technique. In addition, using the "shift" technique can extend the application of the ARM to solve large Peclet number problems. The shift factor ϱ should have a value that makes $\mathbf{K}$ and $\varrho\mathbf{M}$ similar in absolute value. It is suggested that $\varrho \geq 2/\Delta t$ be chosen.

6. The Arnoldi reduction technique has been successfully developed for the solution of problems involving multi-species radionuclides decay chain transport in heterogeneous dual-porosity media. The computation and storage savings of the developed model are substantial. These are achieved by solving a much smaller reduced equation system instead of the original system, and also by calculating a mass exchange term for only m reduced nodes. In addition, the ARM requires only one or two Arnoldi reduction processes to reduce all the equations for different species. The method is well-suited for solving the large problems of multi-species with more nodes and more time steps. It is expected that for long period predictions, the method would be very efficient. More computational time and storage saving can be obtained if more species and more finite element nodes are involved in the problem.

7. The formula for calculation of mass exchange between the fractures and the matrix blocks has been presented. The formula is incorporated into the contaminant transport equations for the fractures in a form that the Arnoldi reduction method can be applied. By using a recursion-like scheme, the concentration distributions in the matrix blocks do not need to be updated before the solving of the equations for fractures and all the computations are performed in the reduced space, which leads to the achievement of the high efficiency in the computation of mass exchange terms.

8. Two schemes for choosing a common starting vector for all species have been developed. The chosen common starting vector ensures the convergence of the Arnoldi method. Using these schemes, the most popular first type boundary conditions can be implemented in the ARM. Considering the superposition method for second type boundary conditions discussed for the flow problem, it is clear that most first and second type boundary conditions can be implemented in the ARM.

9. Comparisons with exact analytical solutions have indicated that the Arnoldi method is capable of yielding a highly accurate solution even when relatively small number Arnoldi vectors are used. The example simulation for 3 species decay chain transport in dual-porosity media shows that the Arnoldi reduction method is very efficiency in both memory storage and computational time. It was found that for most cases, less than 100 vectors may be required to match accurately the concentration computed by a traditional method applied to the original system equations with several to ten thousand nodes. Experiences indicates that the growth in the number of Arnoldi vector does not linearly increase with the number of nodes in a system; its real growth is much smaller.

10. The application of the ARM has been successfully extended to the simulation of multi-species TCE biodegradation type solute transport in dual-porosity media. The proposed method is capable of solving multi-species transport problems with parallel and series reactions. The model developed was verified by a seven species parallel and series reaction transport in a single fracture without diffusion into matrix block. The numerical solutions were compared with analytical solutions. Excellent agreement between the Arnoldi method solutions and analytical solutions was achieved. A field

scale problems concerned transport of TCE and its biodegradation daughter products in a dual-porosity medium has been solved. The two-dimensional model was simulated with typical parameters for decay and in-growth of the contaminant species. The problem involves about 7 million unknowns at each time step. To solve such a large problem would normally be considered being a formidable task using a traditional method.

11. The ARM has also been applied to the simulation of multi-species contaminant transport in fractured porous media using the discrete fracture approach. An iterative version of the ARM, in which the ORTHOMIN solver has been adopted in the reduction process, has been developed for the discrete fracture transport model. The largest problem solved by the ARM using the discrete fracture approach involves 8 species contaminant transport and 120,701 nodes for each species. For multi-species contaminant transport problems, the field scale examples show that the ARM is even more efficient than the LTG method in groundwater hydrology, which has been considered one of the most efficient methods. After using the "shift" technique, the reduction ratio (n/m) can be as high as 1700 and the Peclet number of the problem can be as large as 100.

7.2 Suggestions for future research

The efficiency and accuracy of the reduction methods have been demonstrated in this research. It can be concluded that the ARM is a very promising method for multi-species contaminant transport problem. However further work for this method may be necessary in following areas:

1. An efficient method for determining the optimum shift factor needs to be

developed. The shift factor is a very important parameter that influences the efficiency of the reduction method. If an appropriate shift factor is used, the iterative convergence rate and the reduction process recursion convergence rate can be improved dramatically.

2. The superposition method has been used for the implementation of multiple source boundary conditions. This method requires multiple reduction processes for complicated boundary conditions and it may not be the best method for this type of problem. Further investigation on this topic is necessary.

3. It is important to extend the ARM to solve transport equations of the kinetic reaction processes in porous or fractured porous media. This type of problem involves multiple components and would lead to extensive requirements of computing time and storage space. Therefore an efficient numerical method for this type of problem is necessary.

4. Non-linear problems in groundwater practices are quite common. The investigation of the extension of the ARM to solve the non-linear problem could be very interesting to pursue.

References

Arbogast, T., 1992. *A simplified dual-porosity model for two-phase flow, in Computational Methods in Water Resources IX. Volume 2: mathematical Modeling In Water Resources*, Computational Mechanics Publications, Boston, MA, p419-426.

Arnoldi, W. E., 1951. The principle of minimized iterations in the solution of the matrix eigenvalue problem, *Quart. Appl. Math.*, **9**, 17-29.

Baek, I., W. W. Jr. Pitt, 1996. Colloid-facilitated radionuclide transport in fractured porous rock, *Waste Management*, **v 16 n 4**, p 313-325.

Bai, Mao, 1997. Efficient algorithm for evaluating coupled processes in radial fluid flow, *Computers & Geosciences*, **v23(2)**, 195-202.

Barenblatt, G. I., I. P. Zheltov, and I. N. Kochina, 1960. Basic concepts in the theory of seepage of homogeneous liquids in fissured rocks (strata), *J. Appl. Math. Mech. Engl. Transl.*, **24(5)**, 1286-1303.

Bateman, H., 1910. The solution of a system of differential equations occuring in the theory of radioactive transformation. In *Proc. Cambridge Philos. Soc.*, (15), .

Bear, J., 1972. *Dynamics of Fluids in Porous Media*, Elsevier Science, New York.

Behie, A. L., and P. A. Forsyth, 1984. Incomplete factorization methods for fully implicit simulation of enhanced oil recovery, *SIAM J. Stat. Comput.*, **5(3)**,

543-561.

Berkowitz, B., J. Bear, and C. Braester, 1988. Continuum models for contaminant transport in fractured porous formations, *Water Resour. Res.*, **24(8)**, 1225-1236.

Bibby, R., 1981. Mass transport of solutes in dual-porosity media, *Water Resour. Res.*, **17(4)**, 1075-1081.

Cacas, M. C. L., E. de Marsily, G. Tillie, and B. Barbreau, 1990. Modeling fracture flow with a stochastic discrete fracture network: calibration and validation, *Water Resour. Res.*, **26(3)**, p 479-500.

Chen, C. S., 1986. Solutions for radionuclide transport from an injection well into a single fracture in a porous formation, *Water Resour. Res.*, **22(4)**, 508-518.

Chen, C. T., and S. H. Li, 1997. Radionuclide transport in fractured porous media-analytical solutions for a system of parallel fractures with a flux-type boundary condition, *Nucl. Technol.*, **117(2)**, 223-233.

Clement, T. P., sun, Y. , Hooker, B. S., and Petersen, J. N., 1998. Modeling multi-species reactive transport in groundwater aquifers, *Ground Water Monit. rem.*, **18(2)**, 79-92.

Codell R. B., 1996. Improved radionuclide transport models for a nuclear waste repository. In *Materials Research Society Symposium Proceedings*, (v412), 731-738.

Domenico, P. A., and F. W. Schwartz, 1990. *Physical and Chemical Hydrogeology*, John Wiley and Sons Inc..

Dunbar, W. S., and A. D. Woodbury, 1989. Application of the Lanczos algorithm to the solution of the groundwater flow equation, *Water Resour. Res.*, **25(3)**, 551-558.

Dunbar, W. S., A. D. Woodbury and B. Nour-Omid, 1994. Comment on "On time integration of groundwater flow equations by spectral methods" by G. Gambolati, *Water Resour. Res.*, **30(3)**, 2347-2352.

Dverstorp, B., J. Anderson, and W. Nordqvist, 1992. Discrete fracture network interpretation of field tracer migration in sparsely fractured rock, *Water Resour. Res.*, **28(9)**, p 2327-2343.

Dykhuizen, R. C., 1990. A new coupling term for dual-porosity models, *Water Resour. Res.*, **26(2)**, 351-356.

Farrell, A. D., 1997. *An assessment of the role of transient flow on the dispersion of non-reactive solutes in porous media: a numerical study*, Ph.D. Dissertation, The University of Manitoba.

Farrell, D. A., A. D. Woodbury and E. A. Sudicky, 1997. Numerical modeling of mass transport in hydrogeologic environments: performance comparison of the Laplace transform Galerkin and Arnoldi modal reduction schemes, *Advances in Water Resources*, **21**, 217-235.

Fetter, C. W., 1992. *Contaminant Hydrogeology*, MacMillan.

Fillion, E., and M. L. Noyer, 1996. Flow modeling in a dual porosity domain with automatic mesh generation and parameter calibration: application to the Aspo site, *Journal of Hydrology*, **v180 n 1-4**, p 1-19.

Freeze, R. A., and J. A. Cherry, 1979. *Groundwater*, Prentice-Hall Inc., New Jersey.

Gureghian, A. B., and G. Jansen, 1985. One-dimensional analytical solutions for the migration of a three-member radionuclide decay chain in a multilayered geologic medium, *Water Resour. Res.*, **21(5)**, 733-742.

Hantush, M. S., 1964. *Hydraulics of Wells, Adv. Hydrosci.*, Academic Press, 1,

p281-432.

Harada, M., P. L. Chambre, M. Foglia, K. Iwamoto, D. Leung, T. H. Pigford, and D. Ting, 1980. Migration of radionuclides through sorbing media analytical solutions 1, *Tech. Rep. ONWI-359*, **Waste Isolation, Columbus**, Ohio.

Hardermann, J., 1980. Radionuclide transport through heterogeneous media, *Nucl. Technol.*, **47**, 312-323.

Harrison, B., E. A. Sudicky, and Cherry, 1992. Numerical analysis of solute migration through fractured clayey deposits into underlying aquifers, *Water Resour. Res.*, **28(2)**, 515-526.

Hodgkinson, D. P.,and P. R. Maul, 1988. 1-D modeling of radionuclide migration through permeable and fractured rock for arbitrary length decay chains using numerical inversion of Laplace transforms, *Ann. Nucl. Energy*, **15(4)**, 175-189.

Huyakorn, P. S., B. H. Lester and C. R. Faust, 1983. Finite element techniques for modeling groundwater flow in fractured aquifers, *Water resour. Res.*, **19(4)**, 1019-1035.

Huyakorn, P. S., B. H. Lester and J. W. Mercer, 1983. An efficient finite element technique for modeling transport in fractured porous media, 1. Single species transport, *Water Resour. Res*, **19(3)**, 841-854.

Huyakorn, P. S., B. H. Lester and J. W. Mercer, 1983. An efficient finite element technique for modeling transport in fractured porous media, 2. Nuclide decay chain transport, *Water Resour. Res*, **19(5)**, 1286-1296.

Huyakorn, P. S., S. Panday, Y. S. Wu, 1994. Three-dimensional multiphase flow model for assessing NAPL contaminant in porous and fractured media, 1. Formulation, *Journal of Contaminant Hydrology*, **v16 n2**, p109-130.

Huyakorn, P. S., and G. F. Pinder, 1983. *Computational Methods in Subsurface Flow*, Academic Press.

Ibaraki, M., E. A. Sudicky, 1995. Colloid-facilitated contaminant transport in discretely fractured porous media, 1. Numerical formulation and sensitivity analysis, *Water Resour. Res.*, **31(12)**, 2945-2960.

Jain, M. K. and Criddle, C. S., 1995. Metabolism and cometabolism of halogenated C-1 and C-2 hydrocarbon. In *Biotransformations: Microbial Degradation of Health Risk Compounds*, (edited by V. P. Singh), pp. 65-112. Elsevier Sci., New York

Lanczos, C., 1950. An iteration method for the solution of the eigenvalue problem of linear differential and integral operators, *J. Res. Nat. Bur. Standards*, **45**, 255-282.

Lao, C. J., and J. R. Booker, 1996. Time-stepping finite element method for analysis of contaminant transport in fractured porous media, *International Journal for Numerical and Analytical Methods in Geomechanics*, **v20 n12**, p847-864.

Lee, Y. M., and K. J. Lee, 1995. Nuclide transport of decay chain in the fractured rock medium: a model using continuous time markov process, *Ann. Nucl. Energy*, **22(2)**, 71-84.

Lester, D. H., G. Jansen and H. C. Burkholder, 1975. Migration of radionuclide chains through an adsorbing medium, *AIChE Symp. Ser.*, **71(152)**, 202-213.

Li, H., 1996. *Development and application of the unsymmetric reduction Lanczos method*, Ph.D. Dissertation, The University of Manitoba.

Li, H., A. Woodbury and P. Aitchison, 1999. Application of the unsymmetric Lanczos method to radionuclide decay chain transport in porous media, *Int. J. Numer. Meth. Engin.*, **44**, 355-372.

Liggett, J. A., and D. Medina, 1988. *Groundwater Flow and Quality Modeling*, D. Reidel Publishing Co. Boston, p363-374.

Liu, C. W., and T. N. Narasimhan, 1989. Redox-controlled multiple-species reactive chemical transport, 1. Model development, *Water Resour. Res.*, **25(5)**, 869-882.

Long, J. C. S., J. S. Remer, C. R. Wilson, and P. A. Witherspoon, 1982. Porous media equivalents for networks of discontinuous fractures, *Water Resour. Res.*, **18(3)**, 645-658.

MacQuarrie, K. T. B., E. A. Sudicky, and E. O. Frind, 1990. Simulation of Biodegradable organic contaminants in groundwater, *Water Resour. Res.*, **26(2)**, 207-239.

Meijerink, J. A. and H. A. van der Vorst, 1977. An iterative solution method for linear systems of which the coefficient matrix is a symmetric M-matrix, *Matrematics of computation*, **31(137)**, 148-162.

McCarty, P. L., and L. Semprini, 1994. Groundwater treatment for chlorinated solvents. In *Handbook of Bioremediation*, (Edited by Norris *et al.*), pp 5-1 to 5-30.

Miller, C. W., and L. V. Benson, 1983. Simulation of solute transport in a chemically reactive heterogeneous system: model development and application, *Water Resour. Res.*, **19(2)**, 381-391.

Narasimhan, T. N., A. F. White and T. Tokunaga, 1986. Groundwater contaminant from an inactive uranium mill tailings pile, 2. application of a dynamic mixing model, *Water Resour. Res.*, **22(13)**, 1820-1834.

Neretnieks, I., 1993. *Solute transport in fractured rock-application to radionuclide waste repositions*, in Follow and Contaminant transport in Fractured

rock (Edited by Jacob bear, Chin-Fu Tsang, Ghislain de Marsily) Academic press, New York.

Nour-Omid, B., 1987. Lanczos method for heat conduction analysis, *Int. J. Numer. Methods Eng.*, **24**, 251-262.

Nour-Omid, B., 1989. Application of the Lanczos method, *Comput. Phys. Commun.*, **53**, 157-168.

Nour-Omid, B. and R. W. Clough, 1984. Dynamic analysis of structures using Lanczos coordinates, *Earthquake Engineering Structural Dynamic*, **12**, 565-577.

Nour-Omid, B., W. S. Dunbar and A. D. Woodbury, 1991. Lanczos and Arnoldi methods for the solution of convection-diffusion equations, *Computer Methods in Applied Mechanics and Engineering*, **88**, 75-95.

Novak,C. F., 1993. Modeling mineral dissolution and precipitation in dual-porosity fracture-matrix systems, *Journal of Contaminant Hydrology*, **v13 n1-4**, p91-115.

Ostensen, R. W., 1998. Tracer tests and contaminant transport rates in dual-porosity formations with application to the WIPP, *Journal of Hydrology*, **v 204 n 1-4**, p 197-216.

Pini, G., and M. Putti, 1997. Parallel finite element Laplace transform method for the non-equilibrium groundwater transport equation, *International Journal for Numerical Methods in Engineering*, **v 40 n 14**, p 2653-2664.

Press, W. H., Teukolsky, S. A., Vetterling, W. T. and Flannery, B. P., 1992. *Numerical Recipes in FORTRAN: The art of scientific computing*, Cambridge University Press.

Pruess, K., 1991. *TOUGH2–A General -Purpose Numerical Simulator for Multi-*

phase Fluid and Heat Flow, LBL 29400, Lawrence Berkeley Laboratory, University of California, Berkeley, California.

Rasmuson, A., 1984. Migration of Radionuclides in fissured rock: Analytical solutions for the case of constant source strength, *Water Resour. Res.*, **20(10)**, 1435-1442.

Schwartz, F. W., and L. Smith, 1988. A continuum approach for modeling mass transport in fractured media, *Water Resour. Res.*, **24(8)**, 1360-1372.

Schwartz, F. W., L. Smith, and A. S. Crowe, 1983. A stochastic analysis of macroscopic dispersion in fractured media, *Water Resour. Res.*, **19(5)**, 1253-1265.

Semprini, L., P. K. Kitanidis and J. T. Wilson, 1995. Anaerobic transformation of chlorinated aliphatic hydrocarbons in a sand aquifer based on spatial chemical distributions, *Water Resour. Res.*, **31(4)**, 1051-1062.

Simon, Horst D., 1984. Analysis of the symmetric Lanczos algorithm with reorthogonalization methods, *Linear Algebra and its Applications*, **61**, 101-131.

Skeen, R. S., Gao, J. and Hooker, B. S., 1995. Kinetics of chlorinated ethylene dehalogenation under methanogenic conditions, *Biotechnol. Bioeng.*, **48**, 659-666.

Smith, L., and F. W. Schwartz, 1984. An analysis of the influence of fracture geometry on mass transport in fractured media, *Water Resour. Res.*, **20(9)**, 1241-1252.

Song, H., A. L. Woodbury, 1998. *Simulation of Chlorinated solvent transport and remediation performance assessment at the Rockwood Propellant Plant, Manitoba*, Research Report, The University of Manitoba.

Sudicky, E. A., 1989. The Laplace transform Galerkin technique: A time-continuous

finite element theory and application to mass transport in groundwater, *Water Resour. Res.*, **25(8)**, 1833-1846.

Sudicky, E. A., 1990. The Laplace transform Galerkin technique for efficient time-continuous solution of transport in double-porosity media, *Geoderma*, **46**, 209-232.

Sudicky, E. A., and E. O. Frind, 1982. Contaminant transport in Fractured porous media: Analytical solutions for a system of parallel fractures, *Water Resour. Res.*, **18(6)**, 1634-1642.

Sudicky, E. A., and E. O. Frind, 1984. Contaminant transport in Fractured porous media: Analytical solution for a two-member decay chain in a single fracture, *Water Resour. Res.*, **20(7)**, 1021-1029.

Sudicky, E. A., and P. S. Huyakorn, 1991. Contaminant migration in imperfectly known heterogeneous groundwater systems, *Reviews of Geophysics*, **Supplement**, 240-253.

Sudicky E. A., and R. G. McLaren, 1992. The Laplace transform Galerkin technique for large-scale simulation of mass transport in discretely fractured porous formations, *Water Resour. Res.*, **28(2)**, 499-514.

Sudicky E. A., and R. G. McLaren, 1998. *FRACTRAN user's guide-an efficient simulator for two-dimensional, saturated groundwater flow and solute transport in Porous or discretely-fractured porous formations*, Waterloo Centre for Groundwater Research, University of Waterloo, Canada.

Sun, Y., J. N. Petersen, T. P. Clement and R. S. Skeen, 1999. Development of analytical solutions for multi-species transport with serial and parallel reactions, *Water Resour. Res.*, **35(1)**, 185-190.

Sun, Y., J. N. Petersen, T. P. Clement, 1999. Analytical solutions for multiple

species reactive transport in multiple dimensions, *J. Contaminant Hydrology*, **35(4)**, 429-440.

Tang, D. H., E. O. Frind, and E. A. Sudicky, 1981. Contaminant transport in fractured porous media: Analytical solution for a single Fracture, *Water Resour. Res.*, **17(3)**, 555-564.

Taniguchi, T., and E. Fillion, 1996. Numerical experiments for 3-dimensional flow analysis in a fracture rock with porous matrix, *Advances in Water Resources*, **v 19 n 2**, p97-107.

Therrien R., and E. A. Sudicky, 1996. Three-dimensional analysis of variably-saturated flow and solute transport in discretely-fractured porous media, *J. Contam. Hydrol.*, **23**, 1-44.

Tomasko K. R., M. Kelley and V. A. Pickens, 1989. Parameter sensitivity and importance for radionuclide transport in double-porosity systems. In *Proceeding of The Conference on Geostatistical, Sensitivity and Uncertainty Methods for Groundwater Flow and radionuclide Transport Modeling*, (Battelle Press, Columbus, Ohio), p297-321.

Townley, L. and J. L. Wilson, 1980. *Description of and user's manual for a finite element aquifer flow model, AQUIFEM-1, rep. 252*, Ralph M. Parsons Lab. for Water Resour. and Hydrodyn., Mass. Inst. of technol., Cambridge.

Travis, B. J., 1984. *TRACR3D: A Model of Flow and Transport in Porous/Fractured Media*, LA-9667-MS, Los Alamos National Laboratory, Los Alamos, N. M..

van der Lee, J., E. Ledoux, and G. de Marsily, 1992. Modeling of colloidal uranium transport in a fractured medium, *Journal of Hydrology*, **v 139**, p 135-158.

VanderKwaak, J. E., and E. A. Sudicky, 1996. Dissolution of non-aqueous-phase liquids and aqueous-phase contaminant transport in discretely-fractured porous media, *J. Contam. Hydrol.*, **23**, 45-68.

Vinsome, P. K. W., 1976. *an iterative method for solving sparse sets of simultaneous linear equations*, Pap. SPE 5729, SPE-AIME Symp., Numer. Simulation Reservoir Performance, Los Angeles.

Vogel, T. M., and P. L. McCarty, 1985. Biotransformation of tetrachlorethylene to trichloroethylene, dichloroethylene, vinyl chloride, and carbon dioxide under methanogenic transformation, *Appl. Environ. Microbiol.*, **49(5)**, 1080-1083.

Wiedemeier, T. H., J. T. Wilson, D. H. Kampbell, 1996. Natural attenuation of chlorinated aliphatic hydrocarbons at Plattsburgh air force base, New York. In *Proceeding of Symposium on Natural Attenuation of Chlorinated Organics in Ground Water*, (74-82), .

Willis, C., and J. Rubin, 1987. Transport of reactive solutes subject to a moving dissolution boundary: Numerical methods and solution, *Water Resour. Res.*, **23(8)**, 1561-1574.

Woodbury, A. D., W. S. Dunbar and B. Nour-Omid, 1990. Application of the Arnoldi algorithm to the solution of the advection-dispersion equation, *Water Resour. Res.*, **26(10)**, 2579-2590.

Woodbury, A. D. and Li, H., 1998. The Arnoldi finite element method for solving transport of reacting solutes in porous media. In *Proc. Remediation of Chlorinated and Recalcitrant Compounds*, (Monterey, Calif.), .

Xu, L. and M. L. Brusseau, 1995. A combined Laplace transform and streamline upwind approach for nonideal transport of solutes in porous media, *Water Resour. Res.*, **31(10)**, 2483-2489.

Zimmerman, R. W. and G. S. Bodvarsson, 1989. Integral method solution for diffusion into a spherical block, *Journal of Hydrology*, **111 (1-4)**, 213-224.